MODELING AND CONTROL OF HIGH TEMPERATURE OVEN FOR LOW TEMPERATURE CO-FIRED CERAMIC (LTCC) DEVICE MANUFACTURING

A THESIS SUBMITTED TO
THE GRADUATE SCHOOL OF NATURAL AND APPLIED SCIENCES
OF
MIDDLE EAST TECHNICAL UNIVERSITY

BY

AYŞE TUĞÇE YÜCEL

IN PARTIAL FULFILLMENT OF THE REQUIREMENTS
FOR
THE DEGREE OF MASTER OF SCIENCE
IN
CHEMICAL ENGINEERING

SEPTEMBER 2012

Approval of the thesis:

MODELING AND CONTROL OF HIGH TEMPERATURE OVEN FOR LOW TEMPERATURE CO-FIRED CERAMIC (LTCC) DEVICE MANUFACTURING

Submitted by **AYŞE TUĞÇE YÜCEL** in partial fulfillment of the requirements for the degree of **Master of Science in Chemical Engineering Department, Middle East Technical University** by,

Prof. Dr. Canan Özgen ______________
Dean, Graduate School of **Natural and Applied Sciences**

Prof. Dr. Deniz Üner ______________
Head of Department, **Chemical Engineering**

Asst. Dr. Serkan Kıncal
Supervisor, **Chemical Engineering Dept., METU** ______________

Examining Committee Members:

Prof. Dr. İnci Eroğlu ______________
Chemical Engineering Dept., METU

Asst. Dr. Serkan Kıncal ______________
Chemical Engineering Dept., METU

Prof. Dr. Raşit Turan ______________
Physics Dept., METU

Assoc. Dr. Görkem Külah ______________
Chemical Engineering Dept., METU

Eyüp Töngel, M.Sc. ______________
ASELSAN Inc.

Date: September 05, 2012

I hereby declare that all information in this document has been obtained and presented in accordance with academic rules and ethical conduct. I also declare that, as required by these rules and conduct, I have fully cited and referenced all material and results that are not original to this work.

Name, Last name : AYŞE TUĞÇE YÜCEL

Signature :

ABSTRACT

MODELING AND CONTROL OF HIGH TEMPERATURE OVEN FOR LOW TEMPERATURE CO-FIRED CERAMIC (LTCC) DEVICE MANUFACTURING

Yücel, Ayşe Tuğçe
M.Sc., Department of Chemical Engineering
Supervisor : Asst. Dr. Serkan Kıncal

September 2011, 165 pages

In the electronics the quality, reliability, operational speed, device density and cost of circuits are fundamentally determined by carriers. If it is necessary to use better material than plastic carrier, it has to be made of ceramics or glass-ceramics. This study dealt with the ceramic based carrier production system. The types of the raw ceramics fired at low temperature (below 1000°C) are called Low Temperature Co-Fired Ceramics (LTCC).

In this study, a comprehensive thermal model is described for the high temperature oven which belongs to a Low Temperature Co-fired Ceramic (LTCC) substance production line. The model includes detailed energy balances with conduction, convection and radiation heat transfer mechanisms, view factor derivations for the radiative terms, thermocouple balances, heating filaments and cooling mechanisms for the system.

Research was conducted mainly on process development and production conditions along with the system modeling of oven. Temperature control was made in high temperature co-firing oven. Radiation View Factors for substrate and thermocouples are determined. View factors between substrate and top-bottom-sides of the oven are calculated, and then inserted into the energy balances. The same arrangement was made for 3 thermocouples at the bottom of the oven. Combination of both expressions gave the final model. Modeling studies were held with energy balance simulations on MATLAB. Data analysis and DOE study were held with JMP Software.

Keywords: LTCC, co-firing oven, view factor, radiation heat transfer.

ÖZ

DÜŞÜK SICAKLIKLI EŞ YANMALI SERAMİK (LTCC) MALZEME ÜRETİMİNDE KULLANILAN YÜKSEK SICAKLIK FIRINININ MODELLENMESİ VE KONTROLÜ

Ayşe Tuğçe Yücel
Yüksek Lisans, Kimya Mühendisliği Bölümü
Tez Yöneticisi : Yard. Doç. Dr. Serkan Kıncal

Eylül 2011, 165 sayfa

Elektronikte; kalite, dayanım, operasyon hızı, cihaz yoğunluğu ve devre maliyetleri temel olarak taşıyıcılar tarafından belirlenir. Eğer plastik taşıyıcılardan daha iyi bir malzeme kullanılması gerekliyse, bunlar seramik ya da cam-seramik bazlı olmalıdır. Bu çalışmada seramik bazlı taşıyıcıların üretim sistemleri incelenmiştir. Düşük sıcaklıklarda (1000^{o}C altında) yanmaya giren ham seramik malzeme tipine, Düşük Sıcaklıklı Eşyanmalı Seramik (LTCC) adı verilir.

Bu çalışmada, Düşük Sıcaklıklı Eş-yanmalı Seramik (LTCC) malzemenin üretim hattına ait olan, yüksek sıcaklık fırını için detaylı bir ısıl model tanımlanmıştır. Model; iletim, taşınım ve ışınım yoluyla ısı aktarımı mekanizmalarını içeren detaylı enerji denkliklerini, radyoaktif terimlere ait görüş katsayılarının çıkarımını, ısıl çift denkliklerini, ısıtıcı filamentleri ve sistemin soğutma mekanizmasını içerir.

Araştırma temel olarak, fırının sistem modellemesinin yanı sıra proses geliştirme ve üretim koşulları üzerine gerçekleştirilmiştir. Yüksek sıcaklıklı yanma fırında sıcaklık kontrolü çalışılmıştır. Malzeme ve ısılçiftler için radyasyon görüş faktörleri belirlenmiştir. Fırının altı, üstü ve yanları ile malzeme arasındaki görüş faktörleri hesaplanmış ve enerji denkliklerine yerleştirilmiştir. Aynı düzenleme, fırının alt bölümünde yer alan 3 ısılçift için de yapılmıştır. İki ifadenin birleşimi son denkliği vermiştir. Modelleme çalışmaları ve enerji denkliği simülasyonları MATLAB ile, veri analizi ve deney tasarımı çalışmaları JMP yazılımı ile gerçekleştirilmiştir

Anahtar sözcükler: LTCC, eşyanma fırını, görüş faktörü, radyasyon ısı transferi

To my family

ACKNOWLEDGEMENTS

Through almost three years, I have been a part of this excited field of research. I owe my deepest gratitude to Dr. Serkan Kıncal. Due to the fact that I have performed this study without a study group, I have always turned to him for his guidance. His unlimited vision and supporting energy led me believe in a different perspective of how a true guidance must be.

I am grateful for the endless love and unconditional support of my family. I cannot express the gratitude and appreciation I have for my no-matter-what supporting father Burhan Yücel, my mother Havva Yücel, the most open minded person on earth and my sister Sibel Ezgi Yücel, whom I would be literally lost without.

I would like to thank Hande Kılıç for simply being her and standing beside me, Yasemin Sönmez and Oya Gökdoğan Aras for being in my life in different time periods. I have enjoyed many hours of study, many hours of laughter and unconditional support from them. And a great appreciation for my lovely friends; Seçil Atalay, Tuğçe Atasoy, Didem Tosun, brilliant Emre Yılmaz, my short term lab-mate Engin Özkol and my extraordinary cousin Dr. Gonca Erbaş.

I would like to acknowledge ASELSAN for providing the experimental setup for the study and the opportunity of the internship that drawn me into this field, years before the project.

TABLE OF CONTENTS

LIST OF TABLES

TABLES

LIST OF FIGURES

FIGURES

CHAPTER 1

1. INTRODUCTION

Following thesis study is not only about the understanding and modeling a unique production line, but also introduces an important footstep for the process development concept of the circuit board manufacturing. The project is supported by ASELSAN, a company of Turkish Armed Forces Foundation, which focuses on research and development activities along with the advancement of the technology. By the support of the company, a tremendous profit was planned to be gained both on industry and on the academic field; a newly developed system to be installed, a trained personnel to continue the future plans, a viable source and an aid for similar academic studies. By this manner following study is held with joint work of the industry and of the university.

Through last decades, Low Temperature Co-fired Ceramics (LTCC) have become an attractive technology for electronic components and substrates which are compact, light, and offer high-speed and functionality for portable electronic devices such as the cellular phones, personal digital assistants (PDA) and personal computers (PC) used for wireless voice and data communication in rapidly expanding mobile network systems. For their wiring, these LTCCs use metals such as Cu, Ag, and Au with considerably small conductor loss and low electrical resistance at high frequencies, while the ceramics selected for LTCCs have lower dielectric loss than organic materials. This makes LTCCs especially suitable for the high frequency circuits required for high-speed data communications [1].

During the late 1980s, U.S. and Japanese manufacturers of computers and ceramic materials conducted extensive research and development of LTCC technology that is now crucial to present day and future communications technologies. At that time Fujitsu and IBM America produced a large, multilayer ceramic substrate (meeting Fujitsu's specifications of 254 x 254 mm with 60 layers) with a copper wire pattern for use in mainframe computers. The substrate was manufactured using very precise control of a host of manufacturing parameters [1]. This study mainly gives an account from the engineering perspective of the technology development for the mainframe computer substrate mentioned above.

The origin of multilayer ceramic substrate technology is said to lie in developments at RCA Corporation in the late 1950s, and the bases of current process technologies (green sheet fabrication technology, via forming technology, and multilayer laminate technology using the doctor blade method) were discovered at this time [2]. Afterwards, progress was made using these technologies with IBM taking the lead and the circuit board (board size: 9 cm^2, with 33 layers, and 100 flip chip bonded LSI components) for IBM's mainframe computer commercialized in the early 1980s was the inheritance [3]. Since this multilayer board was Co-fired at the high temperature of 1600°C with the alumina insulating material and conductor material (Mo, W, Mo/Mn), it is called High Temperature Co-fired Ceramic (HTCC) to distinguish it from the Low Temperature Co-fired Ceramics (LTCC) which developed later.

From the middle of the 1980s, efforts to increase the speed of mainframe computers accelerated, and as the key to increasing computer performance, further improvements were handled to multilayer ceramic substrates for high density mounting applications. By using better wiring in order to increase wiring density in circuit boards for high density mounting, the electrical resistance of the wiring increases, and conspicuous attenuation of the signal occurs. Therefore it is necessary to use materials with low electrical resistance (such as Cu, Au) for the wiring. In addition, with the flip chip method of connecting bare Large Scale Integration (LSI) components directly, poor connection of the interconnects may result if the thermal expansion of the board is not close to that of the silicon components therefore an insulating material with low thermal expansion (ceramic) is desirable. Furthermore, to achieve high speed transmission of signals, it is necessary to ensure that the ceramic has a low dielectric constant.

By the early 1990s, most Japanese and American electronics and ceramics manufacturers had developed multilayer boards that met these requirements [4]. Among them, Fujitsu and IBM were the first to succeed with commercial applications of multilayer substrates using copper wiring material and low dielectric constant ceramics [5]. From the latter half of the 1990s to the present, the focus of applications has shifted to high frequency wireless for the electronic components, modules and so on used in mobile communication devices, primarily mobile phones. For the multilayer circuit board, the low thermal expansion of ceramics was its biggest merit for the purposes of high density mounting of LSI components. However, for high frequency communications applications, its low transmission loss is its key feature, and the low dielectric loss of ceramic gives it an advantage over other materials.

As its name suggests, LTCC is ceramic co fired with metal wiring at low temperature, and its constituent materials are metal and ceramic. The typical metals for LTCCs are those with high electric conductivity and as shown in Table 1-1, they all have a low melting point close to 1000°C. Since it is necessary to co-fire the ceramic material with these metals, extreme precision is required to keep temperatures below the melting point of the metal (900 to 1000°C). In order to ensure high sintered density with low temperature firing, it is common to add amorphous glass, crystallized glass, low melting point oxides and so on to the system to enhance sintering. Besides this type, crystallized glass, composites of crystallized glass and ceramic, and liquid phase sintered ceramic are generally well known types.

The basic manufacturing process for multilayer ceramic substrates consists of several steps. Initially, the ceramic powder and organic binder are mixed to make milky slurry. The slurry is cast into tape using the doctor blade method, to obtain a raw ceramic sheet (green sheet) that before firing is flexible like paper. Vias for conduction between layers and wiring patterns are screen printed on the green sheet using conductive paste. Many layers of these printed green sheets are arranged in layers, and heat and pressure is applied to laminate them (the organic resin in the green sheets acts as glue for bonding the layers during lamination). By firing the conductor metal and ceramic together while driving off organic binder in them, a multilayer ceramic substrate can be obtained. The most important point to bear in mind in the manufacturing process is controlling variation in the dimensional precision and material quality of the finished product, and process conditions must be set so that the micro and macro structures of the work in progress are homogenous at every process step [6].

Table 1-1 - Typical material combination of LTCC and HTCC [1]

	Ceramics		Conductor	
	Material	Firing Temperature (°C)	Material	Melting Point (°C)
LTCC	Glass/Ceramic composite Crystallized Glass Crystallized glass/Ceramic composite Liquid-phase sintered ceramics	900 to 1000	Cu	1083
			Au	1063
			Ag	960
			Ag-Pd	960 to 1555
			Ag-Pt	960 to 1186
HTCC	Alumina Ceramics	1600 to 1800	Mo	2610
			W	3410
			Mo-Mn	1246 to 1500

Furthermore, the technique of laminating and co-firing more than two types of ceramic sheet with different dielectric characteristics, and the process of forming a resistor by co-firing are also well known [7].

CHAPTER 2

2. MANUFACTURING OPERATIONS

In this chapter, the product LTCC and its characteristics are briefly described along with the main units of the manufacturing line. Although the co-firing is the main focus of the study, other units are also discussed in detail.

2.1. PRODUCTION OF LTCC

Low Temperature Co-fired Ceramic manufacturing process is basically a parallel process which individual layers are to be produced separately. This single layer manufacturing is advantageous in the sense of being able to detect any sort of defects prior to firing them together. Production flow sheet is given in Figure 2-1.

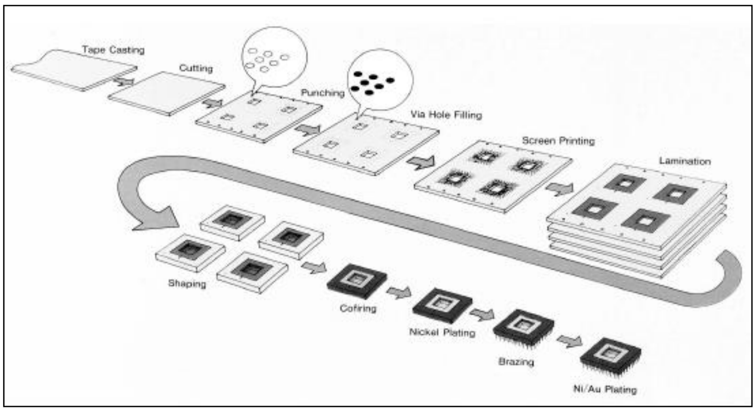

Figure 2-1 - Production Process for Multilayered Ceramics [1]

Each single layer goes through a series of operation individually -such as tape casting, via formation, filling and screen printing. Later on these green sheets stack together for lamination and co-firing oven. After these steps, substrates go through shaping and plating operations due to the demand.

The raw material for the substrate is generally made off of green sheets and ceramic materials in a polymer matrix. This material is tape cast and supplied to the manufacturing operation in the form of rolls or sheets (Figure 2-2). All depends on the application but most of the times; substrate is cut into varying shapes.

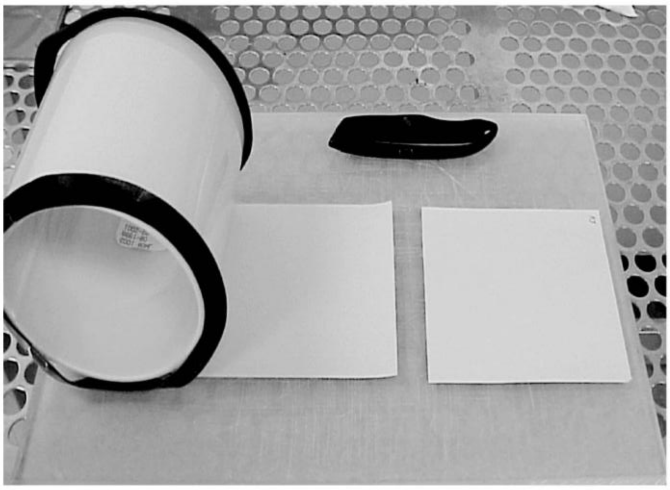

Figure 2-2 - 6 inch (150 mm) square sheet of unfired LTCC attached to a film carrier sheet [3]

Each individual layer is first processed to form holes or vias that will act as connectors between the subsequent layers. These holes may be introduced onto the sheets by mechanical punching or laser-cutting. Next these holes are filled with conductive ink. After this via filling process, each layer is subjected to a screen printing process by which the electrical components are transferred onto the substrate. After the successful generation of the individual layers, they are aligned and stacked onto each other. The process of lamination bonds the polymer components in the tape layers together, forming a semi-permanent bond between the layers. Isostatic lamination is generally the process of choice here although it is possible to achieve the same effect with rollers – with lamination providing superior uniformity. The material at this point is still a flexible sheet. This flexible sheet becomes the hardened final product by a two-step firing process. The first step, carried out under relatively lower temperatures of 300-400^{o}C burns off the polymeric matrix, leaving behind the ceramic and the interconnect material. The final and relatively high temperature (800 – 900^{o}C) firing step, sinters the ceramic and the interconnect material bringing it final electrical properties to the desired levels while forming a perfectly sealed end product

In the scope of this study, three main operations are focused on. Among them, co-firing oven applications are detailed.

2.1.1. Tape Casting

Although the tape is purchased in ready form from a supplier, it is necessary to understand the underlying manufacturing processes in order to develop the correct handling procedures and appreciate the significance of the impact of the processing steps on the tape properties. The tape used in LTCC manufacturing (or multilayer ceramic manufacturing in general) involves the casting of a thin ceramic-organic layer into a flexible sheet. The key parameters involved in this casting process are the composition, selection of the powders, types of polymers and additives, mixing and milling and finally casting. Of course as for any other manufacturing operation inspection and quality control as well as tape handling and storage significantly impacts the final product quality and repeatability.

The resulting tape generally contains a mixture of crystalline and non-crystalline phases, depending on the types of materials used, the particular composition and the specific operating conditions. Controlled purity, homogeneity, surface and bulk chemistry, particle size distribution and surface area morphology are all critical parameters that need to be accurately monitored and controlled during the tape casting process.

In tape casting of commercial quantities – the process involves large volumes of ceramic powders, large ball mills and multiple banks of tape casters. The process begins with the loading of the ceramic powders, solvent and dispersant into the ball mill. The dispersant in this step prevents the agglomeration of the powders and the stabilization of the de-agglomerated particles that are produced during the milling process. This mixture is generally mixed for a period of 12-24 hours until the desired degree of dispersion is achieved as monitored by the viscosity.

2.1.2. Tape Handling

Due to their fragile nature, it is important to be aware of special handling requirements while the tape is in the green or unfired state. The films are also somewhat flexible through the use of the polymer matrix. A further complication of the polymeric matrix is that it can absorb moisture in the unfired state, expanding and contracting as a function of environmental variables such as temperature and humidity. The five areas of critical control are

1. Humidity control
2. Temperature control
3. Particulate contamination
4. Static control

5. Physical support of fragile green tape layers during handling and manufacturing [1].

Particulate control is maintained by traditional clean-room techniques such as controlled access with proper clothing, laminar air flow and air filtration with the level of cleanliness required driven by the minimum feature size on the product. Higher levels of cleanliness come at a cost but would be an unavoidable consequence based on the minimum feature size.

Temperature and humidity control is somewhat a more contained problem to solve in that its effects are not immediate. That is the environment control may be more robust process then particulate control in the sense that it can tolerate variations during the limited time it takes to prepare the individual layers – whereas even momentary exposure to high levels of particulate contamination will cause product failure. However control and stability of the storage environment is the key as the material is subject to these conditions for long time periods.

Static control is also important even though the tape materials themselves are not static sensitive – unlike many semiconductor devices. Static however will cause undesired bonding of the individual tape layers and the plastic carrier layers. Although it is generally achieved through humidity control, ionizing equipment and proper equipment grounding may be required at times [1].

Since the layers are fragile and flexible in the green state and most of the processing operations take place under this condition. This is a unique requirement to layered ceramics processing. Two preferred methods to deal with this issue is either the use of plastic backing tape or metal frames. Both methods not only provide adequate physical support to the green tape but also provide a mechanism to prevent expansion and contraction during the manufacturing process.

The main difference between plastic backing and metal frames is that, the use of metal plates requires additional processing steps of bonding and separation of the green tape to and from the metal frame. In the use of plastic backing, the green tape simply sits on top of a plastic film to provide physical support while the friction on the surface between the two layers prevents the expansion and contraction of the film to a large extent [1].

The metal frames constrain the green tape by the edges and provide for superior protection against expansion and contraction. The films can be much more easily handled by the edges of the frame. Furthermore the frames may contain alignment marks for the subsequent processing steps. This alignment in the case of plastic backing material is achieved by the drilling of alignment holes onto the tape itself. Of course optical alignment to alignment marks printed on the tape can be used in either case to increase the reliability of alignment.

In the case of metal frames, loss of the edge of the tape is an unavoidable consequence of the nature of the process. There is also time lost to the additional steps. For plastic backing, loss of edge material is also present when holes are used for alignment but with optical alignment features, there is the possibility of eliminating loss of edge material.

Obviously the specific choice of handling will be driven by the competing requirements of process quality and cost reduction objectives [4].

2.1.3. Via and Cavity Formation

Once each tape has been cut to the appropriate size, the next step is the creation of holes through the vertical axis to allow for electrical connections between the subsequent layers and/or the generation of cavities or channels for unique electrical or mechanical features such as embedding integrated circuits such that in the final product the IC is flush with the surface of the top layer. Embedding external components within the device has both mechanical and electrical advantages compared to placing it on the very top layer.

The two predominant methods off forming holes or cavities are laser cutting and mechanical punching. Mechanical punching tends to be more preferred in via formation whereas laser cutting has an obvious edge in forming channels or cavities as it can be programmed to cut arbitrary shapes. These two methods will now be described in further detail.

2.1.4. Laser Processing

In laser processing, the relative location of the green tape and a laser source is changed where the movement and the exposure to the laser through a shutter mechanism is controlled to transfer the desired pattern into the sheet. The movement can be done by moving the sheet relative to a fixed laser source or movement of the laser beam can be modulated through the use of optics. The laser source itself is stationary due to the difficulty in moving such a large system component.

The laser essentially ablates the exposed material, forming the desired cavity or hole. The main benefit of the laser processing is that it can carve out very complex shapes with rounded or curved edges. To achieve the same effect by mechanical punching, multiple punching operations need to be carried out on a CNC (computer numerical control) puncher until the edges of the desired shape are completely covered with holes such that it can be removed. This is a time consuming process.

The laser processing is fundamentally deficient in individual via formation for two main reasons. First it ablates out material which gets re-distributed on the surface as defects. The edges of the laser produced via tend to be non-uniform and also there is partial firing of the material in the immediate vicinity of the via as exposure to the laser causes local heating effects.

2.1.5. Mechanical Punching

The mechanical punching process, as the name implies, is the process of mechanically removing the green sheet material where the via needs to be through the use of mechanical force – identical in principle to the punchers used to make holes in paper.

The advantage of mechanical punching over laser cutting in via formation is illustrated in Figure 2-3 where the top 3 SEM images show holes cut by mechanical punchers and the lower images show equivalent vias created by laser processing. The quality of the mechanically punched holes will depend on the sharpness of the puncher – which generally gets dull with usage. This will cause imperfect holes or chips around the hole but this is easily overcome by properly monitoring the age of the puncher and changing it at regular intervals just like any other consumable in a manufacturing process.

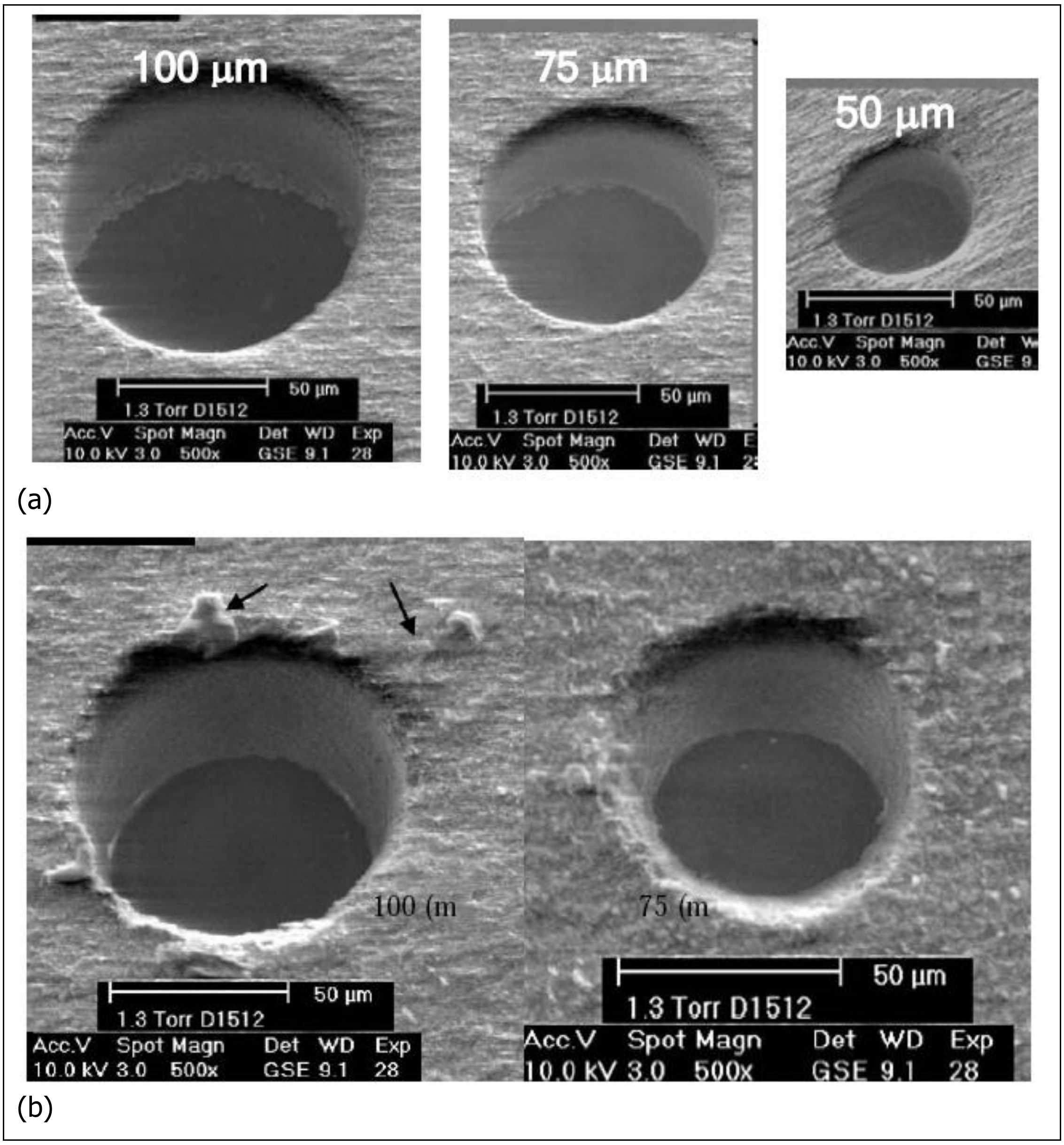

Figure 2-3 - Comparison of (a) Mechanically Punched and (b) Laser Cut Vias [4]

Mechanical punchers can be sub-classified into hard tooling and soft tooling. The tooling here refers to the hole configuration. Hard tooling refers to the mode of operation where multiple holes are punched out in a single action because the tool consists of a dedicated die. This kind of a puncher has a very high throughput but is limited in terms of flexibility as a new die is required for each different layer that needs to be punched. Soft tooling, on the other hand, operates with a single puncher that is located according to the pattern that needs to be transferred to the green sheet. Therefore multiple punches are required to punch in the pattern for the entire layer however multiple layers can be processed using the same piece of hardware. Hard tooling is more suitable for volume production and soft tooling is better suited for pilot scale or prototype production.

2.1.6. Via Fill

This next operation in the sequence is required to enable the holes to act as connectors between the multiple layers. The holes created need to be filled properly with a conductive ink so that they can server their purpose. The process is done by stencil/screen printing or bladder filling. Care must be taken in designing the process as the ink used in this process is more viscous than that used for screen printing on a flat surface. This is because the ink needs to fill in a hole of appreciable diameter and not sag or run prior to drying. Upon firing and loss of the solvent, the hole must remain completely filled in order to ensure a low resistance interconnection.

Stencil or screen printing processes are nearly identical. Both use a shear force created by the movement of a squeegee through a metal mask in stencil printing and a mesh for the screen printing process. The main difference is that in the case of stencil printing, the metal mask is in intimate contact with the green tape, providing a zero snap off distance [1].

Bladder filling is similar to the stencil printing in the sense that it also passes the ink through a metal mask. However the process is fundamentally different in the way it forces the ink through the mask openings and into the holes – it uses a pressurized bladder to apply force to the ink spread over the stencil.

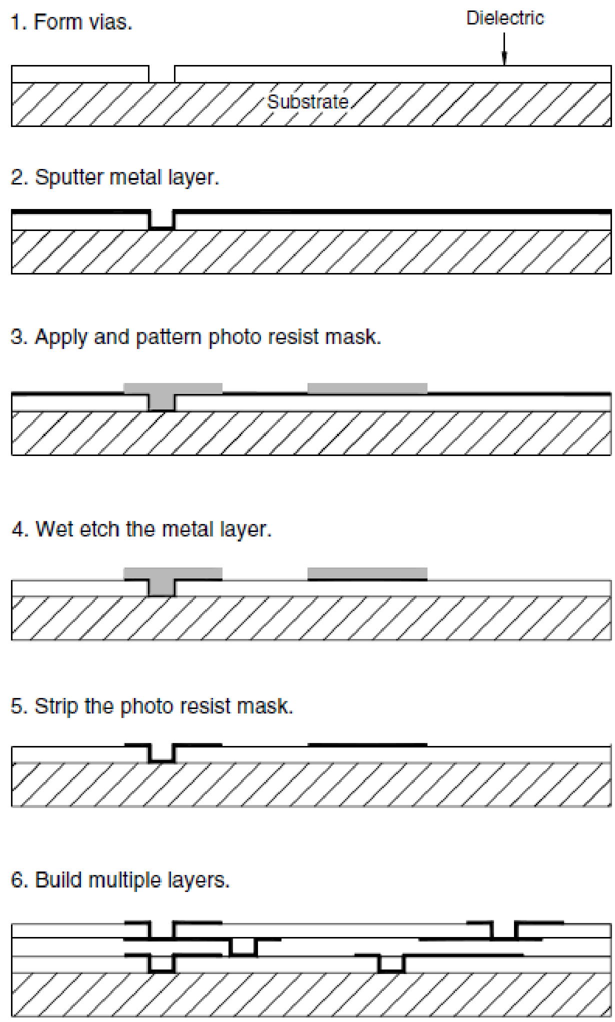

Figure 2-4 - Sputtering Metallization: Wet-Etch Process [1]

In any case, the success of via filling process is judged by the degree of filling. Figure 2-5 illustrates 3 different cases where a proper fill is compared to overfill and misaligned fill. Overfill will cause smearing of the conductive paste around via, possibly causing shorts between adjacent lines.

Under fill would cause improper contact resistance between the layers since the entire area designed for the connection would not be filled with the ink.

Misaligned holes will cause both smearing in undesired locations as well as inadequate contact between adjacent sheet layers.

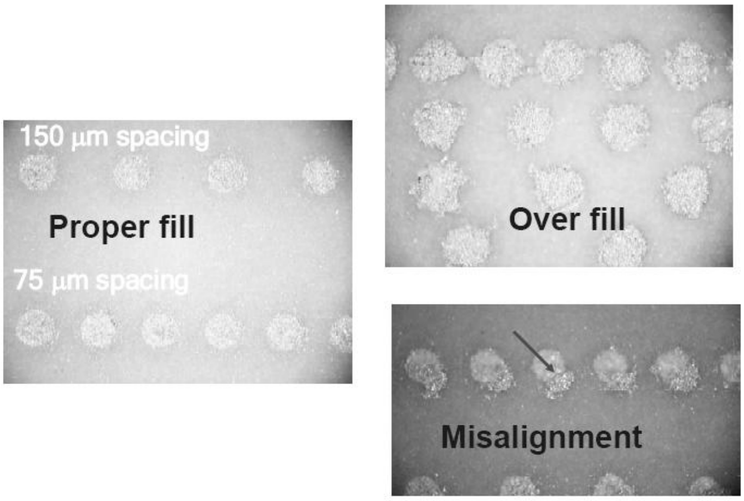

Figure 2-5 - Via Filling Process Success Criteria [1]

2.1.7. Screen Printing

This is perhaps the most challenging and difficult to control and maintain steps in LTCC manufacturing. This is essentially where interconnects are defined on the surface of the individual layers. Screen printing techniques draw upon 50+ years of experience of printing onto pre-fired substrates such as alumina – with some unique modification required in substrate handling such that the fragile green sheets can be accommodated.

The basic steps and critical components of the screen printing process is shown in Figure 2-6. The substrate must be held in with the right amount of force such that it does not move while the pattern is being transferred and yet gentle enough that it does not break the fragile green tape. This is usually achieved by a porous stone chuck which uses many small holes to apply vacuum to the green tape and distribute the force very uniformly across the surface.

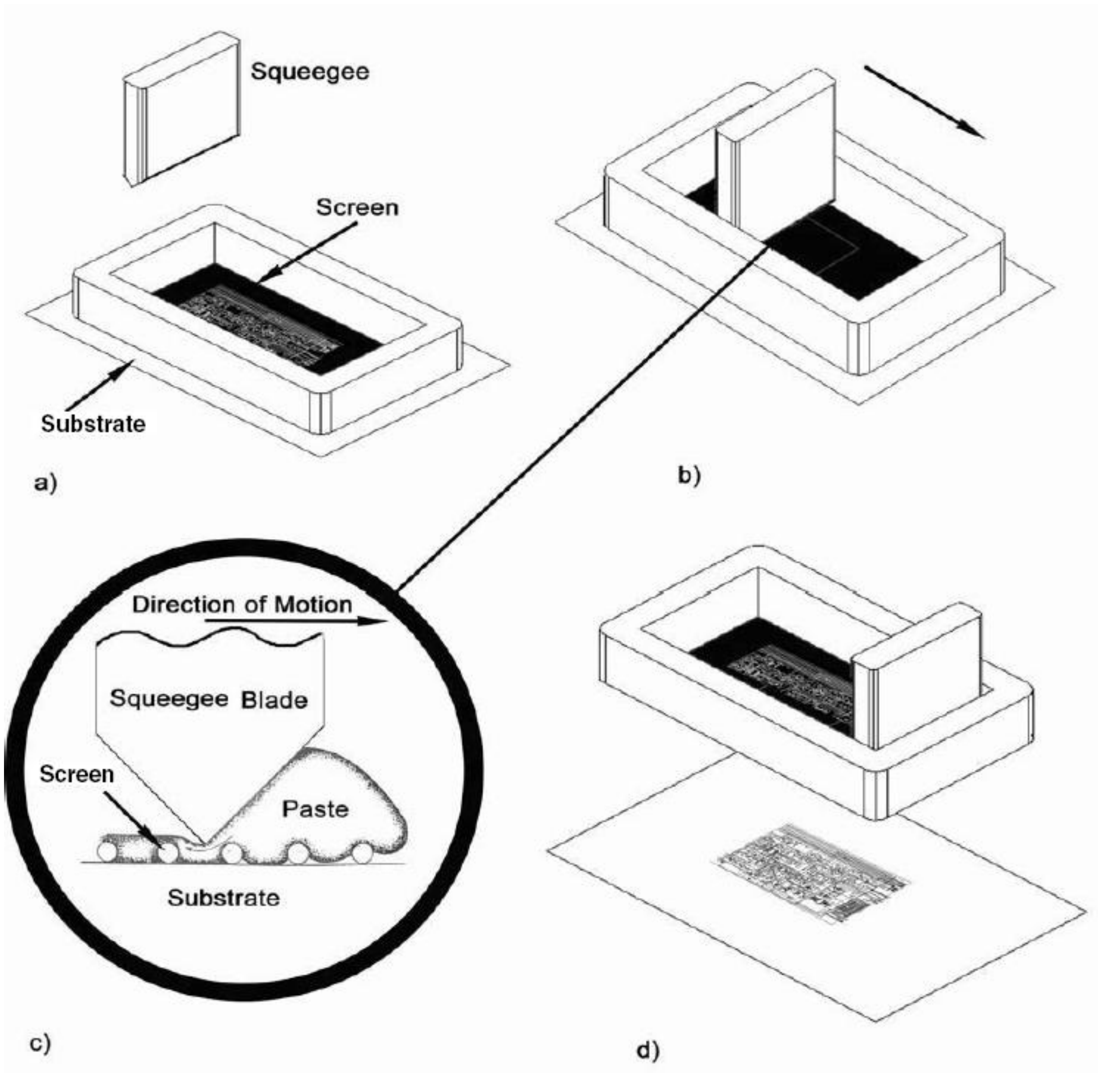

Figure 2-6 - Steps in the Screen Printing Process [1]

The screen is constructed from a thin stainless steel wires mesh. The diameter of the wires usually varies between 0.9 and 1.2 mm. Around 200 to 400 wires per inch are used to form the mesh, with 325 being a more common choice. The mesh may be at 45° or 90° angles with respect to the movement direction of the squeegee. Under identical conditions, a 45° mesh is going to provide superior line quality since it is easier to push the ink through the openings. In general, higher mesh counts and thinner wires result in finer resolution. The screen is held in place by a frame.

The squeegee is simply a piece of rubber or plastic that provides shear force to the ink as it moves horizontally across the screen while applying pressure perpendicular to the screen. This shear force causes the viscosity of the non-Newtonian ink to decrease and easily flow through the openings in the mesh – transferring the image on the stencil onto the substrate. Once the sheer force is gone, viscosity increases again, ensuring that the ink on the surface does not flow freely but keeps its pre-defined shape. During this process, the mesh stays slightly above the substrate by an amount called the snap-off distance – this causes minimal contact with the substrate, the screen only briefly contacts the substrate where the ink is being transferred thus avoiding smearing while the screen is being lifted away from the substrate at the end of the process.

The critical variables that must be tuned and/or maintained for screen printing are

1. Screen to substrate distance – snap off distance
2. Squeegee down-force pressure
3. Squeegee horizontal movement speed
4. Screen to substrate parallelism – must be parallel
5. Screen properties such as mesh size, angle of attack and wire diameter

Where the particular values of these parameters are largely dictated by the specific paste/ink being used as each ink or paste has its own material properties.

After the processes, it follows the inspection stage – which may be dispersed through critical operations of the process – refers to optical inspection of individual layers to ensure quality prior to stacking and lamination. Depending on the degree of resolution required and throughput desires – these steps might be as simple as an operator manually inspecting green sheets under a microscope to fully automated inspection systems with optical alignment and automatic defect identification.

Electrical testing of the finished product is also possible prior to post processing steps for early detection of possible problems.

2.1.8. Film Stacking

This is the final step in the process where the green sheets will exist by themselves for the last time. Here the individual sheets are aligned and placed on top of each other. Similar to the inspection process, this operation may be fully automated with optical alignment features or completely manual through the use of alignment holes. The accuracy and throughput requirements dictate what type of specific strategy to pick as highly automated and accurate systems will come with an associated price tag.

2.1.9. Lamination

Simply overlaying individual layers does not provide adequate levels of surface to surface contact required during the co-firing process. Lamination ensures this surface to surface contact by applying pressure to the stacked layers. Once the stacked films are laminated – it is very difficult to remove them. The particular process conditions applied do depend on the specific materials used in production but values of 3000 psi, 70°C and 10 min are pretty typical settings [7].

There are two types of lamination processes – distinguished by the way they apply the pressure. These are isostatic lamination and uniaxial lamination. Uniaxial lamination uses two heated, parallel plates. The stack is sandwiched in between the heated plates. This process has the advantages of speed and simplicity of equipment but the disadvantage is maintaining a uniform pressure across the entire surface of the plate. A non-uniform pressure applied will result in variability in the density of the material which will eventually cause non-uniform shrinkage during co-firing and possible undesired results.

Isostatic lamination uses a water filled pressure vessel to ensure pressure uniformity across the entire substrate. The substrate must be sealed in some kind of water tight packaging prior to being immersed into the pressure vessel to avoid the unfired ceramic coming into contact with water. Multiple stacks may be laminated in one batch operation to increase throughput – limited by the size of the pressure vessel. Metal backing and cover plates may be used if desired and would help to improve pressure uniformity. Disadvantages of the isostatic lamination process over uniaxial lamination are lower throughput and more complicated equipment [7].

2.1.10. Co-firing Oven

After the individual films have been laminated, they need to be fired to create the dense ceramic material desired for operation. This process takes place in a batch mode in box furnaces for low volume production or continuous belt operation for higher throughput applications. In either case, the substrate must be placed on setters as many of the materials will conform to the surface they are sitting on during the firing process. The setter must be very clean as irregularities on their surface will directly transfer to the substrate. The choice of setter material is also critical such that heat must be uniformly transferred across the surface area and adhesion to the setter must be avoided.

The box furnace operation has the advantages of better control of temperature profiles and smaller, cheaper equipment. However the box furnace is inherently very restrictive in terms of throughput. Larger and larger furnaces may not be practical because maintaining temperature uniformity on identical substrates placed in different locations would get more difficult as multiple substrates are loaded to increase throughput.

In Figure 2-7, there is a typical firing sequence for a LTCC stack. The ramp rates are critical in maintaining spatial temperature uniformity across the substrate. The first plateau in the process, often referred to as the Ash step, is where the volatile components are being driven off the substrate – these include the solvents in the green tape and the various pastes and inks as well as the polymer matrix itself. What should remain pose the ash step is the ceramic material only along with the conductor materials of the inks and pastes.

The substrate at this point is extremely fragile since the polymeric material that was giving it the flexibility has been removed. This material is then heated to higher temperature and held for a certain period of time to allow for the ceramic material to pack closely and sinter forming the mechanically very strong final product that also provides the desired electrical properties [7].

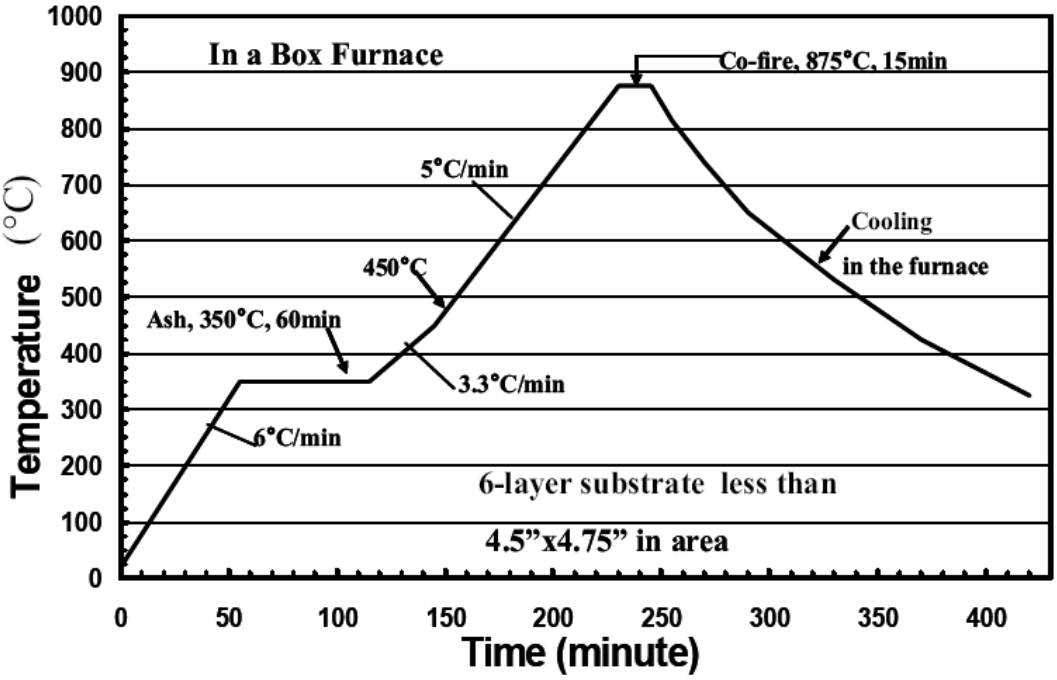

Figure 2-7 - A Typical Firing Sequence for an LTCC Stack [7]

What is of importance during the co-firing process is maintaining a uniform temperature gradient through the entire cycle, making sure the ash and sinter dwell times are long enough to drive all transformations to completion and thereby controlling the amount of shrinkage that happens during the entire cycle. This is critical since variable shrinkage will cause the final dimensions to be different (assuming uniform incoming patter quality) causing eventual differences in electrical properties.

2.2. POST PROCESSING

Once the co-fired stack is manufactured, additional processing steps might need to be carried out depending on the specifics of the application. External connections may need to be made or patterns may need to be printed on the top or bottom surface. If the final design contains embedded IC’s, these must be placed inside the appropriate cavity carved into the stack. These operations will be left outside the scope of this project and report due to the inherent variability in their combination.

2.3. CURRENT STUDIES OF LTCC

The material on focus LTCC does not have a large number of producers. One of the most yielding manufacturers is DuPont. They have a supply of final product LTCC, other than different sources of green tapes for co-fired and post-fired. Co-fired materials have gold and silver/palladium conductors, both externally and internally placed. Green tape post-fired materials are produced with again silver and gold conductors, with glass and glass free encapsulates and post-fired resistors.

Also LTCC is a strong entry for the various production processes. One of the recent studies of Shina et al [12] deals with the production of micro-fuel processor which integrates steam reformer and partial oxidation reactor using LTCCs. Park et al [13] studied a fully integrated micro-channel fuel processor system consisting of vaporizer, steam reformer, heat exchanger and preferential CO oxidation which also developed using LTCCs. The performance is measured at varying conditions such as ratio of the feed flow rate, ratio of H_2O/CH_3OH, CO clean-up system, and operating temperature of the reactor [13].

There are several experimental studies of the molding types for the material in the point of view of attachment LTCC based micro-electromechanical systems (MEMS) or micro system technology (MST) devices. Khanna et al dealt with the test structures which are fabricated by molding single layer green tapes into cylindrical form in order to investigate the penetration of the cracks and the bonding of LTCC modules to metal parts with a dissimilar coefficient of thermal expansion [14].

CHAPTER 3

3. MODELING

This study takes a 3 prong approach to the characterization of the dynamics of the firing oven for the purpose of understanding the mechanisms leading to temperature non-uniformities on the substrate. We begin with a comprehensive model built using commercial finite element solver software, namely ANSYS 13 of ANSYS Inc. This model is going to be described in the next section, 3.1.

Although having the capability of accurately describing and modeling the physical system, the approach of using commercial finite element solvers is hindered by the fact that the solution of the modeling equations take a long time, making it impossible to be used for real time control applications that require faster than real time solution to these modeling equations. Furthermore the results of such commercial packages cannot be easily incorporated into actual control applications due to the high cost of license for such software packages.

This is where the second approach of building a simplified dynamic model becomes relevant. In this case, we use a simplified approach to modeling the dynamics using MATLAB of MathWORKS in order to implement a real time solution to the temperature dynamics inside the oven that can effortlessly be incorporated into actual control applications. The simplifications that enable the real time solution capability for this second modeling approach are derived from and justified by the more complex modeling approach of the finite element solver. This is going to be the topic of section 3.2.

Finally, no modeling effort is complete unless they are confirmed by actual experimental results. In fact even the most complex modeling approach will require some level of tuning of the physical constants that are involved in the system behavior which cannot be measured accurately. The experimental plan based on fundamental concepts of experimental design will be outlined in section 3.3.

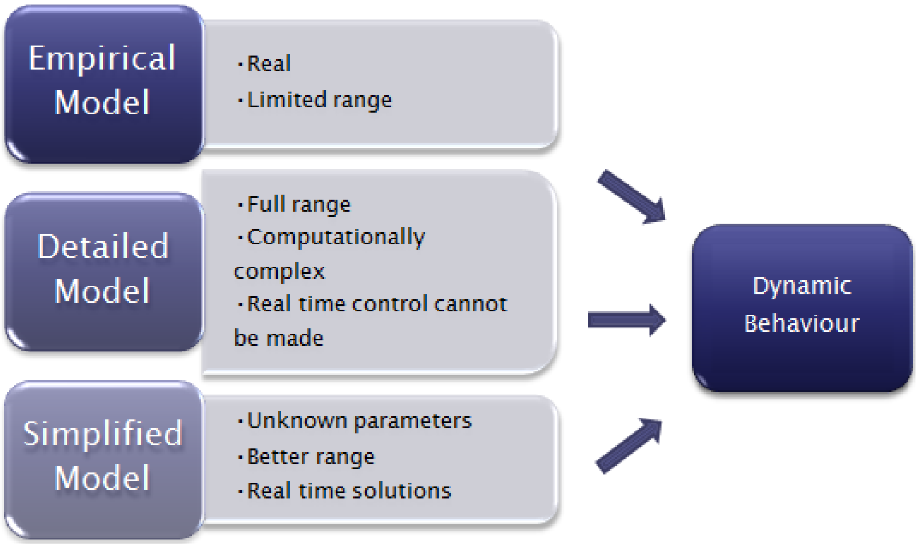

Figure 3-1 – Flow Chart for the Dynamic Behaviour Solution

3.1. Finite Element Solver Model – Complete Dynamics

The finite element solver package provides a solution to the equations of conservation of energy once the proper geometry, material system are defined along with the appropriate boundary conditions. The details of the equations will not be listed here as they are the same ones upon which the simplified model, described in section 3.2, is based. Instead a brief outline of the model built into ANSYS will be described here. The detailed report as produced by ANSYS is included as part of Appendix A.

The geometry of the oven is defined into ANSYS using the graphical user interface with all dimensions and material descriptions based on the system's user manual. Figure 3-2 shows a snapshot of the very outside of the model geometry – which shows the entire oven contents (quartz tube, filaments, substrate and thermocouples) enclosed inside a cylinder of insulation. Figure 3-3 is showing the system with part of the insulation hidden from view in order to reveal the quartz tube that houses the heated enclosure. Figure 3-4 further hides parts of the quartz tube so that the inside of the oven can be seen clearly. This figure shows the 12 main filaments situated around the substrate, the front and back filaments installed for better temperature uniformity and the substrate. What is not very clearly visible here are the thermocouple beads as they are very small. These are located right under the substrate and at the front and the back of the oven at the same vertical position.

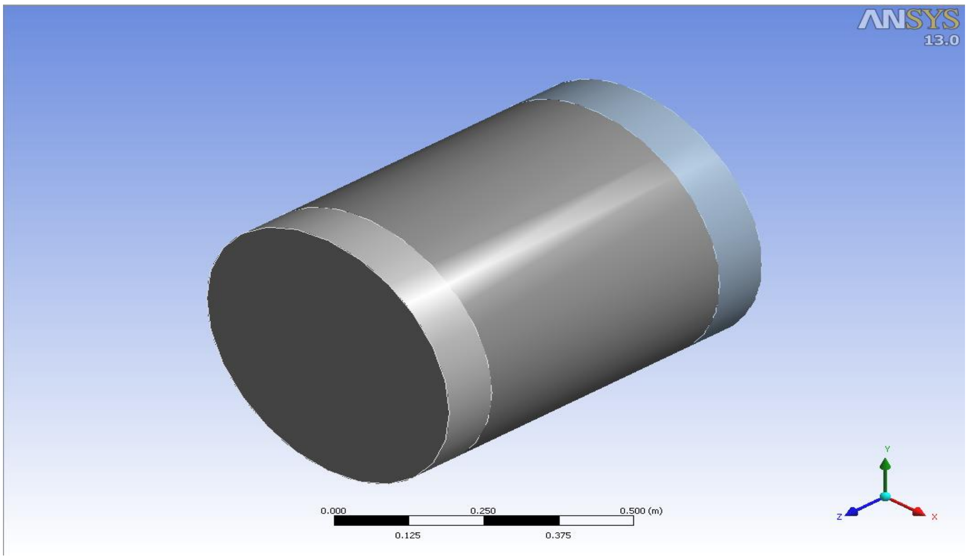

Figure 3-2 - The Oven Enclosed Inside The Insulator

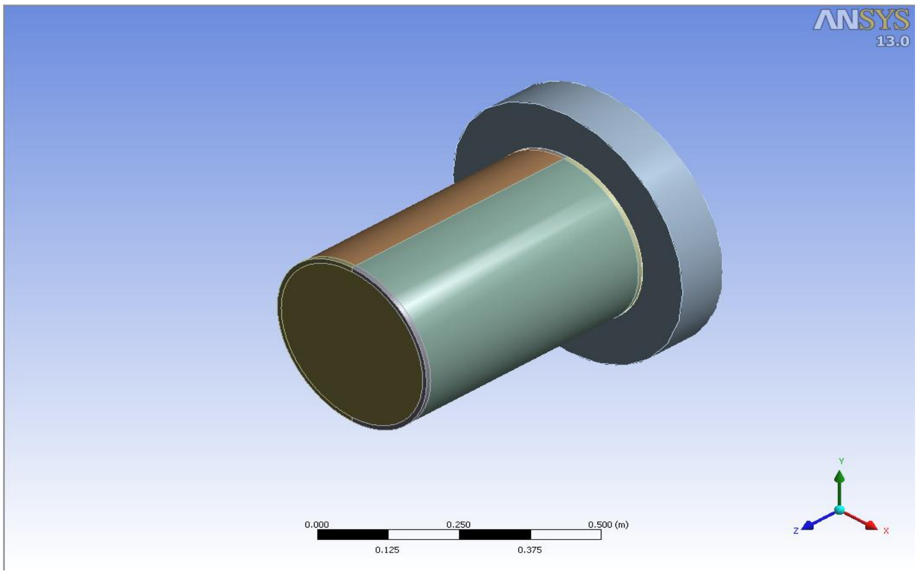

Figure 3-3 - The Insulator Peeled Back At The Front And On The Sides

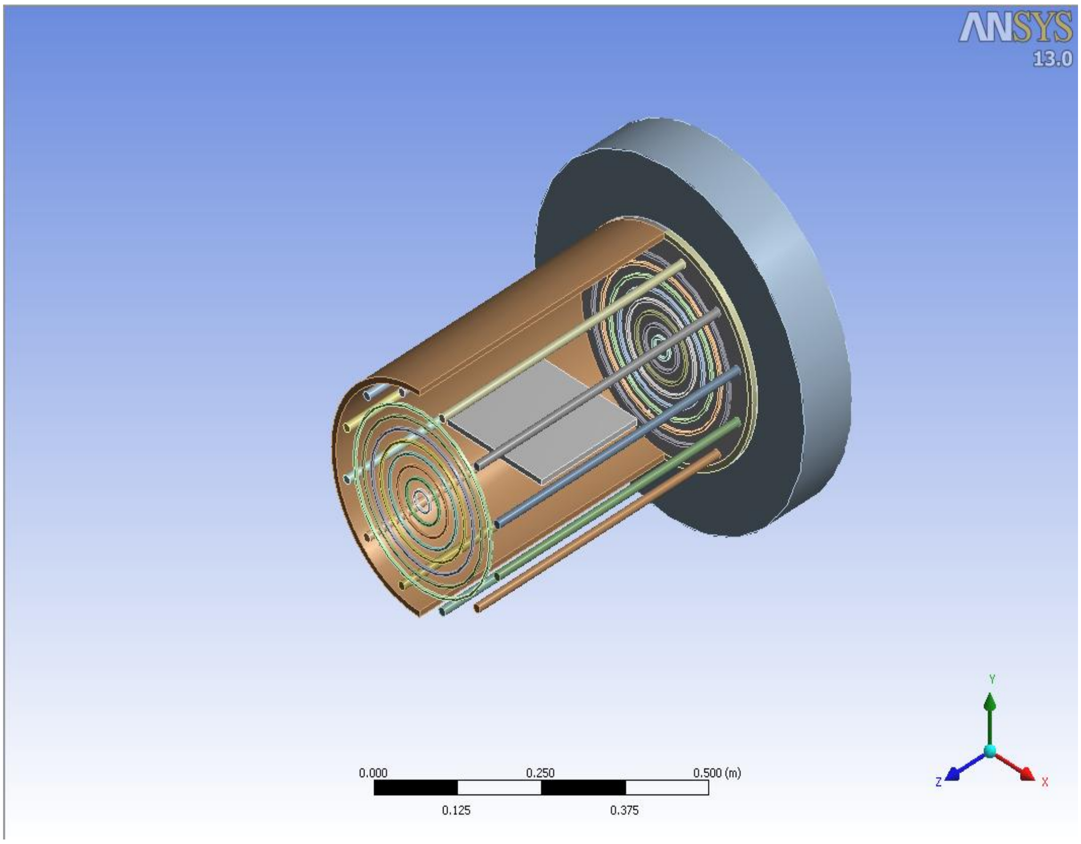

Figure 3-4 - Parts of the Quartz Tube Hidden from View to Reveal the Heated Enclosure

Once the geometry is defined, the mesh needs to be defined over which the equations of energy conservation will be solved. The default mesh options of the software create too many nodes and elements – which introduces an unnecessary amount of computational burden.

The desired level of accuracy can be achieved using the optimized mesh as shown in Figure 3-5. Here several simplifications are made. For instance since the filaments are made of a highly thermally conductive material, the temperature distribution within the filament will be very small thus no elements need to be defined in the radial dimension. This approach reduces the number of elements to approximately 2500 as compared to the approximately 37000 by the default approach. A sensitivity analysis will be summarized in the results section that justifies this reduction of elements.

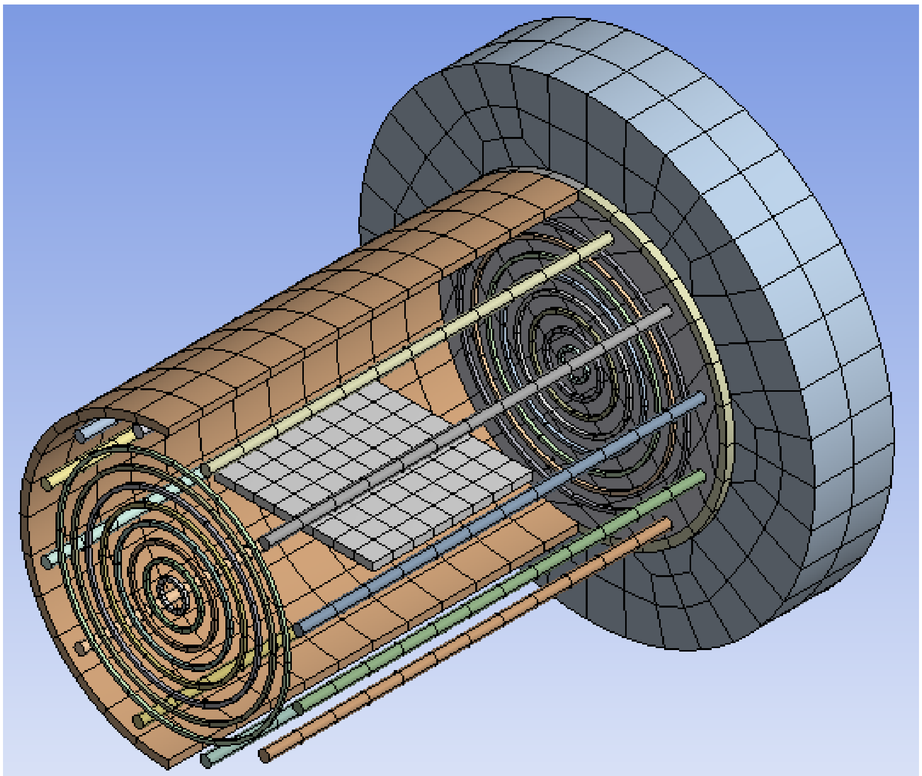

Figure 3-5 - The Meshed Geometry

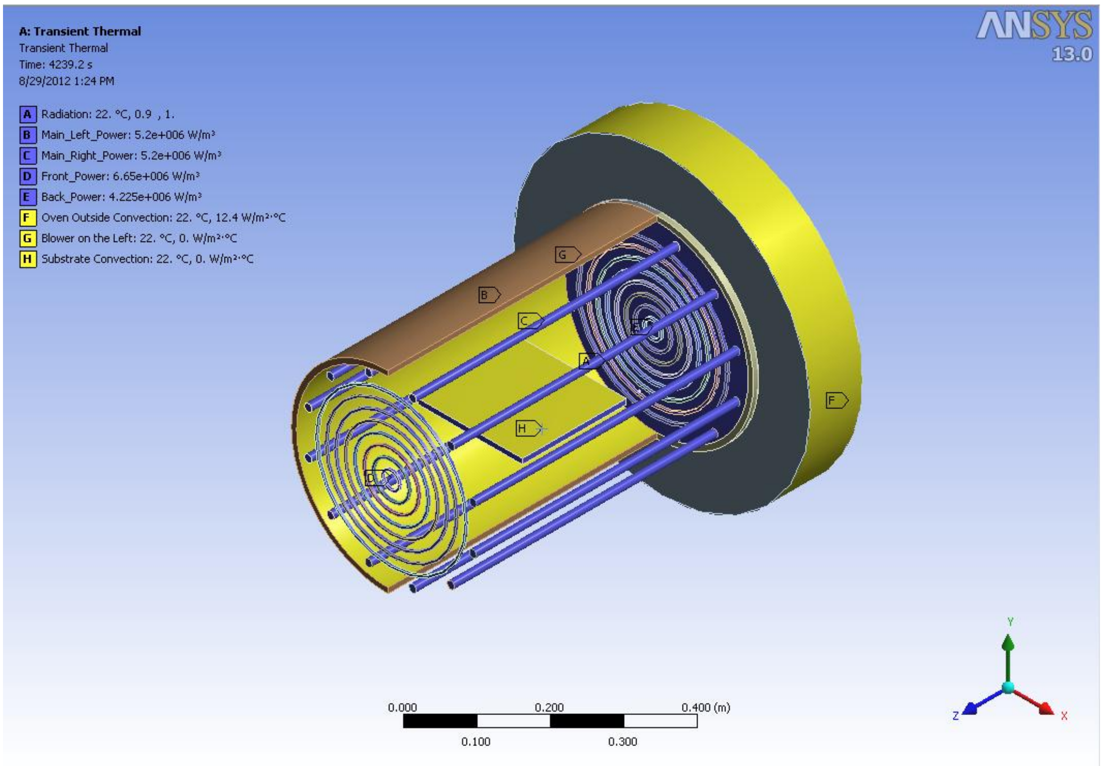

Figure 3-6 - The Boundary Conditions

The final step in defining the model is the specification of appropriate boundary conditions for the entire geometry. Starting from the very outside, the exposed surfaces of the insulation are in contact with stagnant room air – for which convective heat transfer for a horizontal cylinder with stagnant air is appropriate. So the convective heat transfer coefficient as a function of temperature is defined. The filaments are resistive heating elements rated at 1600W each. This is converted to an internal rate of heat generation through the volume of the filaments and defined independently for each filament. The power outputs of the filaments are set-up to be defined as time dependent functions.

Within the oven enclosure, the important mode of heat transfer is radiation and this is defined by including the interior surface of the quartz tube, the filaments and the substrate which are enclosed inside the quartz tube. The solids that are in thermal contact with each other exchange energy through conduction. Conductive heat transfer also takes place within each solid material. Two more modes of convection are defined. First one is over the substrate to simulate the possibility of blowing nitrogen over the substrate during the soak cycle. The other one simulates the behavior of the fan that is turned on during the cooling cycle to be able to control the rate of cooling. This is defined only on the left side of the oven as that is the way the oven is configured. Once the fan is turned on, the convection is turned on by proportionally increasing the convective heat transfer coefficient as a function of blower speed. This coefficient is defined as zero otherwise when the blower is switched off.

3.2. MATLAB MODEL – SIMPLIFIED DYNAMICS

In this section, energy balances were conducted including conduction, convection and radiation heat transfer mechanisms. For the substrate finite difference method was applied. Among the heat transfer mechanisms, radiative term consists of view factor coefficients which were derived for substrate and thermocouples.

3.2.1. Conservation of Energy

Governing temperature distribution of the substrate is constructed as follows:

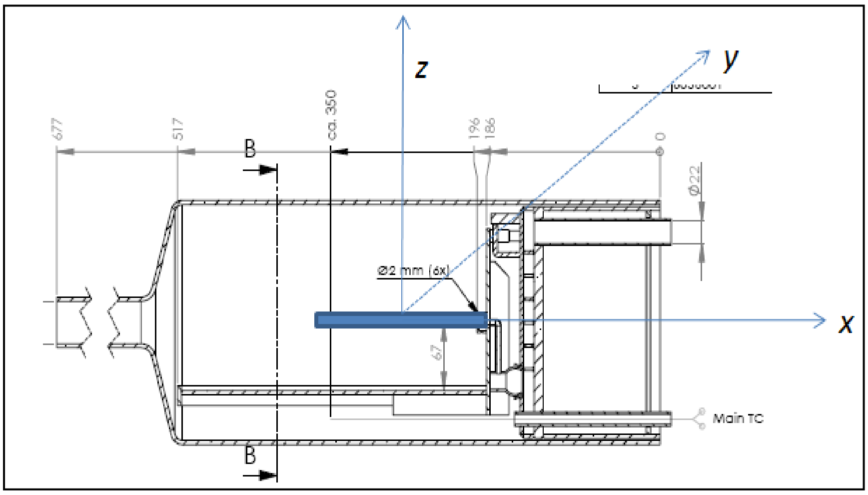

Figure 3-7 - Placement in the Co-firing Oven

$$(Conduction\ in\ x - direction)_{in} - (Conduction\ in\ x - direction)_{out} + (Conduction\ in\ y - direction)_{in} - (Conduction\ in\ y - direction)_{out} + (Radiation\ on\ top\&bottom)_{in} - (Radiation\ on\ top\&bottom)_{out} + (Convection\ on\ top)_{in} - (Convection\ on\ top)_{out} = Accumulation \quad (3.1)$$

$$\left[q_x|_x \Delta y \Delta z \Delta t - q_x|_{x+\Delta x} \Delta y \Delta z \Delta t + q_y|_y \Delta x \Delta z \Delta t - q_y|_{y+\Delta y} \Delta x \Delta z \Delta t\right]_{cond} + [q_z|_z \Delta x \Delta y \Delta t - q_z|_{z+\Delta z} \Delta x \Delta y \Delta t]_{conv} + [q_z|_z \Delta x \Delta y \Delta t - q_z|_{z+\Delta z} \Delta x \Delta y \Delta t]_{radn} = \Delta x \Delta y \Delta z\left[\rho C_p (T|_{t+\Delta t} - T|_t)\right] \quad (3.2)$$

Dividing both sides with $(\Delta x \Delta y \Delta z)\Delta t$;

$$\left[\frac{q_x|_x - q_x|_{x+\Delta x}}{\Delta x} + \frac{q_y|_y - q_y|_{y+\Delta y}}{\Delta y}\right]_{cond} + \left[\frac{q_z|_z - q_z|_{z+\Delta z}}{\Delta z}\right]_{conv} + \left[\frac{q_z|_z - q_z|_{z+\Delta z}}{\Delta z}\right]_{radn} = \rho C_p \left[\frac{T|_{t+\Delta t} - T|_t}{\Delta t}\right] \quad (3.3)$$

Taking the limit as $\Delta x \to 0, \Delta y \to 0, \Delta z \to 0 \; and \; \Delta t \to 0$;

$$\left[-\frac{\partial}{\partial x}(q_x) - \frac{\partial}{\partial y}(q_y)\right]_{cond} - \left[\frac{\partial}{\partial z}(q_z)\right]_{conv} - \left[\frac{\partial}{\partial z}(q_z)\right]_{radn} = \frac{\partial}{\partial t}(\rho C_p T) \quad (3.4)$$

Where conduction heat transfer terms are represented with;

$$q_x = -kA\frac{\partial T}{\partial x} \quad (3.5a)$$

$$q_y = -kA\frac{\partial T}{\partial y} \quad (3.5b)$$

Convection heat transfer term is represented with;

$$[q_z]_{conv} = hA(T - T_a) \quad (3.6)$$

Radiation heat transfer term is represented with;

$$[q_z]_{radn} = AF_{ij}\left(E_{b,i} - E_{b,j}\right) = AF_{ij}\sigma(T^4 - T_s^4) \quad (3.7)$$

Combining these equations;

$$-\frac{\partial}{\partial x}\left[-kA\frac{\partial T}{\partial x}\right] - \frac{\partial}{\partial y}\left[-kA\frac{\partial T}{\partial y}\right] - \frac{\partial}{\partial z}[hA(T - T_a)] - \frac{\partial}{\partial z}\left[F_{ij}A\sigma(T^4 - T_s^4)\right] = \frac{\partial}{\partial t}(\rho C_p T) \quad (3.8)$$

The terms k, ρ, C_p, σ are assumed to be constant;

$$k\left[\frac{\partial^2 T}{\partial x^2}+\frac{\partial^2 T}{\partial y^2}\right]-h\frac{\partial}{\partial z}(T-T_a)-F_{ij}\sigma\frac{\partial}{\partial z}(T^4-T_s^4)=\rho C_p\frac{\partial T}{\partial t} \tag{3.9}$$

$$q|_x\Delta yb - q|_{x+\Delta x}\Delta yb + q|_{y+\Delta y}\Delta xb - q|_y\Delta xb - 2\Delta x\Delta y\sigma(\epsilon T^4-\alpha T_s^4)F_{ij} - \Delta x\Delta yh(T-T_a) = \Delta y\Delta xbC_p\rho\frac{\Delta T}{\Delta t} \tag{3.10}$$

With this basic description and the simplifying assumptions, the generic equation governing the temperature distribution within the substrate is a partial differential equation of the form

$$V\rho C_p\frac{\partial T}{\partial t}=-k\frac{\partial^2 T}{\partial x^2}-k\frac{\partial^2 T}{\partial y^2}+\dot{Q}_{radiation}+\dot{Q}_{convection} \tag{3.11}$$

where the assumptions of temperature and position independence of physical parameters has allowed them to be taken out of the partial derivative terms. The model also ignores the possibility of heat generation or consumption while the green sheet material undergoes a phase change in the firing process. The radiation term can be expressed as:

$$\dot{Q}_{radiation}=F_{s-f}A\sigma(\varepsilon T^4-\alpha T_f^4)+F_{s-t}A\sigma(\varepsilon T^4-\alpha T_t^4)+F_{s-b}A\sigma(\varepsilon T^4-\alpha T_b^4) \tag{3.12}$$

where $F_{s\text{-}f}$, $F_{s\text{-}t}$ and $F_{s\text{-}b}$ refer to the geometric view-factor between the substrate and the main filaments, the top surface of the oven and the bottom surface of the oven respectively. A is the surface area of the substrate, σ is the Stefan-Boltzmann constant, α is the absorptivity of the substrate surface, ε emissivity of the substrate surface. Finally the temperature variables T_f, T_t and T_b denote the temperatures of the filaments, the top surface and the bottom surface respectively.

The form of the convective term is simpler where the rate of convective heat transfer depends on the temperature difference between the substrate surface temperature and the ambient air temperature, Ta, with a proportionality constant h.

$$\dot{Q}_{convection} = Ah(T - T_a) \tag{3.13}$$

The substrate is initially uniformly at the room temperature and the appropriate boundary conditions on the edges of the substrate need to be defined. There will be total of 4 boundary conditions to be able to solve this problem – one at each extreme edge of the substrate. Different boundary conditions to will be considered in the solution ranging from an assumption of no heat transfer at the edges due to very small thickness to radiative and convective mode of heat transfer for these edges just like the larger surfaces.

According to the form of equation, it is apparent that there is not an analytic solution to this system. So the approach to this problem will be to numerically solve the system using a finite difference method. The basis of the finite difference method is outlined with the aid of following figure:

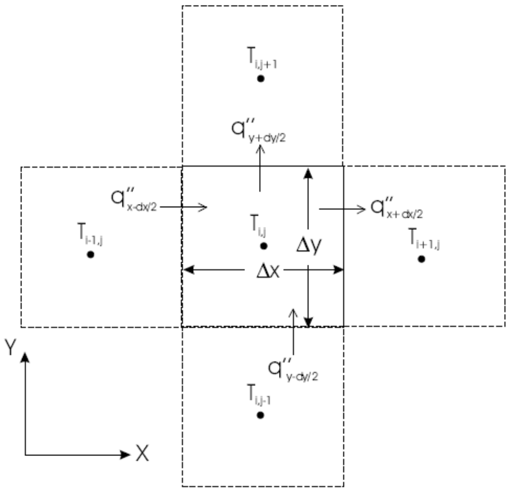

Figure 3-8 - The Finite Difference Method

The substrate is divided into cells of size *Δx* and *Δy* along the *x* and *y* directions. No discretization is required in the z-direction since the substrate has been assumed to be thin enough. Then an energy balance can be written for any arbitrary element whose temperature is given by $T_{i,j}$ – where the equation has now become a system of ordinary differential equation due to the fact that the substrate has been broken down into a network of *n* by *m* cells where n is the number of cells in the *x* direction and *m* the number of cells in the y direction – which depend on the resolution of the discretization as defined by the values of *Δx* and *Δy*.

$$V\rho C_p \frac{dT_{i,j}}{dt} = q''_{x-dx/2} + q''_{y-dy/2} - q''_{x+dx/2} - q''_{x+dx/2} + \dot{Q}_{radiation} + \dot{Q}_{convection} \tag{3.14}$$

The individual heat fluxes can be approximated by the local gradient of the temperature at each surface as:

$$q''_{x-dx/2} = -k\Delta y d \frac{T_{i,j}-T_{i-1,j}}{\Delta x} \tag{3.15a}$$

$$q''_{y-dy/2} = -k\Delta xd\frac{T_{i,j}-T_{i-1,j}}{\Delta y} \tag{3.15b}$$

$$q''_{x+dx/2} = -k\Delta yd\frac{T_{i,j}-T_{i-1,j}}{\Delta x} \tag{3.15c}$$

$$q''_{x+dx/2} = -k\Delta xd\frac{T_{i,j}-T_{i-1,j}}{\Delta y} \tag{3.15d}$$

Where d is the thickness of the substrate. If one chooses the same mesh size in the x and y directions, that is *Δx=Δy*, the 4 expressions above can be simplified and substituted into the original energy balance as

$$V\rho C_p\frac{dT_{i,j}}{dt} = kd(T_{i+1,j} + T_{i-1,j} + T_{i,j+1} + T_{1,j-1} - 4T_{i,j}) + \dot{Q}_{radiation} + \dot{Q}_{convection} \tag{3.16}$$

At this point, the model will also be discretized in the time domain as well, that is

$$\frac{dT_{i,j}}{dt} = \frac{T_{i,j}^{k+1}-T_{i,j}^{k}}{\Delta t} \tag{3.17}$$

where the superscript denotes the time dimension. With this definition, the present time temperature values, denoted by the superscript k, can be isolated into one side of the expression

$$T_{i,j}^{k+1} = T_{i,j}^{k} + \frac{\Delta t}{\Delta \mathrm{xx}\cdot\Delta \mathrm{yy}\cdot\rho\cdot C_p}\Big[k(T_{i+1,j}^{k} + T_{i-1,j}^{k} + T_{i,j+1}^{k} + T_{i,j-1}^{k} - 4T_{i,j}^{k}) + \frac{1}{d}\dot{Q}_{radiation} + \frac{1}{d}\dot{Q}_{convection}\Big] \tag{3.18}$$

Where the volume of the element has been replaced by

$$V = \Delta x\cdot\Delta y\cdot d \tag{3.19}$$

which allows for the direct calculation of the temperatures for the next instance in time based on the knowledge of only the present values of temperature. In the same context, the radiative and convective terms become

$$\dot{Q}_{radiation} = \Delta x \cdot \Delta y \cdot \sigma \left[F_{i,j-f}\left(\varepsilon {T_{i,j}^{k}}^{4} - \alpha T_f^4\right) + F_{i,j-t}\left(\varepsilon {T_{i,j}^{k}}^{4} - \alpha T_t^4\right) + F_{i,j-b}\left(\varepsilon {T_{i,j}^{k}}^{4} - \alpha T_b^4\right)\right] \qquad (3.20)$$

$$\dot{Q}_{convection} = \Delta x \cdot \Delta y \cdot h(T_{i,j}^{k} - T_a) \qquad (3.21)$$

Systems boundary and initial conditions form a specific nature. The initial condition is incorporated into the finite difference form of the energy balance by letting

$$T_{i,j}^{0} = T_0 \qquad (3.22)$$

in the simplest form. One is also free to define any temperature profile by assigning a specific temperature for each of the *n*x*m* elements of the matrix $T_{i,j}$ at k=0 if desired. The boundary conditions are accounted for slightly modifying the energy balance depending on the specific location of the grid element.

1	2	2	2	2	2	1
2	3	3	3	3	3	2
2	3	3	3	3	3	2
2	3	3	3	3	3	2
2	3	3	3	3	3	2
2	3	3	3	3	3	2
1	2	2	2	2	2	1

Figure 3-9 - The x-y Grid

Figure 3-9 shows an arbitrary 7 by 7 grid. The number in each grid refers to the condition of the grid element in terms of the neighboring grid elements. The most abundant type is "9" where all four edges are covered by grid elements, thus the energy balance developed above holds for these types of grid elements. For the remaining grid elements, the heat fluxes need to be modified. For instance for a type "6" cell, there is conduction through the top and right surfaces only. The bottom and left surfaces are open to the oven, where the heat flux needs to be modified in accordance with the specific boundary conditions.

For the simplest case when one assumes no heat transfer through this surface (which justified by the fact that the substrate is very thin compared to the exposed surface area), the energy balance simplifies to

$$T_{i,j}^{k+1} = T_{i,j}^{k} + \frac{\Delta t}{\Delta \mathrm{xx} \cdot \Delta \mathrm{yy} \cdot \rho \cdot C_p}\left[k(T_{i+1,j}^{k} + T_{i,j+1}^{k} - 2T_{i,j}^{k}) + \frac{1}{d}\dot{Q}_{radiation} + \frac{1}{d}\dot{Q}_{convection}\right] \tag{3.23}$$

Which is derived by eliminating the temperature gradients for the edge exposed surfaces. Similar equations can be derived for the remaining nodes. The conductive heat transfer terms for the 9 different grid locations as summarized in Figure 3-9 written for the no heat transfer at the edge boundary condition are given in Table 3-1.

Table 3-1 - Energy Balance by Grid Element Location

Node	Conductive Term
1	$k(T_{i+1,j}^{k} + T_{i,j+1}^{k} - 2T_{i,j}^{k})$
2	$k(T_{i+1,j}^{k} + T_{i-1,j}^{k} + T_{i,j+1}^{k} - 3T_{i,j}^{k})$
3	$k(T_{i-1,j}^{k} + T_{i,j+1}^{k} - 2T_{i,j}^{k})$
4	$k(T_{i+1,j}^{k} + T_{i,j+1}^{k} + T_{i,j-1}^{k} - 3T_{i,j}^{k})$
5	$k(T_{i+1,j}^{k} + T_{i,j+1}^{k} + T_{i,j-1}^{k} - 3T_{i,j}^{k})$
6	$k(T_{i+1,j}^{k} + T_{i,j+1}^{k} - 2T_{i,j}^{k})$
7	$k(T_{i+1,j}^{k} + T_{i-1,j}^{k} + T_{i,j+1}^{k} - 3T_{i,j}^{k})$
8	$k(T_{i-1,j}^{k} + T_{i,j+1}^{k} - 2T_{i,j}^{k})$
9	$k(T_{i+1,j}^{k} + T_{i-1,j}^{k} + T_{i,j+1}^{k} + T_{i,j-1}^{k} - 4T_{i,j}^{k})$

3.2.2. View Factor Theory

The radiation heat transfer mechanism consists of coefficients such as emissivity, absorptivity and radiative view factors. Among these, view factor is a bit more complicated due to the fact that is depends on the positioning of radiative units. Through the system, the agents of the focus are in fact placed in several positions and in every line of the computation, view factor component changes rather than staying the same as of the emissivity and absorptivity. Following step of the study simply states the computation of view factors between any given positions on the assumed coordinate system [15].

Now that each node has a relevant energy balance equation, the only remaining unknowns, apart from the material properties, are the view factors in the radiative transfer term, referenced in Equation 3.20.

The view factors quantify the ratio of the radiation leaving one surface that lands on the other surface based on the relative position of the different surfaces involved in the radiative heat exchange. In general, the view factor between to generic surfaces 1 and 2 is given by

$$F_{1-2} = \frac{1}{|S_1|} \iint_{S_1} dS_1 \iint_{S_2} \frac{cos\beta_1 \cdot cos\beta_2}{\pi \cdot r^2} dS_2 \tag{3.24}$$

where the nomenclature is- given in Figure 3-8. In this form, this is a quadruple integral – taken across both surfaces. In finite difference model being developed for this work, the surface S_1 is small enough compared to the rest of the geometry such that the view factor is constant across it. This allows for the independent evaluation of the outer surface integral, simplifying the view factor expression into

$$F_{1-2} = \iint_{S_2} \frac{cos\beta_1 \cdot cos\beta_2}{\pi \cdot r^2} dS_2 \tag{3.25}$$

In evaluating the angles appearing in the expression above, it is convenient to use the dot product of the unit normal to each surface with the vector connecting the two surfaces. Then we can define the two points in space in the parametric form as

$$P_1 = \langle x_1, y_1, z_1 \rangle \tag{3.26a}$$

$$P_2 = \langle x_2, y_2, z_2 \rangle \tag{3.26b}$$

From which the vector connecting the two points can be directly calculated as

$$S = \langle x_1 - x_2, y_1 - y_2, z_1 - z_2 \rangle \tag{3.27}$$

Then once the unit normal vectors are also defined as $\hat{n}_1$ and $\hat{n}_2$, the view factor expression can be written as

$$F_{1-2} = \frac{1}{\pi}\iint_{S_2} \frac{(\hat{n}_1 \cdot S)(\hat{n}_2 \cdot S)}{(S \cdot S)^2} dS_2 \tag{3.28}$$

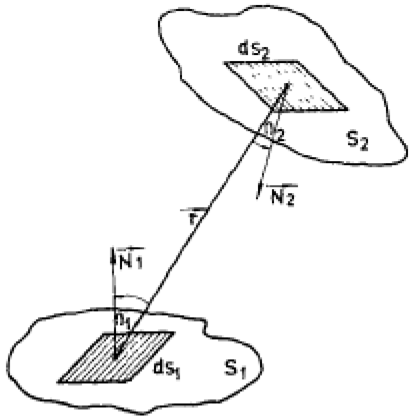

Figure 3-10 - Nomenclatures for View Factor Definition [15]

The final step in determining the exact values of the various view factors is the correct definition of the geometry that will fix the values of the vectors and the limits of the integration. This needs to be done separately for the 3 different types of view factors appearing in the radiative heat transfer terms.

3.2.2.1. View Factor between the Substrate and the Oven Filaments

View factor calculations of the substrate with respect to oven filaments were calculated with the division into 3 parts of the oven, which are between (1) substrate and filaments, (2) substrate and front lid and (3) substrate and back lid.

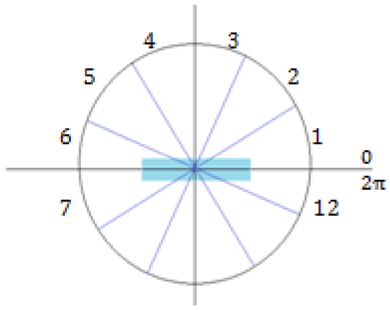

Figure 3-11 – Heating Filaments Around the Oven

Twelve filaments were numbered in the following fashion and angle in Figure 3-11. General expression for the view factors are usually defined as follows:

$$F_{s-f} = \iint \frac{|\hat{n}_s . s| . |\hat{n}_f . s|}{|s . s|^2} dxdy$$

(3.29)

After the integration, dF_{s-f} values were defined depending on the integral limitations. When the number of filament, *k*, less equal than 7 or ant other words, upper case filaments represented with the view factor of

$$dF_{s-f} = \frac{(Rsint).(xcost - R)}{[R^2 + x^2 - 2xRcost + (z-y)^2]^2} Rdtdz$$

(3.30)

And by the same manner, when the number of filament, *k*, greater equal than 7 or ant other words, lower case filaments represented with the view factor of

$$dF_{s-f} = -\frac{(Rsint).(xcost - R)}{[R^2 + x^2 - 2xRcost + (z-y)^2]^2} Rdtdz$$

(3.31)

For both cases, axial variable z has the limits of $z \to -\frac{L}{2}, \frac{L}{2}$ for both of them and the angle, t has the limits of $t \to 0, \pi$ and $t \to \pi, 2\pi$ respectively for upper and lower cases.

View factor expression for the front and the back lid were defined with the angle t and radius r, instead of angle t and axial variable z. Expressions for view factor between the substrate and the front lid and the substrate and the back lid are;

$$dF_{s-t} = \frac{R\ .(Rsint).(-A - y)}{[R^2 + x^2 - 2xRcost + (-A - y)^2]^2} Rdtdr \qquad (3.32a)$$

$$dF_{s-b} = -\frac{R\ .(Rsint).(+A - y)}{[R^2 + x^2 - 2xRcost + (+A - y)^2]^2} Rdtdr \qquad (3.32b)$$

With the limitations of $t \to 0, \pi$ and $r \to 0, R$.

3.2.2.2. View Factor between TCs and the Oven Filaments

Thermocouples are placed inside a tube at the bottom of the co-firing oven. They are called as the front thermocouple (TC_{front}), central thermocouple (TC_{center}) and the back thermocouple (TC_{back}). View factor calculations for the three TCs were made with 2 different surfaces, which are upper and lower surfaces of TCs and with respect to three different cases, which are for the front lid of the oven, back lid of the oven and filaments around the oven (defined as ‘sides’).

View Factors between (Fx_xx);

Oven \ TC	TC front		TC center		TC back	
	upper	Lower	upper	Lower	upper	Lower
Oven front	Ff_ft	Ff_fb	Fc_ft	Fc_fb	Fb_ft	Fb_fb
Oven sides	Ff_st	Ff_sb	Fc_st	Fc_sb	Fb_st	Fb_sb
Oven back	Ff_bt	Ff_bb	Fc_bt	Fc_bb	Fb_bt	Fb_bb

Fx_xx;
* First x: TC
* Second x: oven
* Third x: upper or lower surface of TCs

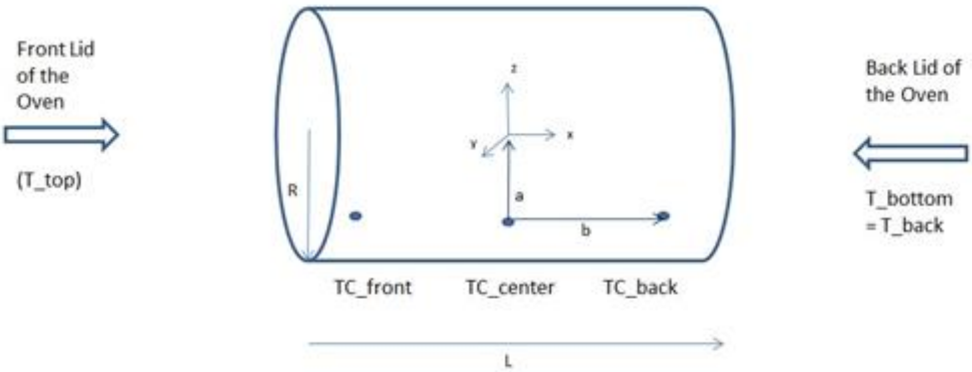

Figure 3-12 – View Factor Definitions between Oven and TCs

3.3. EMPIRICAL MODELING – EXPERIMENTAL DESIGN

In extracting empirical information from a system, the resolution of the information acquired is inversely proportional to the amount of time and cost invested to carry out the experiments. The concepts and approaches of design of experiments (DOE) enable the extraction of the required information with minimal effort. For putting together an effective experimental design, one must be competent not only in the statistical tools and techniques involved but also have a good idea of the physics behind the system under study.

The ideal method to carry out identification experiments for model building purposes is to execute experiments in an open loop fashion, where by the variables that impact the outputs are modulated directly and their effects recorded. However the software installed on the oven does not allow for this mode of an operation for safety reasons. Therefore the experiments had to be designed under a closed loop setting, where the temperature set-points are specified and the equipment adjusts the power of the various filaments according to un-published internal control algorithms. The fact that the details of the control algorithms are not released by the equipment manufacturer further complicates the analysis as these algorithms cannot be directly de-convolved from the results – revealing the true dynamics of the system.

The critical operating variables impacting the substrate temperature were determined to be the heat-up and cool-down rates and the temperature of set-point of the soak step. A secondary variable is the amount of air flow over the substrate during the soak step. Since radiation is the dominating mode of heat transfer and is a non-linear function of temperature – a simple 2 level experimental design is not going to yield enough information about the system. To capture the non-linear characteristics at least 3 levels are required for each critical variable. For 3 critical variables, that makes a total of 27 experiments. Some exploratory experiments showed that only a single experiment can be performed in one day since the oven takes a long time to cool back down to room temperature for the start of the next experiment. Reserving 27 days for experimentation on manufacturing equipment is not a possible proposal so the design needs to be simplified.

When one considers the experimental sequence, it becomes apparent that the heats-up and cool-down rates are independent variables, since they are separated by a long soak step which takes the temperature distributions to equilibrium. Thus the same non-linear information can be extracted using a sequence of 9 experiments. On top of this, we make the assumption that the convection over the substrate is an independent variable and the decision is made to study its impact at some constant value of the other variables.

Table 3-2 - Experimental Design With Individual Variable Levels

Run No	Ramp-up	Ramp-down	SP Temperature	Comment
1	30	30	600	Main DOE
2	20	30	900	Main DOE
3	20	20	600	Main DOE
4	10	10	600	Main DOE
5	10	30	300	Main DOE
6	30	10	900	Main DOE
7	20	10	300	Main DOE
8	10	20	900	Main DOE
9	20	20	300	Main DOE
10	20	30	900	Run 2 Repeat
11	20	30	900	Run 2 – 15.8slm
12	20	30	900	Run 2 – 31.6 slm
13	20	20	600	Run 3 – 15.8 slm

The detailed experimental conditions are listed above in Table 3-2 where runs 1-9 are the actual design, run 10 is a repeat experiment for confirming repeatability and reproducibility. Runs 11-13 are checking the impact of air flow over the substrate during the experiment.

CHAPTER 4

4. RESULTS AND DISCUSSION

This chapter is parallel to the previous one where the modeling approach was outlined in the sense that there will be 3 distinct sections, going over the results and findings for the 3 different modeling approaches. There will be a minor change in which the models are covered in terms of findings in order to improve the flow of findings. The modeling section ended with the experimental plan, this analysis section will begin with the results of the experiments since these findings will be referred to in the results and analysis of the two modeling studies.

4.1. EMPIRICAL MODELING – EXPERIMENTAL DESIGN

4.1.1. Summary of Oven Metrics

The data collected in each experiment is a time trend of the various parameters that are collected during the course of the experiment. These include the temperatures collected by the 3 TC's installed inside the oven for temperature control purposes, the power supplied to the three sets of filaments used to maintain the temperature inside the oven and the readings of the 5 TC's installed on the temperature collection substrate. These data are collected every second during the entire ramp-up, soak and cool-down cycle as well as for some time after the end of the cool-down step – tracking the final characteristics of oven and substrate cool-down. As such, each dataset is contains 8000 to 20000 data-points depending on the duration of the experiment. Such large sets of data cannot be analyzed effectively in their raw state. They must be summarized in some key metrics which can then be interpreted for understanding the oven characteristics. The upcoming sections, prior to the analysis summary, outline these summary metrics along with some justification as to why the particular ones are picked.

4.1.2. Thermocouple Temperatures

A few typical time - temperature overlay plots for the three thermocouples recording the temperature inside the oven for control purposes is shown below. Identical plots for the entire set of experimental runs appear inside Appendix D.

The first plot here focuses in on the main firing step – for which the constant set-point temperature is regulated. One can see here that the center thermocouple (denoted by the red color and identified by the acronym TCC) shows the best tracking performance, followed by the front thermocouple (denoted by the green color and the acronym TCF). The back thermocouple (denoted by the blue color and identified by the acronym TCB) follows the other two by a slight offset. Parameters of steady state analysis for this processing step have been decided as the average value of each TC and the off-set between each TC pair at the steady state point (occurring approximately after a time of ~4500s for this particular example along with the amount of variation of the temperature value throughout the step (to be characterized by the range metric).

Next we look at the cooling step of the firing sequence. Again Run 03 is provided here as the typical example with the rest appearing in Appendix D.

The parameters that might be of interest here are again the temperature values and the offset between each TC pair at the end of the step. It does not make sense to consider the variation here as the variation is almost always the same, correlated to the ramp-down rate. The reasons for the lack of variation as compared to the previous step will become apparent during the analysis of the power input to the filaments.

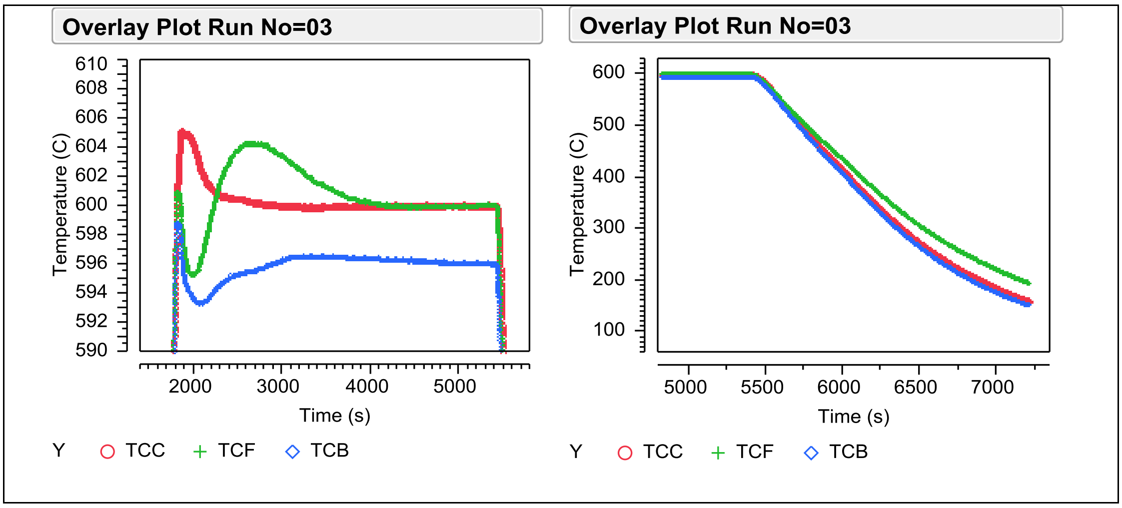

Figure 4-1 – Cooling Step for Run 3

4.1.3. Filament Powers

As mentioned at the beginning of this section, filament powers are adjusted through unpublished internal algorithms of the oven software. The time trend of power supplied to the filaments in Run 03 are provided again for demonstration purposes. In the plot below, the color coding refers to the step number where red is the warm-up, green is the steady-state temperature bake and blue is the ramp-down. Note that the main power also takes on negative values; this is during the phase of the cooling cycle where the fan has been turned on.

The majority of the heat supplied to the oven comes from the 12 main filaments. The front and main power are auxiliary filaments that provide supplemental power at the positions where the main filaments are not present to provide for better edge temperature uniformity.

Important note on the units of power – is that they are not explicitly stated by the equipment manufacturer. Although each filament has a maximum rated power, the recorded values do not even correspond to percentages of these maximum ratings – as evidenced by the 0 mean power provided by the main filament for the 300C set-point experiments. Therefore these recorded values will need to be calibrated to measured temperatures during the modeling efforts. Here we will include the final steady-state values of each filament during the constant temperature bake step (denoted by the green color as mentioned above) and the amount of variation that the filament encounters during the same step – in the hopes that this will correlate to the temperature variations of the 3 thermocouples.

Note here that as soon as the firing cycle enters the cool-down phase, all filaments are essentially shut down and the blower is turned on relatively quickly. This is the reason why the temperature fluctuations at this step are minimal – there essentially no active closed loop control.

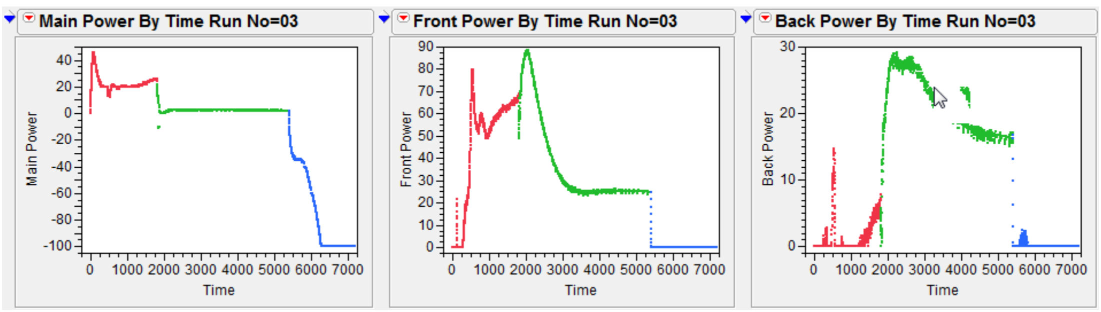

Figure 4-2 – Analysis for the Run 3

4.1.4. Substrate Temperature Measurements

A close investigation of the substrate temperature measurements show that there are very slight variations of the within substrate temperatures during the constant temperature bake step. The final steady state temperature of each substrate temperature will be included in the analysis. More interesting things happen in the cool-down phase as shown in the plot on the left below. The dynamic range between each substrate point can be as high as 25-30C.

This within substrate temperature range is better visualized on a range versus time plot as shown in the figure below. The analysis will include the maximum temperature ranges demonstrated during the ramp-up and ramp-down phases along with the final steady-state temperature range on the substrate towards the end of the constant temperature bake step. Another set of parameters of interest.

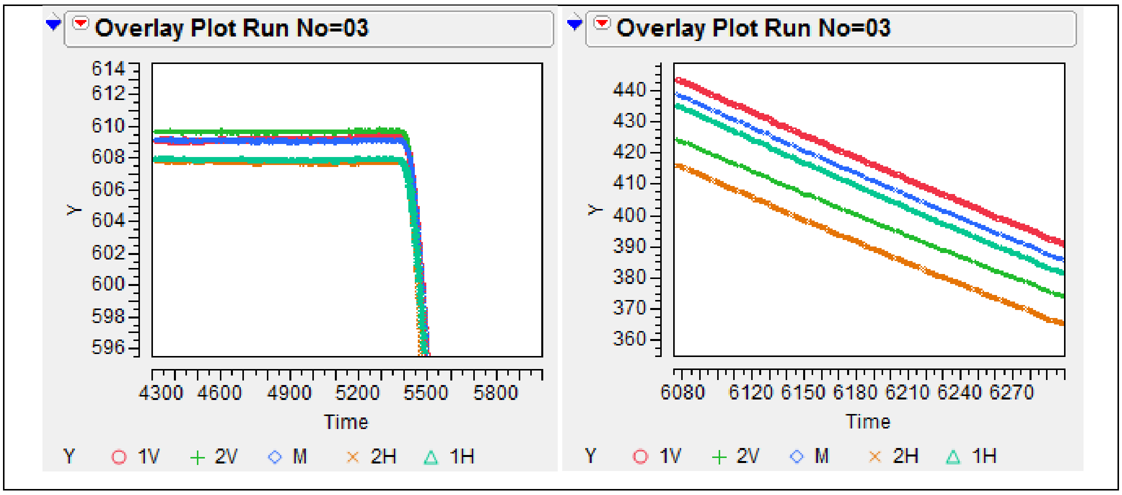

Figure 4-3 – Overlay Plots for Run 3

4.1.5. Summary of Oven Metrics

As per the brief explanations provided above, the experimental parameters of ramp-up and ramp-down rates, the steady state soak temperature will be correlated to the following variables:

Table 4-1 - Oven Thermocouple Related Parameters

Run No	Soak Step SS			Soak Step Variation			Soak Step SS Range	Ramp Down Final		
	TCC	TCF	TCB	TCC	TCF	TCB		TCC	TCF	TCB
1	600	600	596	5.8	22.4	14.5	4	225	261	216
2	900	900	896	5.7	6.8	3.3	4	253	299	248
3	600	600	596	5.8	9	5.6	4	161	196	154
4	600	600	596	5.0	2.6	2.5	4	98	123	94
5	300	300	296	8.8	9.8	6.6	4	181	197	177
6	900	900	896	6.0	15.4	6.1	4	103	130	101
7	300	300	296	10.3	10.2	15.9	4	86	103	81
8	900	900	896	4.2	3.8	3.1	4	180	221	175
9	300	300	296	8.8	20.3	26.1	4	141	160	135
10	900	900	896	7.9	11.1	4.0	4	248	304	237
11	900	900	896	7.7	14.5	5.4	4	248	302	239
12	900	900	896	8.0	14.6	3.9	4	239	287	243
13	600	600	596	6.9	6.6	6.7	4	160	202	150

Table 4-2 - Filament Power Related Parameters

Run No	Soak Step SS			Soak Step Variation		
	Main	Front	Back	Main	Front	Back
1	2.3	26.0	17.1	1.0	4.0	7.3
2	6.2	63.6	34.4	2.0	7.2	6.1
3	2.3	25.2	16.7	1.0	2.6	4.8
4	2.0	24.4	16.2	1.0	3.1	5.0
5	0.0	11.1	6.7	0.0	12.1	4.8
6	6.2	65.3	36.1	2.0	10.7	5.6
7	0.0	10.7	6.7	1.0	16.0	4.8
8	6.0	62.8	32.2	2.0	4.1	4.7
9	0.0	11.6	6.4	0.0	15.3	4.9
10	6.8	59.4	33.4	2.0	6.4	5.3
11	7.2	72.1	30.0	2.0	7.0	4.3
12	7.9	99.9	23.1	2.0	2.2	3.8
13	2.9	31.3	13.3	2.0	2.7	4.8

Table 4-3 - Substrate Temperature Related Parameters

Run No	Soak Step SS Values					Soak Step SS Range	Ramp-up Max Range	Ramp-up Min Range	Ramp-down Order
	1V	2V	M	2H	1H				
1	610	610	610	608	608	2.0	16.1	28.7	1V M 1H 2V 2H
2	910	910	910	908	908	2.2	11.0	38.0	
3	609	610	609	608	608	2.0	10.9	27.5	
4	610	610	609	608	608	2.0	5.6	23.5	
5	312	312	312	311	311	0.7	5.4	11.4	
6	910	910	909	908	908	2.4	16.8	26.9	
7	312	312	312	311	312	0.9	9.7	11.1	
8	911	911	910	909	909	2.2	5.8	34.8	
9	312	312	312	311	311	0.8	13.2	11.3	
10	907	907	907	906	905	1.8	18.9	59.8	
11	903	904	904	904	903	1.2	18.6	58.0	
12	902	903	904	904	903	2.0	20.7	56.0	
13	604	604	604	603	603	0.6	19.3	38.7	

4.1.6. Analysis of Oven Doe Data

4.1.6.1. Repeatability

As summarized in the DOE table, Run #2 was repeated twice – once at the start of the experiment runs and another time at the end of the experiment runs to monitor and justify the stability of the oven operation and the repeatability of the measurements. One may question the fact that only two repeat experiments were done, however this is justified in this case as each experiment does not result in a single data point but rather a sequence of ~10000 data points. Furthermore we are monitoring the stability of industrial class manufacturing equipment that is operated under closed loop control. These two aspects of this work can be stated to justify this otherwise somewhat limited repeatability analysis.

Repeatability and operational stability is analyzed based on the time trends of the relevant operational parameters. When one compares the average temperature measurements on the substrate (5 locations) and the oven (3 locations), one sees that the difference at any given time is less than 3C for identical times in the processing sequence.

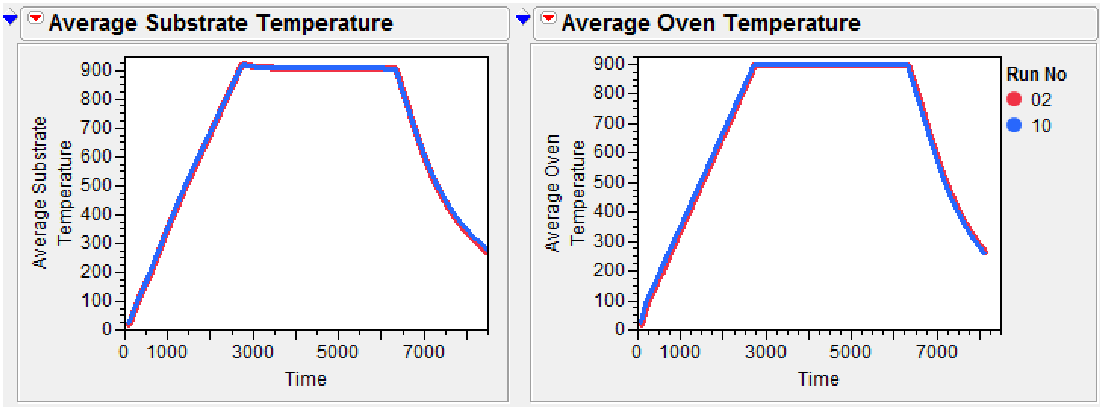

Figure 4-4 – Average Substrate and Oven Temperature

The individual temperature measurements show more of a variability, particularly in the cool-down step. This is best demonstrated by looking at the time trend of the substrate temperature range. The red and blue trends in the plot correspond to the within substrate temperature range recorded over runs 02 and 10 respectively. The shape of these trends are identical for both cases, however the temperature range is far greater for run 10 then run 02, in particular for the cool-down phase. If one looks further into the reason for this difference, it is noted that the active cooling for the two runs are significantly different. In Run 10, the cooling fan is turned on at a greater rate compared to the more gentle and gradual rate of Run 02. The mechanism for this observation will be explained in greater detail through the rest of the analysis and modeling sections. However to summarize this has to do with the fact that the fan blows air on one side of the oven only, thereby cooling that side more effectively than the other side. The temperature range is driven by this imbalance during the cooling cycle. Thus for Run 10, where the fan is turned on more aggressively, more temperature gradient builds-up on the substrate.

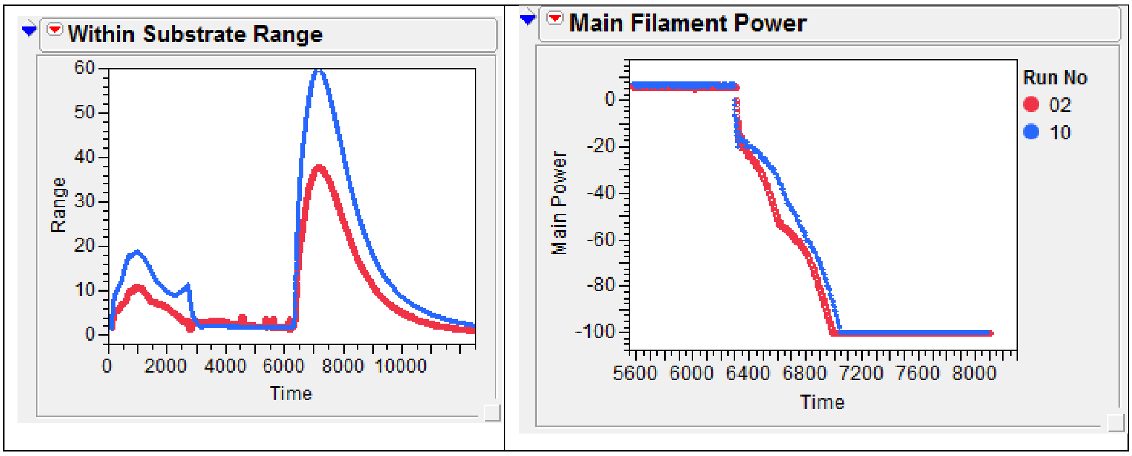

Figure 4-5 – Range and Main Power vs Time Trends

The fundamental reason behind this mis-match between two identical experiments is the power sequence that was applied to the filaments and later to the blower. As demonstrated in the Main Power vs Time trend, Run 10 has the fan turned on more aggressively – resulting in a higher temperature difference between the right and left side of the furnace during the cooling cycle thereby producing a higher temperature gradient on the substrate.

4.1.6.2. Heating, Cooling Rates and Set Point Temperature Analysis

A typical experimental sequence is shown in Figure 4-6. The SP temperature refers to the constant temperature that the oven is held at for 60 minutes in the middle of the sequence. The ramp-up and ramp down rates refer to the slope of the temperature SP profile on either side of the soak step where the temperature is held constant at the SP temperature.

On the other hand, Figure 4-6 shows the actual temperature recorded on the substrate during the experiment. A close inspection of the two plots will reveal that there are different dynamics governing the monitoring TC's and the actual substrate temperature. The first obvious difference is the initial overshoot of the substrate temperature – which is due to the significantly higher thermal mass of the substrate as compared to the monitoring TC. After the cool-down phase is started, one can also see that the substrate temperatures settle less rapidly, again due to the difference in thermal mass. It will not be practical to separately analyze the 10 different profiles – therefore some appropriate metrics need to be defined – which can then be modeled based on operating conditions. The temperature range that exists within the substrate at any given time, particularly during heat-up phase where the film stack is still not solidified, is critical otherwise mechanical stress build-up within the substrate may cause non-uniform shrinkage or even breakage. Another critical parameter would be the off-set between the measured, specified and actual substrate temperatures.

In the following Figures 4-6; TCF, TCB and TCM refer to the thermocouples located at the front, back and the middle of the oven, respectively. The heaters are controlled to track TCM. In Figure 4-7, 1V, 1H, M, 2V and 2H refer to the thermocouples located inside the special temperature monitoring substrate shown in Figure 4-6.

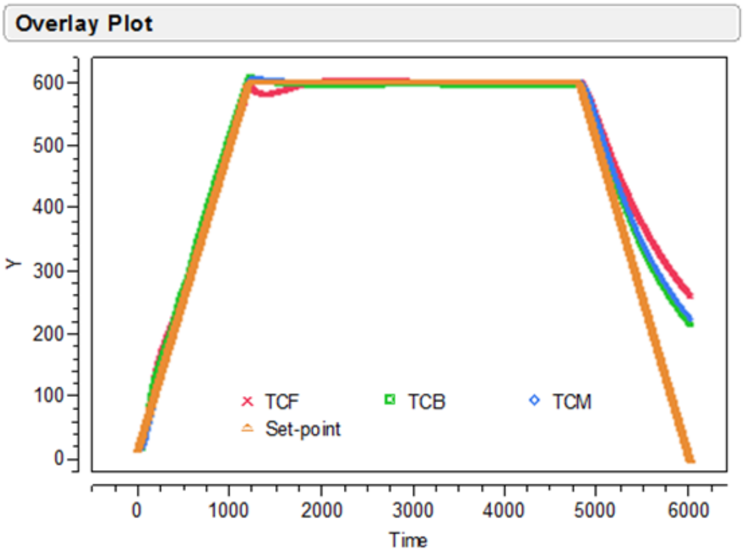

Figure 4-6 - The Firing Cycle – TCF, TCB, TCM

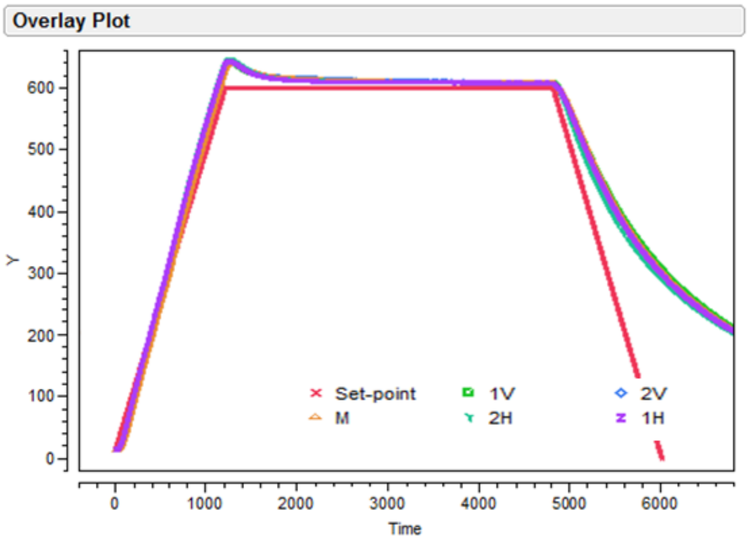

Figure 4-7 - The Firing Cycle – 1V, 1H, M, 2V, 2H

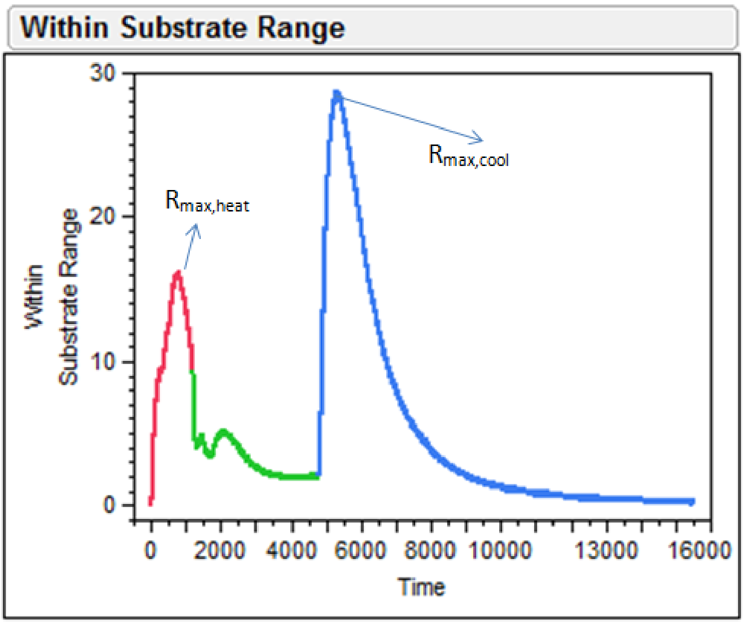

Figure 4-8 - The Two Range Parameters to be Modeled

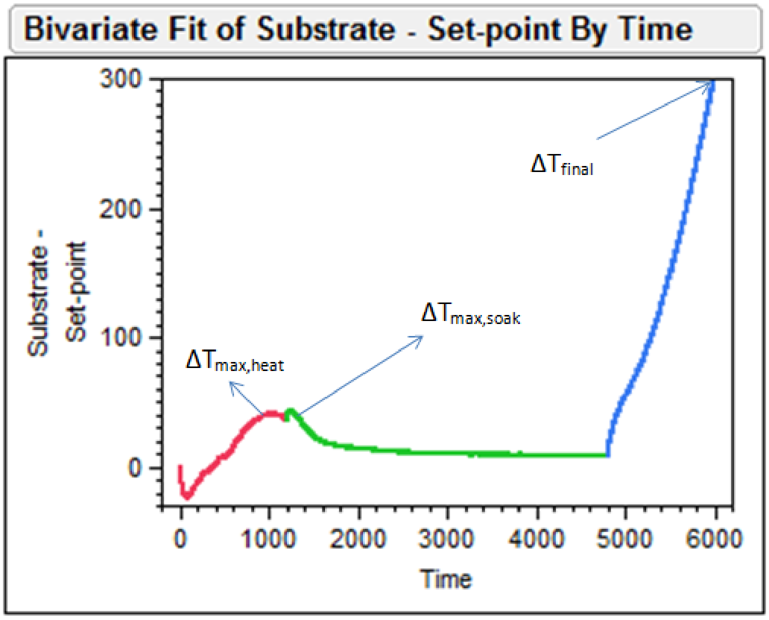

Figure 4-9 - The Two Temperature Difference Parameters To Be Modeled

The time progression of the within substrate range and the difference between the substrate temperature and SP temperature are given in Figure 4-6 and Figure 4-7. Note that there is a huge difference between the SP and substrate temperatures during the cool-down phase as indicated by the blue color in Figure 4-6. This is due to the fact that the oven is not designed to control the cool-down phase very precisely – the rate of SP temperature ramp-down is simply faster than the cooling capacity of the oven. Although this is not as critical for the process performance as the SP tracking while the LTCC sheets are still soft, it is not preferable to cool-down the substrate in an uncontrolled fashion. Therefore the final temperature difference is included for monitoring how well the cool down temperature is controlled.

Out of the two range parameters defined, the first one is likely to be more critical to process performance. This is because the substrate is subjected to this temperature range while the sheets are still in the soft, uncured state. Thus the reactions and phase changes may occur in a non-uniform fashion, leading to shrinkage dependence on position as well as film breakage due to internal mechanical stress.

Figure 4-10 shows the prediction profiles of the critical parameters defined above to the operational characteristics of the oven for the ramp rate and SP temperature DOE as outlined in Table 3-1. The general statement to be made for the four models is that the interactions or quadratic terms are not important. All observations are accurately modeled with only the individual factors; the correlation coefficients of all models are above 0.95.

Furthermore, not all the factors are important for every output. Particularly the within substrate range parameters are completely driven by a single factor which is the ramp-rate for the initial heating phase and the SP temperature for the cool-down phase. In terms of process control, it would be possible to maintain a 5-6°C temperature range within the substrate if the ramp-up rate is restricted to less than 10 °C/min.

The within substrate range during the cool down can be as high as 35°C at the SP of 900°C and is quite independent of the cool-down rate. This is in part due to the physical limitation of the oven for during the cool-down phase. This can be best illustrated by the aid of the overlay plot in Figure 3.6. Note in this figure that as soon as the cooling phase begins, the oven TC through which the PLC is controlling the system begins to decrease fairly rapidly – pretty close to the rate of SP decrease (at least in the initial phases). However the substrate, with its very large thermal mass as compared to that of the oven TC has to radiate out a lot more heat and thus begins to cool down quite slowly. Furthermore, the side of the substrate on which the 2H and 2V TC's are installed becomes colder than the rest of the substrate – this location difference is consistent across all experiments carried out. The reason for this is that this side of the substrate is exposed to the open side of the oven (shown in Figure 4-6). It is this open side of the oven through which the ambient air is drawn for providing the cooling action. Since the ambient air at the low temperature sees this side of the oven first, the walls on this side become cooler, allowing for the adjacent side of the substrate to radiate more heat and build in the temperature profile. This effect will also be validated through the modeling work in the latter sections. There is no way that this range can be overcome without a major design modification to the cooling mechanism of the oven. The flow of air within the oven itself will also be considered in the proceeding sections but the convective heat transfer mechanism is driven by the first power of the temperature difference while the radiative mechanism that causes the temperature difference on the substrate is driven by the fourth power of the temperature difference. So overcoming this difference by providing more cooling action through convective heat transfer likely will not be possible.

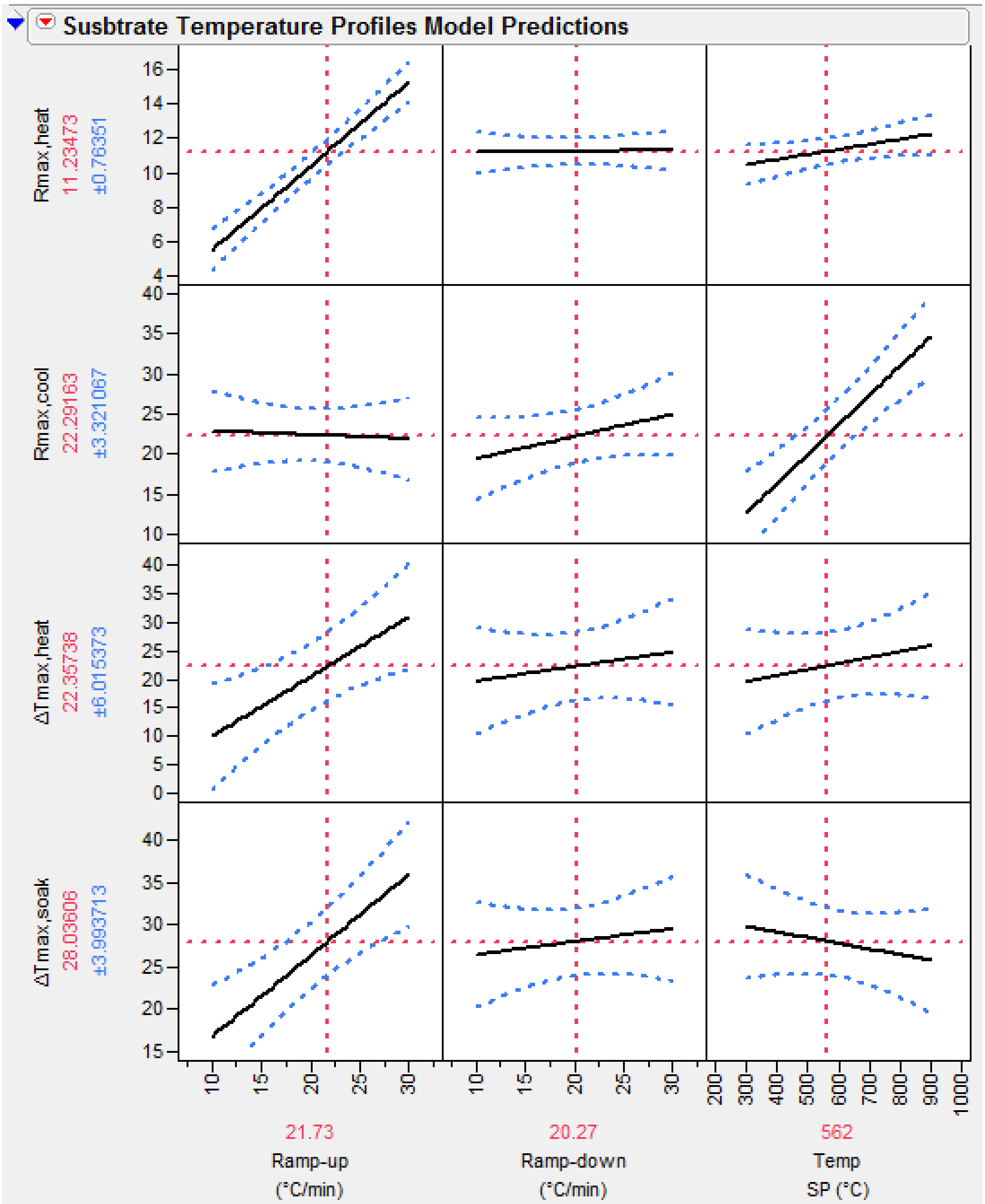

Figure 4-10 - The Critical Parameters Modeled To Experimental Conditions

The mean temperature difference between the substrate and the oven TC can be reduced significantly by keeping the ramp-up rate under control – the impact direction is same to that of the within temperature range so by reducing the ramp-up rate, one can minimize all three variables under evaluation.

The ΔT_{final} parameter that was mentioned at the beginning of this section was not accurately modeled by any of the operating parameters meaning that the cool down process is essentially an uncontrolled process under the range of variables studied. Once again due to the differences in the thermal mass of the substrate and that of the oven TC, this cannot be brought under control unless a model based predictive control algorithm is used along with a state estimation technique. Fortunately temperature control and temperature non-uniformities are far less critical during the cool down phase where all the reactions have taken place and the film stack has been completely cured and solidified.

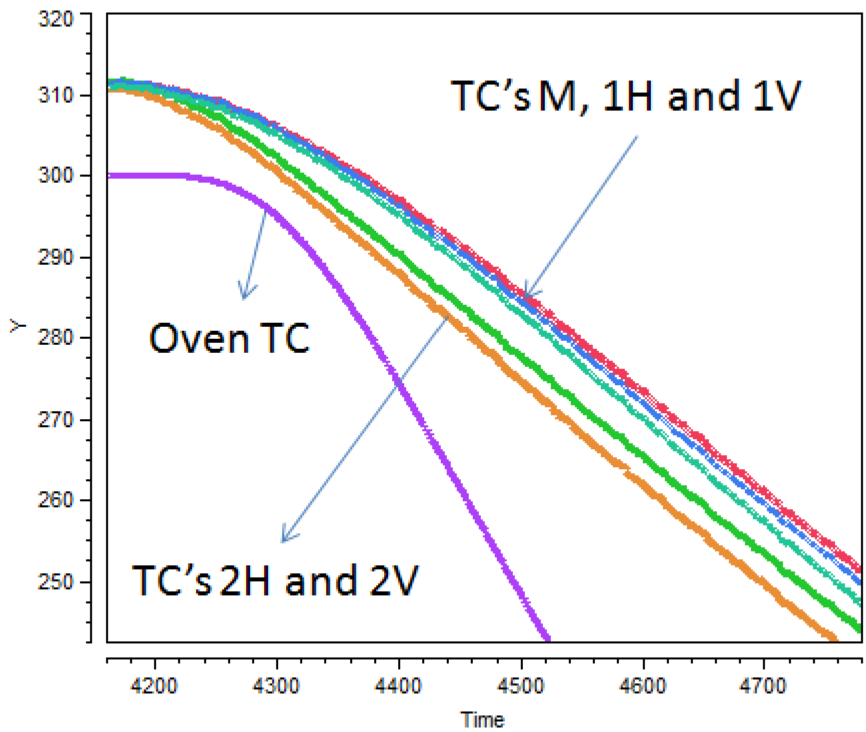

Figure 4-11 - The Non-Uniform Cooling On The Substrate

4.1.6.3. Air Flow Rate Analysis

The impact of air flow rate will be summarized through the plots in Figure 4-12 and Figure 4-13. These plots show a very effective impact during the ramp-up and initial soak phases. One could realize more than a 50% improvement in within substrate range by flowing 31.6 slm of ambient air through the oven and also obtain very good settling times as the substrate begins its constant temperature soak phase.

As effective as the improvement is during the ramp-up phase, the impact is equally ineffective during the cool-down phase. There is a trending improvement with increasing air flow – however the magnitude of the impact is on the order of 2-3%. This is because the cooling is dominated by the uncontrolled radiative mechanism outlined in the previous section. Once again the only way of improving this non-uniformity is by providing uniform cooling to the quartz tube walls, just like uniform heating is applied through accurate control of the heater filaments.

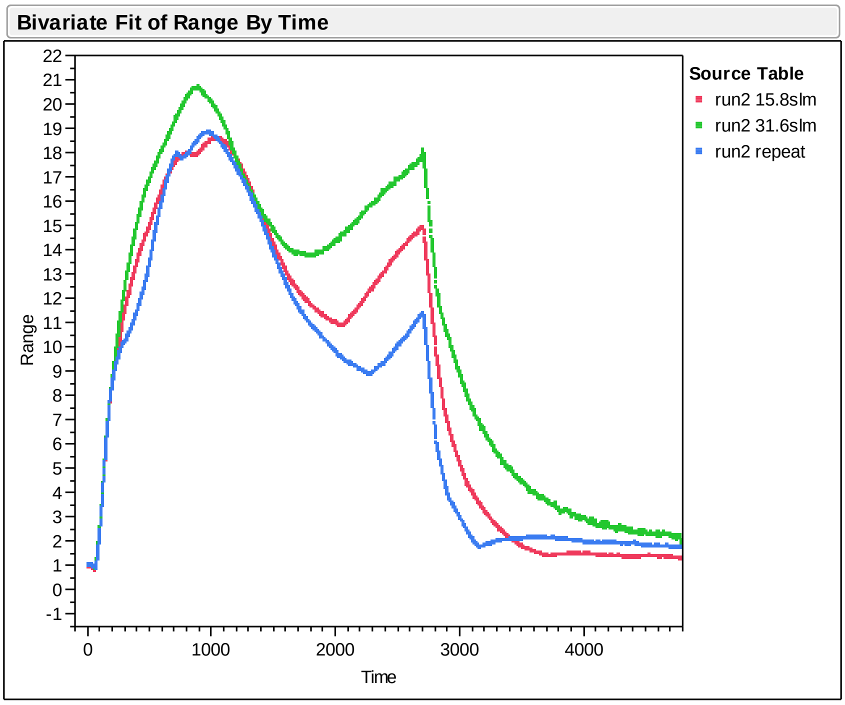

Figure 4-12 - The Within Substrate Range During Ramp-Up and Initial Soak

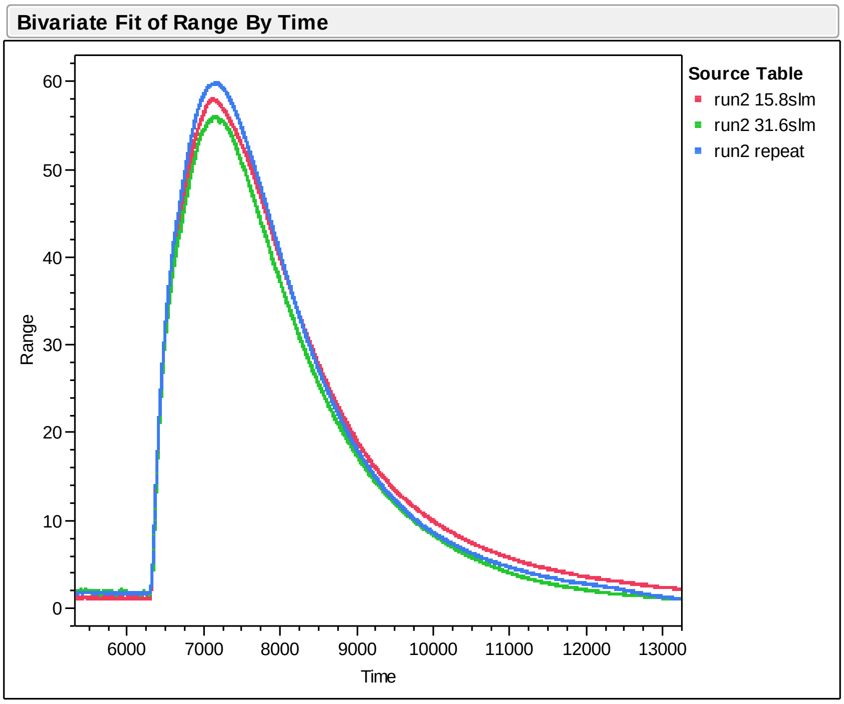

Figure 4-13 – The Within Substrate Range During The Initial Cool Down Period

4.2. FINITE ELEMENT SOLVER MODEL – COMPLETE DYNAMICS

4.2.1. Experimental Results Reproduction – System Identification

The finite element model coded into ANSYS is very well defined in terms of geometrical dimensions and accurately represents the actual oven. However in terms of material properties, some tuning needs to be done in order to match model predictions to actual oven behavior. For this purpose, a two on experimental design is executed, using the simulations as a platform. Objective is to identify the parameters of critical importance among the many material properties involved.

Table 4-4 lists all of the material properties involved that are likely to have an impact on the thermal behavior of the system.

Table 4-4 - Material Properties and Default Values

Material	Cp ($J.kg^{-1}.^{o}C^{-1}$)	K ($W.m^{-1}.^{o}C^{-1}$)
Quartz (oven tube)	964	1.38
Insulation	680	0.02
Substrate (alumina)	930	22
Filaments (Kanthal®)	420	30

The initial exploratory experimental design considers the first order impact of each of these parameters. For the sake of computational simplicity, a representative oven condition is picked, namely Run 2 – taking place at a soak temperature of 600^{o}C. Figure 4-14 below shows the temperature profile of this particular run and indicate the two metrics that will be used to match the modeling results. The first one is the mean substrate temperature and the second one is the slope of the temperature profile during the stabilized soak phase. Note that the set-point temperature needs to be as close to 600 ^{o}C as possible while the slope of the temperature profile must be as close to zero as possible, perhaps slightly negative. These will be quantified by the temperature measurements at 2500s, 3500s and 4500s respectively.

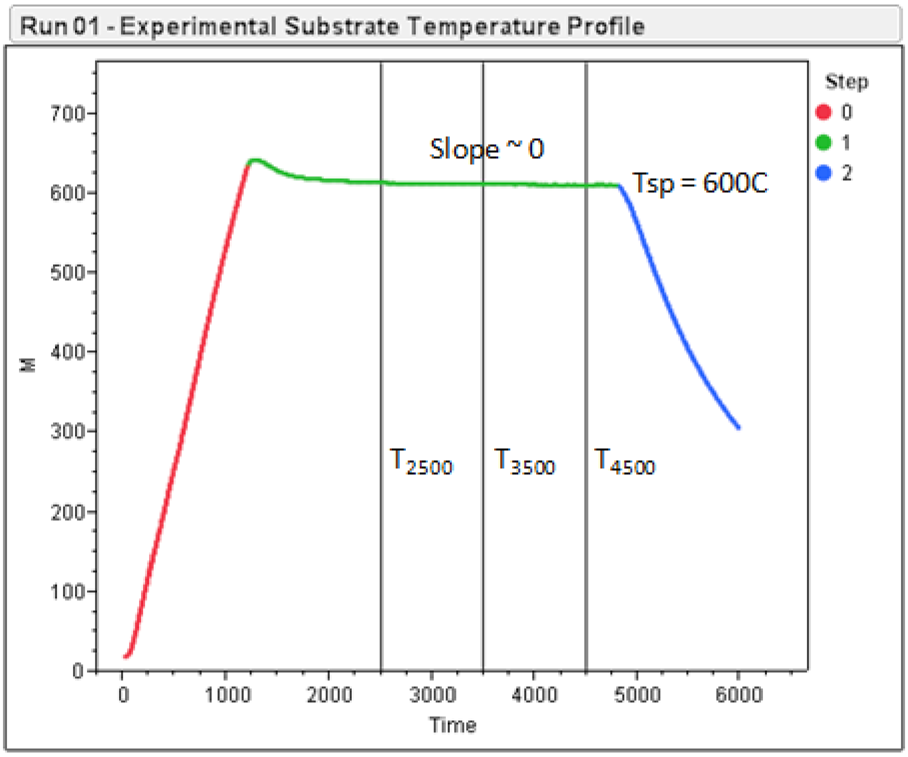

Figure 4-14 – Run 2 Experimental Substrate Temperature Profile

Next, each parameter was varied by an order of magnitude around their default values as stated in Table 4-4. This resulted in a total of 18 simulations. The critical values were derived from the average substrate temperature at 3500s, 4500s and 5500s.

Table 4-5 - Impact Estimates – Average Substrate Temperature

Stabilized Substrate Temperature - Impact Estimates

Term	Estimate	Std Error	t Ratio	Prob>|t|
P29 - Cp Quartz	-0.035614	0.011309	-3.15	0.0040*
P31 - Cp Substrate	-0.029597	0.012156	-2.43	0.0218*
P34 - Cp Filament	-0.060749	0.026918	-2.26	0.0323*
P28 - Cp Insulation	-0.019974	0.016477	-1.21	0.2359
P27 - k insulation	-65.53162	58.24954	-1.13	0.2705
P30 - k Quartz	-8.806508	7.991823	-1.10	0.2802
P33 - k Filament	-0.247394	0.376847	-0.66	0.5171
P32 - k Substrate	-0.332309	0.513882	-0.65	0.5233

Table 4-6 - Impact estimates – Substrate Profile Flatness

Substrate Profile Flatness - Impact Estimates

Term	Estimate	Std Error	t Ratio	Prob>|t|
P27 - k insulation	-0.047119	0.007035	-6.70	<.0001*
P29 - Cp Quartz	-2.66e-6	1.366e-6	-1.95	0.0619
P30 - k Quartz	0.0010238	0.000965	1.06	0.2982
P28 - Cp Insulation	-2.015e-6	1.99e-6	-1.01	0.3202
P34 - Cp Filament	3.2476e-6	3.251e-6	1.00	0.3267
P31 - Cp Substrate	1.0551e-6	1.468e-6	0.72	0.4785
P33 - k Filament	1.6176e-5	4.551e-5	0.36	0.7251
P32 - k Substrate	1.8728e-5	0.000062	0.30	0.7652

The results in Tables 4-5 and 4-6 indicate that the most significant driver for the average substrate temperature are the heat capacities of the substrate, quartz and filament. This parameter directly impacts the temperature of these materials and thereby determines the amount of radiative heat exchange between them. The insulator is not included in this picture as it does not participate in radiative heat transfer, only conduction with the quartz tube. The insulator comes into the picture when the rate of stabilization of temperature is concerned. This is because the insulator is the rate limiting step in the loss of heat to the surroundings – thereby its thermal conductivity determining the characteristics of substrate temperature stabilization.

Based on the findings of the above variation study, the results of the experimental Run 01 were reproduced, using the filament powers as the input to the simulations.

4.2.2. Substrate Temperature Distribution Dynamics

Figure 4-15 below shows the comparison of the predicted vs actual representation of temperature dynamics. Note that there is a constant off-set between the steady-state temperatures – which can be remedied with further fine tuning of the experimentally determined thermal characteristics of the system.

The trend of the substrate range is within reasonable agreement as far as the shape is concerned. There is again some further fine tuning to be done – particularly with the convective heat transfer coefficient of the blower side during the ramp-down cycle to make the magnitudes match. It appears that the simulation blower introduces more heat losses than reality at these current settings.

Finally the thermal conductivity of the substrate needs to be fine-tuned to match the initial warm-up rate as well as the slightly higher observed within substrate range during soak.

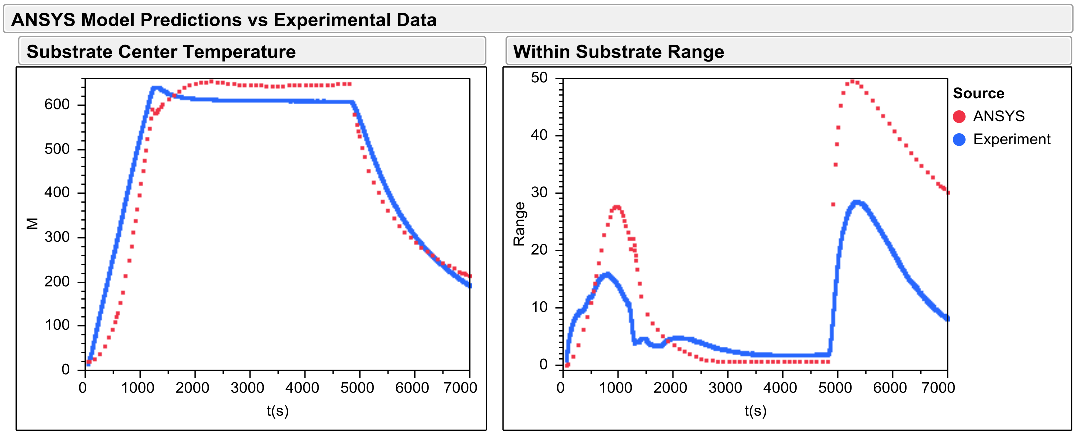

Figure 4-15 - ANSYS Model Predictions vs. Reality

4.2.3. Right and Left Side Temperature Difference During Cool-Down

The experimentally observed within substrate temperature difference is explained by the uneven cooling between the blower (left) and natural convection (right) sides of the oven. Figure 4-16 shows the temperature distribution on the quartz tube during warm-up, soak and cool-down respectively. Note that the initial distribution shows the impact of the filaments, with hot-spots located near the filaments. Then during soak the temperature has time to equalize and achieve a steady state, constant value. Finally as the blower forces air on the left side, a temperature gradient builds-up between the two sides – causing the un-even temperature distribution on the substrate.

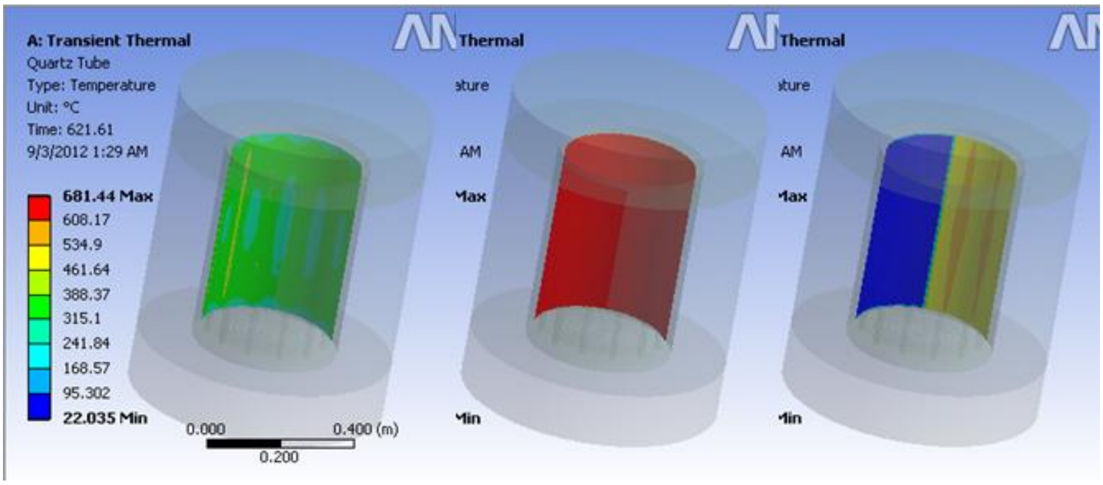

Figure 4-16 - Blower Impact for Cool-Down

4.3. MATLAB MODEL – SIMPLIFIED DYNAMICS

4.3.1. View Factor Confirmations

As outlined before, the definition of view factors involves many operations whose results must be confirmed by some means to ensure accuracy. The oven-substrate system is special in the sense that the substrate is completely contained within the quartz tube. Thus the summation of all view factors must be equal to unity.

For this confirmation study, the oven dimensions given in the Appendix D are used. Namely the quartz tube length L is 331 mm, radius at which the filaments are located, R is 164 mm. The first filament makes an angle of 15° with the horizontal line and each filament is located at 30° intervals after that. The substrate under study is 200mm by 200mm, that is A = 200mm. For demonstration purposes, Δx and Δy will be fixed at 10mm.

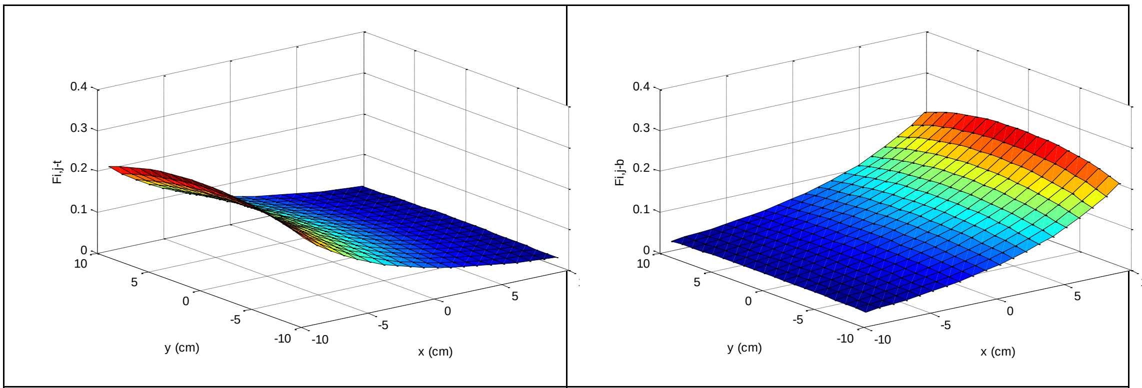

(a) (b)

Figure 4-17 - Top (a) and Bottom (b) Surface View Factors

Another approach for the verification of the thermocouple view factors were detailed with the analysis for the view factors with respect to locations. The values *a* and *b* represent the horizontal and vertical coordinates of the thermocouples, respectively. The view factor theory indicates the fact that, in an enclosed system, summation of the factors must be equal to unity. Considering the thermocouples were assumed to be cylindrical volumes and view factors were estimated for upper and lower halves, separately; there were 2 different results, both equal to unity. Thus following graph has a y-axis with close numerical values to 2 as in Table 4-7.

Table 4-7 – View Factor Unity Results

	Oven Front		Oven Back		Oven Sides		Σ
TC_f	Upper	Lower	Upper	Lower	Upper	Lower	2.000
TC_c	0.2774	0.0137	0.0414	0.0003	0.6812	0.9860	2.000
TC_b	0.1015	0.0011	0.1015	0.0011	0.7969	0.9978	2.000

Since the thermocouples were aligned inside a tube right at the bottom of the co-firing oven, the abovementioned study was held with basic axial movement. Thermocouples were hypothetically moved from a=0 (both on the front and back lid of the oven) to a=16.5 cm (central line of the oven).

Following assessment was made with the movement of the front thermocouple, along the axial line. As the front thermocouple got more away from the front lid of the oven, view factor value (F_{f_f}) was increased dramatically, because the possible area for the TC_{front} to cover was increased.

In Figure 4-18, front thermocouple view factors with respect to front lid of the oven were represented, while the other thermocouples

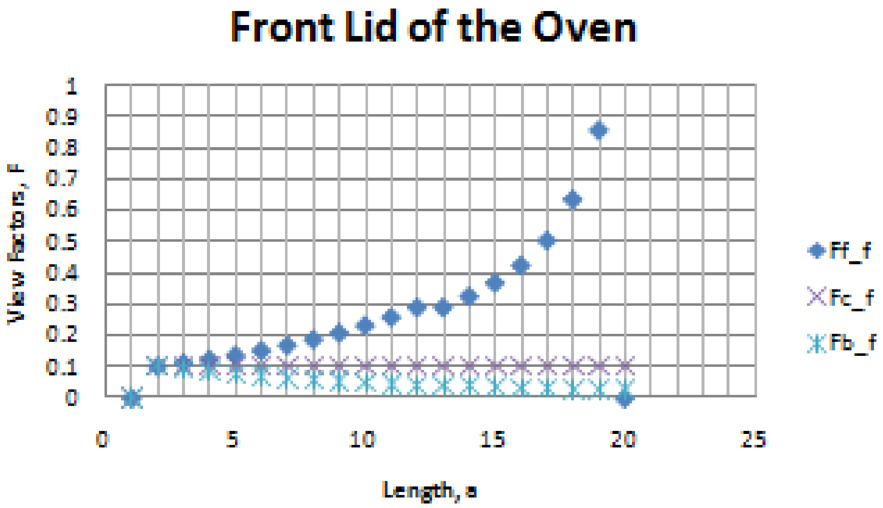

Figure 4-18 – TC_{front} – T_{front} Movement on Axial Line

Other than the placement study, all the view factor summation for the oven gave the unity with a maximum deviation on the order of 10^{-5} as in Figure 4-19.

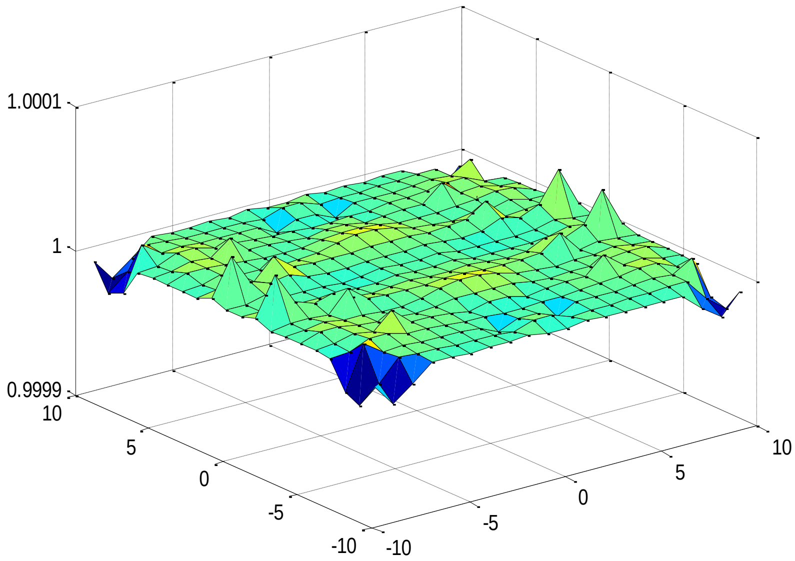

Figure 4-19 - Summation of the View Factors

4.3.2. Sensitivity Analysis

Before proceeding any further toward the correlation of the model predictions with the experimental results, the 3 mesh sizes appearing in the model need to be optimized with respect to computational burden and solution stability. This can be done by executing a set of designed experiments where the factors are Δx, Δy and Δt. The final time will be fixed such that the system reaches a steady state from a set of initial conditions.

As expected the computational burden for calculating the view factors (F_{ij}) increases linearly with the number of cells the grid is divided into – which grows with the square of decreasing mesh size. This is not a very significant problem since the view factors are to be calculated once, determined by the geometrical arrangement. The smallest grid size for which the 20cm substrate is broken into 1mm by 1mm squares, the CPU time used is less than 1hr. If one wants further resolution, there is also the possibility of interpolating between the calculated view factors at a higher resolution. The F_{ij} calculation time per cell remains relatively constant throughout the range studied at less than 0.08s per cell.

The more critical mesh size is in the time domain as this would be expected to impact the stability of the algorithm. The sensitivity analysis indicates an exponential relationship between the mesh size in the time domain and CPU time – as expected. The critical issue here at what point does the algorithm lose stability and whether this point is a very small mesh size, requiring excessively long simulation times.

This measure of stability is a more elusive parameter to define. So far the simulations carried out at a Δt of 0.2 (larger than the largest value that was reported in Table 4-8) shows reasonable stability performance. Under these stable conditions, an 8hr run takes approximately 35 minutes to simulate – which is a reasonable time period.

Table 4-8 - Sensitivity Analysis Results

delx (cm)	dely (cm)	delt (s)	Cells	Fij CPU Time (s)	Tij CPU Time (s)	Fij CPU time per Cell
1	1	0.1	400	31	35	0.077
0.5	0.5	0.1	1600	122	93	0.076
0.2	0.2	0.1	10000	744	226	0.074
0.4	0.4	0.1	2500	186	79	0.075
0.1	0.1	0.1	40000	3130	564	0.078
0.1	0.1	0.01	40000	3130	5912	0.078
0.1	0.1	0.02	40000	3130	2858	0.078
0.1	0.1	0.05	40000	3130	1243	0.078

The algorithm still has room for efficiency improvement in its structure. At this point, it has been deemed unnecessary to spend time for further optimization since the simulation times in the present form are reasonable.

4.3.3. Experimental Results Reproduction – System Identification

Modeling approach for the study was made through the separation the system into two parts. Temperatures of the oven (which are T_{front}, T_{back} and T_{sides}) were assumed as not measured throughout the operation; on the other hand thermocouple temperatures (TC_{front}, TC_{back} and TC_{center}) were assumed to be the values to be measured all through the operation. With this approach, expressions between the filaments and substrate met the expressions between the filaments and thermocouples. Those led to substrate and thermocouple energy balances and finally to the final temperature distribution.

Note that this is slightly different compared to the ANSYS model where the input to the model is the fundamental property (i.e. the filament powers) that derive the temperature increases. This requires a thermal model for the entire system, including the insulation and quartz oven tube. The simplified MATLAB approach correlates the temperature of the oven thermocouples to the temperatures on the substrate through the different view-factors involved in the geometry. Therefore less computational power is required at the expense of somewhat lower accuracy.

A typical plot of model estimations vs experimentation is shown below for Run 01.

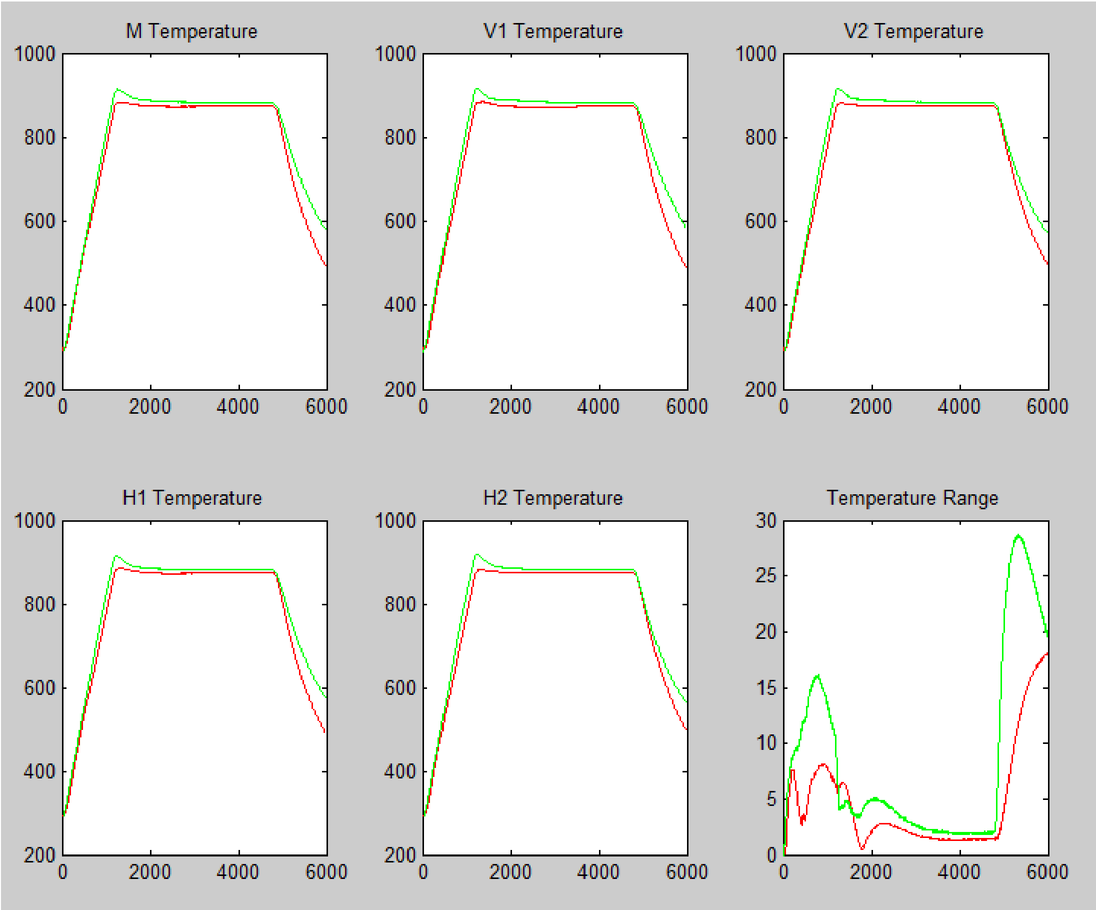

Figure 4-20 – Model Estimations vs Experimentation for Run 1

Steady-state estimations are relatively accurate – with predicted substrate temperatures falling within 3% of the measured values. Dynamic predictions are within the same trend; however their magnitudes are about 2x lower than the actual values.

CHAPTER 5

5. CONCLUSIONS and FUTURE WORK

5.1. CONCLUSIONS

In this thesis study, detailed experimental and modeling work carried out on the furnace, which is perhaps the most important process in the LTCC manufacturing flow was summarized. The experimental observations and model predictions were within reasonable agreement. The dynamic behavior of the process and its limitations had been well supported by fundamental physical laws. With this detailed understanding of the furnace process, it will be possible to design the optimal process for the co-firing of the LTCC stack. Specific conclusions include.

1. Demonstration of an effective modeling strategy for process optimization. We have successfully been able to predict oven temperature distribution dynamics by using complex as well as simplified, efficient models in connection with an effective experimental design. This is a good recipe for effective process development in manufacturing environments. The models allow us to understand the unmeasured (and perhaps un-measurable) factors that fundamentally derive the final temperature distributions.

2. Oven thermocouple to substrate temperature correlation is reasonable under steady state operating conditions. However due to differences in installation location and more importantly the significant difference in thermal mass – oven thermocouples fail to predict the within substrate temperature distributions while the system is dynamically changing.

3. Significant temperature profiles within the substrate may exist during the ramp-up and cool-down stages. The range during cool-down is more significant since the cooling is done in an unbalanced manner through the use of a blower passing room temperature air on one side of the oven. It is possible to address this issue through the use of advanced control algorithms or equipment re-designs. Similar approaches are possible during the warm-up stage – where temperature profiles could have a more significant impact on the LTCC product performance.

5.2. FUTURE WORK

Further work will be carried out on the modeling front – by reducing the gap between the model predictions and reality through parameter fitting. At the end of this work it will be possible to propose an improved control strategy for the control of the oven temperature profiles.

More sensitivity studies need to be conducted on the remaining operation parameters (such as ramp rates for warm-up and cool-down as well as the steady state soak temperature) to reproduce the result of all experimental runs – not just Run 01 and the air-flow impacts.

The material selection has been completed for the green sheets and the compatible pastes and inks. Once these materials arrive on site – the characterization of the screen printing process will begin using the test chip developed.

CHAPTER 6

6. RECOMMENDATIONS

- In order to obtain the uniform temperature distribution, cooling stage can be controlled more effectively. In the system, cool-down part was done with forced convection – more effective on one side of the oven. In order to have a better control over the system, this forced convection can be more uniformly applied by re-designing the blower system to achieve the same air flow-rate over the entire surface area of the furnace. Since this redesign would require a hardware change, it is not very practical. The same effect can be mimicked by adjusting the power ramp down rates independently on either side of the furnace.

- Inside the substrate there are another 5 thermocouples in order to achieve a uniform distribution. They are placed as four in corners and one in the center. Placement might be made on the edges to have a better surveillance over the temperature distribution.

- Thermocouple shape assumption can be tested and selected among dot, spherical or cubical.

- As the most complicated part of the study, view factor assessment was conducted with the individual estimations. Instead of the assumption of the substrate not being in the way of the thermocouples, it is recommended to conduct view factors when thermocouples are accompanied by the substrate.

REFERENCES

[1] Imanaka, Y., Multilayered Low Temperature Co-fired Ceramics (LTCC) Technology, Japan: Springer, 2004

[2] Stetson H., "Multilayer Ceramic Technology," *Ceramics and Civilization*, No. 3, 1987, pp. 307-321,

[3] Blodgett A. J. and Barbour, D. R. "Thermal conduction module: A high performance multilayer ceramic package," *IBM J. Res. Develop.*, Vol. 26, No.3 , 1982, pp. 30.

[4] "Low-Temperature Fireable Multi-layer Ceramic Circuit Board", Nikkei New Materials, 1987, pp. 93-103.

[5] Niwa K., Horikoshi E. and Imanaka Y., "Recent Progress in Multilayer Ceramic Substrates," *Ceramic Transactions* Vol. 97, Multilayer Electronic Ceramic Devices, 1999, pp. 171-182.

[6] Kamehara N., Imanaka Y., and Niwa K., "Multilayer Ceramic Circuit Board with Copper Conductor", Tokyo, 1987, pp. 143-148.

[7] Utsumi K., Shimada Y., Ikeda T., Takamizawa H., Nagasako S., Fujii S. and Nanamatsu S., "Monolithic Multicomponents Ceramic (MMC) Substrate", *NEC Res. & Develop.*, No. 77, 1985, pp. 1-12.

[8] Kamehara N., Imanaka Y. and Niwa K., "Multilayer Ceramic Circuit Board with Copper Conductor", Denshi Tokyo, No. 26, 1987, pp. 143-148.

[9] Usui Y., "Quantitative Analysis Overcomes Design Bottleneck for PCB's with Speeds over IGHz", Nikkei Electronics, 2002, pp. 107-113.

[10] Mohammed A. A., "LTCC for High-Power RF Application", *Advanced Packaging*, 1999, pp. 46-50.

[11] Amey D. I., Dirks M. T., Draudt R. R., Horowitz S. J. and Needs C. R. S., "Opening the door to wireless innovations", *Advanced Packaging*, 2000, pp. 37-54.

[12] Shina Y., Kima O., Hongb J. C., Ohb J. H. and Kimb W. J. "The Development Of Micro-Fuel Processor Using Lowtemperature Co-Fired Ceramic (LTCC)", *International Journal of Hydrogen Energy*, 31, 2006, pp 1925-1933.

[13] Park J. J., Shin Y., Oh J.H. and Chung C.H. "The Development Of A Fully Integrated Micro-Channel Fuel Processor Using Low Temperature Co-Fired Ceramic (LTCC)", *Journal of Industrial and Engineering Chemistry*, 15, 2009, pp 618–623.

[14] Fournier Y., Rouelle G.B., Craquelin N. and Maeder T., "SMD pressure and flow sensor for compressed air in LTCC technology with integrated electronics", *Procedia Chemistry*, 1, 2009, pp 1471–1474.

[15] Al-Bahadili H., Wood J., "View Factor For Radiation Heat Exchange Between The Wall And End Of A Cylinder", *Ann. Nucl. Energy*, Vol. 18, No: 4, 1991, pp 229-231.

[16] Jantunen H., Kangasvieri T., Vahakangas J., Leppavuori S. "Design aspects of microwave components with LTCC technique", J*ournal of the European Ceramic Society*, 23, 2003, pp 2541–2548.

[17] Devlin, L., Pearson, G. and Pittock, J. "RF and microwave component in LTCC", In Proc. of the 38th IMAPS Nordic Conference, Oslo, Norway, 2001, pp. 96–110.

[18] Jantunen, H. A Novel Low Temperature Co-firing Ceramic (LTCC) Material for Telecommunication Devices. PhD Thesis, Department of Electrical Engineering, University of Oulu, Finland, 2001.

[19] Harper C. A., Sampson R.M., Electronic Materials and Processes Handbook, McGraw-Hill, New York, 1993

[20] Fathy E., ”Design of Embedded Passive Components in Low-Temperature Cofired Ceramic on Metal (LTCC-M) Technology,” Microwave Symposium Digest, 1998 IEEE MTT-S Symp., v. 3, 1998, pp. 1281-1284.

[21] Jones H. R. N., “Radiation Heat Transfer”, Oxford Chemistry Primers, Oxford University Press, 2000.

[22] Sparrow E. M., Cess R. D., “Radiation Heat Transfer”, CRC Press, 1978.

APPENDICES

APPENDIX A. MODEL DEVELOPMENT

Model for the study was held with two main arteries; substrate energy balances and thermocouple energy balances. Each line has its own complicated view factor estimations.

1. SUBSTRATE ENERGY BALANCES

On the process of modeling the substrate, finite element method was used with the partial differential equations and non-uniform temperature distribution assumption.

Substrate was divided into grids as follows and treated by the proper heat transfer mechanisms.

1	2	2	2	2	2	1
2	3	3	3	3	3	2
2	3	3	3	3	3	2
2	3	3	3	3	3	2
2	3	3	3	3	3	2
2	3	3	3	3	3	2
1	2	2	2	2	2	1

Figure A. 1 - Substrate Grid Division

Conductive term for the mechanism and its interpretations are;

$$\frac{dT_{i,j}}{dt} = \frac{T_{i,j}^{k+1} - T_{i,j}^{k}}{\Delta t}$$

Table A. 1 - Conductive Terms for the Grids

Node	Conductive Term
1 - Corners	$k(T_{i+1,j}^{k} + T_{i,j+1}^{k} - 2T_{i,j}^{k})$
2 – Edges	$k(T_{i+1,j}^{k} + T_{i,j+1}^{k} + T_{i,j-1}^{k} - 3T_{i,j}^{k})$
3 - Center	$k(T_{i+1,j}^{k} + T_{i-1,j}^{k} + T_{i,j+1}^{k} + T_{i,j-1}^{k} - 4T_{i,j}^{k})$

The convective term for the general expression for the

2. SUBSTRATE VIEW FACTORS

Following figure represents the nomenclature for the temperatures of the oven and thermocouples.

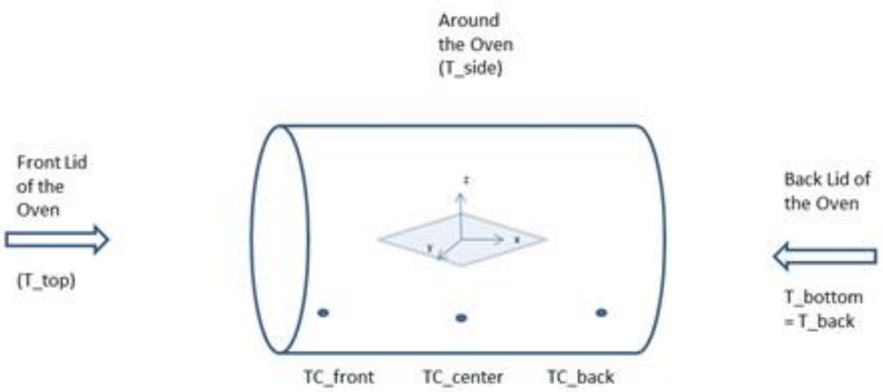

Figure A. 2 - Thermocouple Placements on the Oven

2.1. Equations for Front Lid of the Oven

General expression between Thermocouples and the front lid temperature (T_{front})

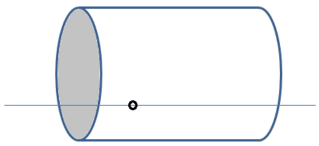

Figure A. 3 - T_{front} Placement on the Oven

2.1.1. General Expressions for the Upper Surface of Thermocouples

Thermocouple: P_1 = <a, 0, -b> ; n_1' = <0, 1, 0>

Cylinder: P_2 = <rcost, rsint, -L/2> ; n_2' = <1, 0, 0>

$$s = P_2 - P_1 = < rcost - a, rsint, -\frac{L}{2} + b > \quad \text{(A.2.1)}$$

$$s.s = r^2 - 2a.rcost + a^2 + (b - \frac{L}{2})^2 \quad \text{(A.2.2)}$$

$$dF = \frac{|n_1'.s||n_2'.s|}{|s.s|^2} rdrdt \quad \text{(A.2.3)}$$

$$dF = \frac{(r)(sint)(rcost-a)}{\left[-2a.rcost+a^2+r^2+(b-\frac{L}{2})^2\right]^2} drdt \quad \text{(A.2.4)}$$

$$dF = \int_0^{t_2}\int_0^{R} f(r,t)drdt + \int_{t_1}^{2\pi}\int_0^{R} f(r,t)drdt + \int_{\frac{3\pi}{2}-acos\frac{b}{R}}^{\frac{3\pi}{2}+acos\frac{b}{R}}\int_0^{\frac{b}{cost}} f(r,t)drdt$$

(A.2.5)

2.1.2. General Expressions for the Lower Phase of Thermocouples

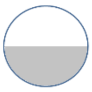

Thermocouple: P_1 = <a, 0, -b> ; n_1' = <0, -1, 0>

Cylinder: P_2 = <rcost, rsint, -L/2> ; n_2' = <1, 0, 0>

$$s = P_2 - P_1 = < rcost - a, rsint, -\frac{L}{2} + b > \quad (A.2.6)$$

$$s.s = r^2 - 2a.rcost + a^2 + (b - \frac{L}{2})^2 \quad (A.2.7)$$

$$dF = \frac{|n_1'.s||n_2'.s|}{|s.s|^2} rdrdt \quad (A.2.8)$$

$$dF = -\frac{(r)(rsint)(rcost-a)}{\left[-2a.rcost+a^2+r^2+(b-\frac{L}{2})^2\right]^2} drdt \quad (A.2.9)$$

$$dF = \int_0^{t_2}\int_0^{R} f(r,t)drdt + \int_{t_1}^{2\pi}\int_0^{R} f(r,t)drdt + \int_{\frac{3\pi}{2}-acos\frac{b}{R}}^{\frac{3\pi}{2}+acos\frac{b}{R}}\int_{\frac{b}{cost}}^{R} f(r,t)drdt$$

(A.2.10)

2.1.3. Front Lid Temperature and Front Thermocouple

Due to the placement, location of the front thermocouple TC_{front} is represented as (-a).

Function for upper surface:

$$f_1(r,t) = \frac{(r)(rsint)(rcost+a)}{\left[2a.rcost+a^2+r^2+(b-\frac{L}{2})^2\right]^2} \quad (A.2.11)$$

$$dF_1 = \int_0^{t_2}\int_0^{R} f_1(r,t)drdt + \int_{t_1}^{2\pi}\int_0^{R} f_1(r,t)drdt + \int_{\frac{3\pi}{2}-acos\frac{b}{R}}^{\frac{3\pi}{2}+acos\frac{b}{R}}\int_0^{\frac{b}{cost}} f_1(r,t)drdt$$

(A.2.12)

Function for lower surface:

$$f_2(r,t) = -\frac{(r)(rsint)(rcost+a)}{\left[2a.rcost+a^2+r^2+(b-\frac{L}{2})^2\right]^2} \quad (A.2.13)$$

$$dF_2 = \int_0^{t_2}\int_0^{R} f_2(r,t)drdt + \int_{t_1}^{2\pi}\int_0^{R} f_2(r,t)drdt + \int_{\frac{3\pi}{2}-acos\frac{b}{R}}^{\frac{3\pi}{2}+acos\frac{b}{R}}\int_{\frac{b}{cost}}^{R} f_2(r,t)drdt$$

(A.2.14)

2.1.4. Front Lid Temperature and Central Thermocouple

Due to the placement, location of the central thermocouple TC_{center} is represented as 0.

Function for upper surface:

$$f_3(r,t) = \frac{(r)(rsint)(rcost)}{\left[r^2+(b-\frac{L}{2})^2\right]^2} \quad (A.2.15)$$

$$dF_3 = \int_0^{t_2}\int_0^R f_3(r,t)drdt + \int_{t_1}^{2\pi}\int_0^R f_3(r,t)drdt + \int_{\frac{3\pi}{2}-acos\frac{b}{R}}^{\frac{3\pi}{2}+acos\frac{b}{R}}\int_0^{\frac{b}{cost}} f_3(r,t)drdt$$

(A.2.16)

Function for lower surface:

$$f_4(r,t) = -\frac{(r)(rsint)(rcost)}{\left[r^2+(b-\frac{L}{2})^2\right]^2} \quad \text{(A.2.17)}$$

$$dF_4 = \int_0^{t_2}\int_0^R f_4(r,t)drdt + \int_{t_1}^{2\pi}\int_0^R f_4(r,t)drdt + \int_{\frac{3\pi}{2}-acos\frac{b}{R}}^{\frac{3\pi}{2}+acos\frac{b}{R}}\int_{\frac{b}{cost}}^{R} f_4(r,t)drdt$$

(A.2.18)

2.1.5. Front Lid Temperature and Back Thermocouple

Due to the placement, location of the back thermocouple TC_{back} is represented as (+a).

Function for upper surface:

$$f_5(r,t) = \frac{(r)(rsint)(rcost-a)}{\left[-2a.rcost+a^2+r^2+(b-\frac{L}{2})^2\right]^2} \quad \text{(A.2.19)}$$

$$dF_5 = \int_0^{t_2}\int_0^R f_5(r,t)drdt + \int_{t_1}^{2\pi}\int_0^R f_5(r,t)drdt + \int_{\frac{3\pi}{2}-acos\frac{b}{R}}^{\frac{3\pi}{2}+acos\frac{b}{R}}\int_0^{\frac{b}{cost}} f_5(r,t)drdt$$

(A.2.20)

Function for lower surface:

$$f_6(r,t) = -\frac{(r)(rsint)(rcost-a)}{\left[-2a.rcost+a^2+r^2+(b-\frac{L}{2})^2\right]^2} \quad \text{(A.2.21)}$$

$$dF_6 = \int_0^{t_2}\int_0^R f_6(r,t)drdt + \int_{t_1}^{2\pi}\int_0^R f_6(r,t)drdt + \int_{\frac{3\pi}{2}-acos\frac{b}{R}}^{\frac{3\pi}{2}+acos\frac{b}{R}}\int_{\frac{b}{cost}}^{R} f_6(r,t)drdt$$

(A.2.22)

2.2. Equations for the Back Lid of the Oven

General expression between thermocouples and the back lid temperature

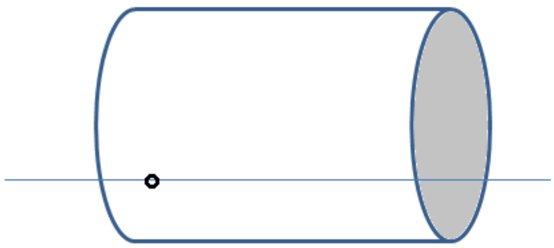

Figure A. 4 - T_{back} Placement on the Oven

2.2.1. General Expressions for the Upper Phase of Thermocouples

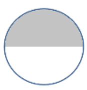

Thermocouple: P_1 = <a, 0, -b> ; n_1' = <0, 1, 0>

Cylinder: P_2 = <rcost, rsint, L/2> ; n_2' = <-1, 0, 0>

$$s = P_2 - P_1 = < rcost - a, rsint, \frac{L}{2} + b > \quad \text{(A.2.23)}$$

$$s.s = -2a.rcost + r^2 + a^2 + (b+\frac{L}{2})^2 \quad \text{(A.2.24)}$$

$$dF = \frac{|n_1'.s||n_2'.s|}{|s.s|^2} rdrdt \tag{A.2.25}$$

$$dF = -\frac{(r)(rsint)(rcost-a)}{\left[-2a.rcost+a^2+r^2+(b+\frac{L}{2})^2\right]^2} drdt \tag{A.2.26}$$

$$dF = \int_0^{t_2}\int_0^{R} f(r,t)drdt + \int_{t_1}^{2\pi}\int_0^{R} f(r,t)drdt + \int_{\frac{3\pi}{2}-acos\frac{b}{R}}^{\frac{3\pi}{2}+acos\frac{b}{R}}\int_0^{\frac{b}{cost}} f(r,t)drdt \tag{A.2.27}$$

2.2.2. General Equations for the Lower Surface of Thermocouples

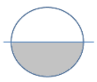

Thermocouple: P_1 = <a, 0, -b> ; n_1' = <0, -1, 0>

Cylinder: P_2 = <rcost, rsint, L/2> ; n_2' = <-1, 0, 0>

$$s = P_2 - P_1 = < rcost - a, rsint, \frac{L}{2} + b > \tag{A.2.28}$$

$$s.s = -2a.rcost + r^2 + a^2 + (b+\frac{L}{2})^2 \tag{A.2.29}$$

$$dF = \frac{|n_1'.s||n_2'.s|}{|s.s|^2} rdrdt \tag{A.2.30}$$

$$dF = \frac{(r)(sint)(rcost-a)}{\left[-2a.rcost+a^2+r^2+(b+\frac{L}{2})^2\right]^2} drdt \tag{A.2.31}$$

$$dF = \int_0^{t_2}\int_0^{R} f(r,t)drdt + \int_{t_1}^{2\pi}\int_0^{R} f(r,t)drdt + \int_{\frac{3\pi}{2}-acos\frac{b}{R}}^{\frac{3\pi}{2}+acos\frac{b}{R}}\int_{\frac{b}{cost}}^{R} f(r,t)drdt \tag{A.2.32}$$

2.2.3. Back Lid Temperature and Front Thermocouple

Due to the placement, location of the front thermocouple TC_{front} is represented as (-a).

Function for upper surface:

$$f_7(r,t) = -\frac{(r)(rsint)(rcost+a)}{\left[2a.rcost+a^2+r^2+(b+\frac{L}{2})^2\right]^2} \quad \text{(A.2.33)}$$

$$dF_7 = \int_0^{t_2}\int_0^{R} f_7(r,t)drdt + \int_{t_1}^{2\pi}\int_0^{R} f_7(r,t)drdt + \int_{\frac{3\pi}{2}-acos\frac{b}{R}}^{\frac{3\pi}{2}+acos\frac{b}{R}}\int_0^{\frac{b}{cost}} f_7(r,t)drdt$$

(A.2.34)

Function for lower surface:

$$f_8(r,t) = \frac{(r)(rsint)(rcost+a)}{\left[2a.rcost+a^2+r^2+(b-\frac{L}{2})^2\right]^2} \quad \text{(A.2.35)}$$

$$dF_8 = \int_0^{t_2}\int_0^{R} f_8(r,t)drdt + \int_{t_1}^{2\pi}\int_0^{R} f_8(r,t)drdt + \int_{\frac{3\pi}{2}-acos\frac{b}{R}}^{\frac{3\pi}{2}+acos\frac{b}{R}}\int_{\frac{b}{cost}}^{R} f_8(r,t)drdt$$

(A.2.36)

2.2.4. Back Lid Temperature and Central Thermocouple

Due to the placement, location of the central thermocouple TC_{center} is represented as 0.

Function for upper surface:

$$f_9(r,t) = -\frac{(r)(rsint)(rcost)}{\left[r^2+(b+\frac{L}{2})^2\right]^2} \qquad \text{(A.2.37)}$$

$$dF_9 = \int_0^{t_2}\int_0^{R} f_9(r,t)drdt + \int_{t_1}^{2\pi}\int_0^{R} f_9(r,t)drdt + \int_{\frac{3\pi}{2}-acos\frac{b}{R}}^{\frac{3\pi}{2}+acos\frac{b}{R}}\int_0^{\frac{b}{cost}} f_9(r,t)drdt$$

(A.2.38)

Function for lower surface:

$$f_{10}(r,t) = \frac{(r)(rsint)(rcost)}{\left[r^2+(b+\frac{L}{2})^2\right]^2} \qquad \text{(A.2.39)}$$

$$dF_{10} = \int_0^{t_2}\int_0^{R} f_{10}(r,t)drdt + \int_{t_1}^{2\pi}\int_0^{R} f_{10}(r,t)drdt + \int_{\frac{3\pi}{2}-acos\frac{b}{R}}^{\frac{3\pi}{2}+acos\frac{b}{R}}\int_{\frac{b}{cost}}^{R} f_{10}(r,t)drdt$$

(A.2.40)

2.2.5. Back Lid Temperature and Back Thermocouple

Due to the placement, location of the central thermocouple TC_{center} is represented as (+a).

Function for upper surface:

$$f_{11}(r,t) = -\frac{(r)(rsint)(rcost-a)}{\left[-2a.rcost+a^2+r^2+(b+\frac{L}{2})^2\right]^2} \qquad \text{(A.2.41)}$$

$$dF_{11} = \int_0^{t_2}\int_0^{R} f_{11}(r,t)drdt + \int_{t_1}^{2\pi}\int_0^{R} f_{11}(r,t)drdt + \int_{\frac{3\pi}{2}-acos\frac{b}{R}}^{\frac{3\pi}{2}+acos\frac{b}{R}}\int_0^{\frac{b}{cost}} f_{11}(r,t)drdt$$

(A.2.42)

Function for lower surface:

$$f_{12}(r,t) = \frac{(r)(rsint)(rcost-a)}{\left[-2a.rcost+a^2+r^2+(b+\frac{L}{2})^2\right]^2} \quad \text{(A.2.43)}$$

$$dF_{12} = \int_0^{t_2}\int_0^{R} f_{12}(r,t)drdt + \int_{t_1}^{2\pi}\int_0^{R} f_{12}(r,t)drdt + \int_{\frac{3\pi}{2}-acos\frac{b}{R}}^{\frac{3\pi}{2}+acos\frac{b}{R}}\int_{\frac{b}{cost}}^{R} f_{12}(r,t)drdt$$

(A.2.44)

2.3. Equations for the Sides of the Oven

General expression between Thermocouples and the oven side temperatures are explained below:

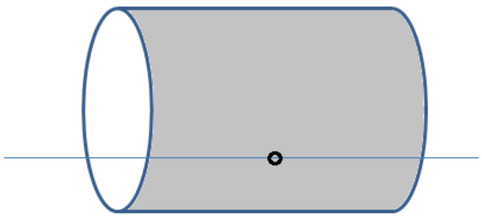

Figure A. 5 - T_{side} Placement on the Oven

2.3.1. General Expressions of the Upper Surface of the Thermocouples

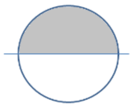

Thermocouple: P_1 = <a, 0, -b> ; n_1' = <0, 1, 0>

Cylinder: P_2 = <Rcost, Rsint, z> ; n_2' = <-cost, -sint, 0>

$$s = P_2 - P_1 = < Rcost - a, Rsint, z + b > \quad \text{(A.2.45)}$$

$$s.s = - 2a.Rcost + R^2 + a^2 + (z + b)^2 \quad \text{(A.2.46)}$$

$$dF = \frac{|n_1'.s||n_2'.s|}{|s.s|^2} rdrdt \quad \text{(A.2.47)}$$

$$dF = \frac{(R)(Rsint)[(-cost)(Rcost - a) + (-sint)(Rsint)]}{[- 2a.Rcost + R^2 + a^2 + (z + b)^2]^2} dzdt$$

$$dF = \frac{(R)(Rsint)(-Rcos^2t + acost - Rsin^2t)}{[- 2a.Rcost + R^2 + a^2 + (z + b)^2]^2} dzdt$$

$$dF = \frac{(R)(Rsint)(-R+acost)}{[- 2a.Rcost + R^2 + a^2 + (z+b)^2]^2} dzdt \quad \text{(A.2.48)}$$

$$dF = \int_0^{t_2} \int_{-\frac{L}{2}}^{+\frac{L}{2}} f(z,t)dzdt + \int_{t_1}^{2\pi} \int_{-\frac{L}{2}}^{+\frac{L}{2}} f(z,t)dzdt \quad \text{(A.2.49)}$$

2.3.2. General Expressions of the Lower Surface of the Thermocouples

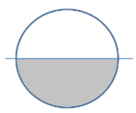

Thermocouple: P_1 = <a, 0, -b> ; n_1' = <0,- 1, 0>

Cylinder: P_2 = <Rcost, Rsint, z> ; n_2' = <-cost, -sint, 0>

$$s = P_2 - P_1 = < Rcost - a, Rsint, z + b > \quad (A.2.50)$$

$$s.s = -2a.Rcost + R^2 + a^2 + (z+b)^2 \quad (A.2.51)$$

$$dF = \frac{|n_1'.s||n_2'.s|}{|s.s|^2} rdrdt \quad (A.2.52)$$

$$dF = -\frac{(R)(Rsint)(-R+acost)}{[-2a.Rcost + R^2 + a^2 + (z+b)^2]^2} dzdt \quad (A.2.53)$$

$$dF = \int_{t_1}^{t_2} \int_{-\frac{L}{2}}^{+\frac{L}{2}} f(z,t)dzdt \quad (A.2.54)$$

2.3.3. Side Temperature and Front Thermocouple

Due to the placement, location of the front thermocouple TC_{front} is represented as (-a).

Function for upper surface:

$$f_{13}(z,t) = -\frac{(R)(Rsint)(R+acost)}{[2a.Rcost + R^2 + a^2 + (z+b)^2]^2} \quad (A.2.55)$$

$$dF_{13} = \int_{0}^{t_2} \int_{-\frac{L}{2}}^{+\frac{L}{2}} f_{13}(z,t)dzdt + \int_{t_1}^{2\pi} \int_{-\frac{L}{2}}^{+\frac{L}{2}} f_{13}(z,t)dzdt$$

(A.2.56)

Function for lower surface:

$$f_{14}(z,t) = \frac{(R)(Rsint)(R+acost)}{[2a.Rcost + R^2 + a^2 + (z+b)^2]^2} \quad (A.2.57)$$

$$dF_{14} = \int_{t_1}^{t_2} \int_{-\frac{L}{2}}^{+\frac{L}{2}} f_{14}(z,t) dz dt$$

(A.2.58)

2.3.4. Side Temperature and Central Thermocouple

Due to the placement, location of the central thermocouple $TC_{central}$ is represented as 0.

Function for upper surface:

$$f_{15}(z,t) = -\frac{(R)(R)(R)}{\left[R^2 + (z+b)^2\right]^2} \tag{A.2.59}$$

$$dF_{15} = \int_{0}^{t_2} \int_{-\frac{L}{2}}^{+\frac{L}{2}} f_{15}(z,t) dz dt + \int_{t_1}^{2\pi} \int_{-\frac{L}{2}}^{+\frac{L}{2}} f_{15}(z,t) dz dt$$

(A.2.60)

Function for upper surface:

$$f_{16}(z,t) = \frac{(R)(R)(R)}{\left[R^2 + (z+b)^2\right]^2} \tag{A.2.61}$$

$$dF_{16} = \int_{t_1}^{t_2} \int_{-\frac{L}{2}}^{+\frac{L}{2}} f_{16}(z,t) dz dt$$

(A.2.62)

2.3.5. Side Temperature and Back Thermocouple

Due to the placement, location of the back thermocouple TC_{back} is represented as (+a).

Function for upper surface:

$$f_{17}(z,t) = \frac{(R)(Rsint)(-R+acost)}{\left[-2a.Rcost + R^2 + a^2 + (z+b)^2\right]^2} \quad \text{(A.2.63)}$$

$$dF_{17} = \int_{0}^{t_2} \int_{-\frac{L}{2}}^{+\frac{L}{2}} f_{17}(z,t)dzdt + \int_{t_1}^{2\pi} \int_{-\frac{L}{2}}^{+\frac{L}{2}} f_{17}(z,t)dzdt$$

(A.2.64)

Function for lower surface:

$$f_{18}(z,t) = -\frac{(R)(Rsint)(-R+acost)}{\left[-2a.Rcost + R^2 + a^2 + (z+b)^2\right]^2} \quad \text{(A.2.65)}$$

$$dF_{18} = \int_{t_1}^{t_2} \int_{-\frac{L}{2}}^{+\frac{L}{2}} f_{18}(z,t)dzdt$$

(A.2.66)

2.4. Resulting Equations

2.4.1. Expressions for the Front Lid of the Oven

$TC_{front} - T_{front}$:

$$dF_1 = \int_0^{t_2}\int_0^{R} f_{1,1}(r,t)drdt + \int_{t_1}^{2\pi}\int_0^{R} f_{1,1}(r,t)drdt + \int_{\frac{3\pi}{2}-acos\frac{b}{R}}^{\frac{3\pi}{2}+acos\frac{b}{R}}\int_0^{\frac{b}{cost}} f_{1,1}(r,t)drdt$$

$$+\int_0^{t_2}\int_0^{R} f_{1,2}(r,t)drdt + \int_{t_1}^{2\pi}\int_0^{R} f_{1,2}(r,t)drdt$$

$$+\int_{\frac{3\pi}{2}-acos\frac{b}{R}}^{\frac{3\pi}{2}+acos\frac{b}{R}}\int_{\frac{b}{cost}}^{R} f_{1,2}(r,t)drdt$$

(A.2.67)

Where $f_{1,1}$ and $f_{1,2}$ functions represent frontal thermocouple's upper and lower surfaces, respectively that expressed as follows:

$$f_{1,1}(r,t) = \frac{(r^2 sint)(rcost+a)}{\left[2a.rcost+a^2+r^2+(b-\frac{L}{2})^2\right]^2} \quad \text{(A.2.68a)}$$

$$f_{1,2}(r,t) = -\frac{(r^2 sint)(rcost+a)}{\left[2a.rcost+a^2+r^2+(b-\frac{L}{2})^2\right]^2} \quad \text{(A.2.68b)}$$

TC$_{center}$ – T$_{front}$:

$$dF_2 = \int_0^{t_2}\int_0^{R} f_{2,1}(r,t)drdt + \int_{t_1}^{2\pi}\int_0^{R} f_{2,1}(r,t)drdt + \int_{\frac{3\pi}{2}-acos\frac{b}{R}}^{\frac{3\pi}{2}+acos\frac{b}{R}}\int_0^{\frac{b}{cost}} f_{2,1}(r,t)drdt$$

$$+ \int_0^{t_2}\int_0^{R} f_{2,2}(r,t)drdt + \int_{t_1}^{2\pi}\int_0^{R} f_{2,2}(r,t)drdt$$

$$+ \int_{\frac{3\pi}{2}-acos\frac{b}{R}}^{\frac{3\pi}{2}+acos\frac{b}{R}}\int_{\frac{b}{cost}}^{R} f_{2,2}(r,t)drdt$$

(A.2.69)

Where f$_{2,1}$ and f$_{2,2}$ functions represent central thermocouple's upper and lower surfaces, respectively that expressed as follows:

$$f_{2,1}(r,t) = \frac{r^3.sint.cost}{\left[r^2+(b-\frac{L}{2})^2\right]^2} \quad \text{(A.2.70a)}$$

$$f_{2,2}(r,t) = -\frac{r^3.sint.cost}{\left[r^2+(b-\frac{L}{2})^2\right]^2} \quad \text{(A.2.70b)}$$

TC$_{back}$ – T$_{front}$:

$$dF_1 = \int_0^{t_2}\int_0^{R} f_{3,1}(r,t)drdt + \int_{t_1}^{2\pi}\int_0^{R} f_{3,1}(r,t)drdt + \int_{\frac{3\pi}{2}-acos\frac{b}{R}}^{\frac{3\pi}{2}+acos\frac{b}{R}}\int_0^{\frac{b}{cost}} f_{3,1}(r,t)drdt$$

$$+ \int_0^{t_2}\int_0^{R} f_{3,2}(r,t)drdt + \int_{t_1}^{2\pi}\int_0^{R} f_{3,2}(r,t)drdt$$

$$+ \int_{\frac{3\pi}{2}-acos\frac{b}{R}}^{\frac{3\pi}{2}+acos\frac{b}{R}}\int_{\frac{b}{cost}}^{R} f_{3,2}(r,t)drdt$$

(A.2.71)

Where $f_{3,1}$ and $f_{3,2}$ functions represent back thermocouple's upper and lower surfaces, respectively that expressed as follows:

$$f_{3,1}(r,t) = \frac{(r^2 sint)(rcost-a)}{\left[-2a.rcost+a^2+r^2+(b-\frac{L}{2})^2\right]^2} \qquad \text{(A.2.72a)}$$

$$f_{3,2}(r,t) = -\frac{(r^2 sint)(rcost-a)}{\left[-2a.rcost+a^2+r^2+(b-\frac{L}{2})^2\right]^2} \qquad \text{(A.2.72b)}$$

2.4.2. Expressions for the Sides of the Oven

$TC_{front} - T_{side}$:

$$dF_4 = \int_0^{t_2}\int_{-\frac{L}{2}}^{+\frac{L}{2}} f_{4,1}(z,t)dzdt + \int_{t_1}^{2\pi}\int_{-\frac{L}{2}}^{+\frac{L}{2}} f_{4,1}(z,t)dzdt + \int_{t_1}^{t_2}\int_{-\frac{L}{2}}^{+\frac{L}{2}} f_{4,2}(z,t)dzdt$$

(A.2.73)

Where $f_{4,1}$ and $f_{4,2}$ functions represent frontal thermocouple's upper and lower surfaces, respectively that expressed as follows:

$$f_{4,1}(z,t) = -\frac{(R)(Rsint)(R+acost)}{\left[2a.Rcost+R^2+a^2+(z+b)^2\right]^2} \qquad \text{(A.2.74a)}$$

$$f_{4,2}(z,t) = \frac{(R)(Rsint)(R+acost)}{\left[2a.Rcost+R^2+a^2+(z+b)^2\right]^2} \qquad \text{(A.2.74b)}$$

$TC_{center} - T_{side}$:

$$dF_5 = \int_0^{t_2}\int_{-\frac{L}{2}}^{+\frac{L}{2}} f_{5,1}(z,t)dzdt + \int_{t_1}^{2\pi}\int_{-\frac{L}{2}}^{+\frac{L}{2}} f_{5,1}(z,t)dzdt + \int_{t_1}^{t_2}\int_{-\frac{L}{2}}^{+\frac{L}{2}} f_{5,2}(z,t)dzdt$$

(A.2.75)

Where $f_{5,1}$ and $f_{5,2}$ functions represent central thermocouple's upper and lower surfaces, respectively that expressed as follows:

$$f_{5,1}(z,t) = -\frac{R^3 sint}{\left[R^2+(z+b)^2\right]^2} \tag{A.2.76a}$$

$$f_{5,2}(z,t) = \frac{R^3 sint}{\left[R^2+(z+b)^2\right]^2} \tag{A.2.76b}$$

$TC_{back} - T_{side}$:

$$dF_6 = \int_0^{t_2} \int_{-\frac{L}{2}}^{+\frac{L}{2}} f_{6,1}(z,t)dzdt + \int_{t_1}^{2\pi} \int_{-\frac{L}{2}}^{+\frac{L}{2}} f_{6,1}(z,t)dzdt + \int_{t_1}^{t_2} \int_{-\frac{L}{2}}^{+\frac{L}{2}} f_{6,2}(z,t)dzdt$$

(A.2.77)

$$f_{6,1}(z,t) = \frac{(R)(Rsint)(-R+acost)}{\left[-2a.Rcost + R^2+a^2 + (z+b)^2\right]^2} \tag{A.2.78a}$$

$$f_{6,2}(z,t) = -\frac{(R)(Rsint)(-R+acost)}{\left[-2a.Rcost + R^2+a^2 + (z+b)^2\right]^2} \tag{A.2.78b}$$

2.4.3. Expressions for the Back Lid of the Oven

$TC_{front} - T_{back}$:

$$dF_7 = \int_0^{t_2} \int_0^{R} f_{7,1}(r,t)drdt + \int_{t_1}^{2\pi} \int_0^{R} f_{7,1}(r,t)drdt + \int_{\frac{3\pi}{2}-acos\frac{b}{R}}^{\frac{3\pi}{2}+acos\frac{b}{R}} \int_0^{\frac{b}{cost}} f_{7,1}(r,t)drdt$$

$$+ \int_0^{t_2} \int_0^{R} f_{7,2}(r,t)drdt + \int_{t_1}^{2\pi} \int_0^{R} f_{7,2}(r,t)drdt$$

$$+ \int_{\frac{3\pi}{2}-acos\frac{b}{R}}^{\frac{3\pi}{2}+acos\frac{b}{R}} \int_{\frac{b}{cost}}^{R} f_{7,2}(r,t)drdt$$

(A.2.79)

Where $f_{7,1}$ and $f_{7,2}$ functions represent frontal thermocouple's upper and lower surfaces, respectively that expressed as follows:

$$f_{7,1}(r,t) = -\frac{(r^2 sint)(rcost+a)}{\left[2a.rcost+a^2+r^2+(b+\frac{L}{2})^2\right]^2} \quad \text{(A.2.80a)}$$

$$f_{7,2}(r,t) = \frac{(r^2 sint)(rcost+a)}{\left[2a.rcost+a^2+r^2+(b+\frac{L}{2})^2\right]^2} \quad \text{(A.2.80b)}$$

$TC_{center} - T_{back}$:

$$dF_8 = \int_0^{t_2}\int_0^{R} f_{8,1}(r,t)drdt + \int_{t_1}^{2\pi}\int_0^{R} f_{8,1}(r,t)drdt + \int_{\frac{3\pi}{2}-acos\frac{b}{R}}^{\frac{3\pi}{2}+acos\frac{b}{R}}\int_0^{\frac{b}{cost}} f_{8,1}(r,t)drdt$$
$$+\int_0^{t_2}\int_0^{R} f_{8,2}(r,t)drdt + \int_{t_1}^{2\pi}\int_0^{R} f_{8,2}(r,t)drdt$$
$$+\int_{\frac{3\pi}{2}-acos\frac{b}{R}}^{\frac{3\pi}{2}+acos\frac{b}{R}}\int_{\frac{b}{cost}}^{R} f_{8,2}(r,t)drdt$$

(A.2.81)

Where $f_{8,1}$ and $f_{8,2}$ functions represent central thermocouple's upper and lower surfaces, respectively that expressed as follows:

$$f_{8,1}(r,t) = -\frac{(r^2 sint)(rcost)}{\left[r^2+(b+\frac{L}{2})^2\right]^2} \quad \text{(A.2.82a)}$$

$$f_{8,2}(r,t) = \frac{(r^2 sint)(rcost)}{\left[r^2+(b+\frac{L}{2})^2\right]^2} \quad \text{(A.2.82b)}$$

$TC_{back} - T_{back}$:

$$dF_9 = \int_0^{t_2}\int_0^{R} f_{9,1}(r,t)drdt + \int_{t_1}^{2\pi}\int_0^{R} f_{9,1}(r,t)drdt + \int_{\frac{3\pi}{2}-acos\frac{b}{R}}^{\frac{3\pi}{2}+acos\frac{b}{R}}\int_0^{\frac{b}{cost}} f_{9,1}(r,t)drdt$$
$$+ \int_0^{t_2}\int_0^{R} f_{9,2}(r,t)drdt + \int_{t_1}^{2\pi}\int_0^{R} f_{9,2}(r,t)drdt$$
$$+ \int_{\frac{3\pi}{2}-acos\frac{b}{R}}^{\frac{3\pi}{2}+acos\frac{b}{R}}\int_{\frac{b}{cost}}^{R} f_{9,2}(r,t)drdt$$

(A.2.83)

Where $f_{9,1}$ and $f_{9,2}$ functions represent back thermocouple's upper and lower surfaces, respectively that expressed as follows:

$$f_{9,1}(r,t) = -\frac{(r^2 sint)(rcost-a)}{\left[-2a.rcost+a^2+r^2+(b+\frac{L}{2})^2\right]^2} \quad \text{(A.2.84a)}$$

$$f_{9,2}(r,t) = \frac{(r^2 sint)(rcost-a)}{\left[-2a.rcost+a^2+r^2+(b+\frac{L}{2})^2\right]^2} \quad \text{(A.2.84b)}$$

3. THERMOCOUPLE ENERGY BALANCES

Another aspect of the modeling includes radiation equation with respect to thermocouple temperatures which is stated below in terms of emissivity, absorptivity and Stefan-Boltzmann constants:

$$Q_{radiation} = \sigma F_{i,j}\,(\varepsilon TC^4 - \alpha T^4) \quad \text{(A.2.85)}$$

$$[(q_{in}A - q_{out}A)\Delta t]_{for\ Tback,Tfront,Tside} = V\rho Cp(TC^{k+1} - TC^{k})$$

(A.2.86)

$$\sigma F_{i,j}\left(\varepsilon TC_{back}^{4} - \alpha T_{front}^{4}\right)A + \sigma F_{i,j}\left(\varepsilon TC_{back}^{4} - \alpha T_{side}^{4}\right)A$$
$$+\sigma F_{i,j}\left(\varepsilon TC_{back}^{4} - \alpha T_{back}^{4}\right)A = V\rho Cp\left(\frac{TC_{back}^{k+1} - TC_{back}^{k}}{\Delta t}\right)$$

(A.2.87)

$$TC_{back}^{k+1} = TC_{back}^{k} + C_1\left[\begin{array}{c} F_{i,j}\left(\varepsilon TC_{back}^{4} - \alpha T_{front}^{4}\right) + \\ F_{i,j}\left(\varepsilon TC_{back}^{4} - \alpha T_{side}^{4}\right) + F_{i,j}\left(\varepsilon TC_{back}^{4} - \alpha T_{back}^{4}\right) \end{array}\right]$$

(A.2.88)

Where C_1 is the generalized constant for the expression which includes:

$$C_1 = \frac{\sigma\Delta t}{V\rho Cp}$$

For each thermocouple, named TC_{back}, TC_{center} and TC_{front}; expressions are listed respectively:

$$TC_{back}^{k+1} = TC_{back}^{k} + C_1\left[\begin{array}{c} F_{i,j}\left(\varepsilon TC_{back}^{4} - \alpha T_{front}^{4}\right) + \\ F_{i,j}\left(\varepsilon TC_{back}^{4} - \alpha T_{side}^{4}\right) + F_{i,j}\left(\varepsilon TC_{back}^{4} - \alpha T_{back}^{4}\right) \end{array}\right]$$

(A.2.89)

$$TC_{center}^{k+1} = TC_{center}^{k} +$$
$$C_2\left[\begin{array}{c} F_{i,j}\left(\varepsilon TC_{center}^{4} - \alpha T_{front}^{4}\right) + \\ F_{i,j}\left(\varepsilon TC_{center}^{4} - \alpha T_{side}^{4}\right) + F_{i,j}\left(\varepsilon TC_{center}^{4} - \alpha T_{back}^{4}\right) \end{array}\right]$$

(A.2.90)

$$TC_{front}^{k+1} = TC_{front}^{k} + C_3 \begin{bmatrix} F_{i,j}\left(\varepsilon TC_{front}^4 - \alpha T_{front}^4\right) + \\ F_{i,j}\left(\varepsilon TC_{front}^4 - \alpha T_{side}^4\right) + F_{i,j}\left(\varepsilon TC_{front}^4 - \alpha T_{back}^4\right) \end{bmatrix}$$

(A.2.91)

General expression between the thermocouple temperatures and filament temperatures is expressed as follows:

$$\frac{\partial TC_i}{\partial t} = C_{1,i}\left(TC_i^4 - T_f^4\right) + C_{2,i}\left(TC_i^4 - T_s^4\right) + C_{3,i}\left(TC_i^4 - T_b^4\right)$$

(A.2.92)

Again for each thermocouple:

$$TC_{front} \ : \ 0 = C_1\left(TC_{front}^4 - T_{front}^4\right) + C_2\left(TC_{front}^4 - T_{side}^4\right) + C_3\left(TC_{front}^4 - T_{back}^4\right)$$

(A.2.93)

$$TC_{back} \ : \ 0 = C_4\left(TC_{back}^4 - T_{front}^4\right) + C_5\left(TC_{back}^4 - T_{side}^4\right) + C_6\left(TC_{back}^4 - T_{back}^4\right)$$

(A.2.94)

$$TC_{center} \ : \ 0 = C_7\left(TC_{center}^4 - T_{front}^4\right) + C_8\left(TC_{center}^4 - T_{side}^4\right) + C_9\left(TC_{center}^4 - T_{back}^4\right)$$

(A.2.95)

4. THERMOCOUPLE VIEW FACTORS

Thermocouples are placed inside a tube at the bottom of the co-firing oven. They are called as the front thermocouple (TC_{front}), central thermocouple (TC_{center}) and the back thermocouple (TC_{back}). View factor calculations for the three TCs were made with 2 different surfaces, which are upper and lower surfaces of TCs and with respect to three different cases, which are for the front lid of the oven, back lid of the oven and filaments around the oven (defined as 'sides').

View Factors between (Fx_xx);

Oven \ TC	TC front		TC center		TC back	
	upper	Lower	upper	Lower	upper	Lower
Oven front	Ff_ft	Ff_fb	Fc_ft	Fc_fb	Fb_ft	Fb_fb
Oven sides	Ff_st	Ff_sb	Fc_st	Fc_sb	Fb_st	Fb_sb
Oven back	Ff_bt	Ff_bb	Fc_bt	Fc_bb	Fb_bt	Fb_bb

Fx_xx;
* First x: TC
* Second x: oven
* Third x: upper or lower surface of TCs

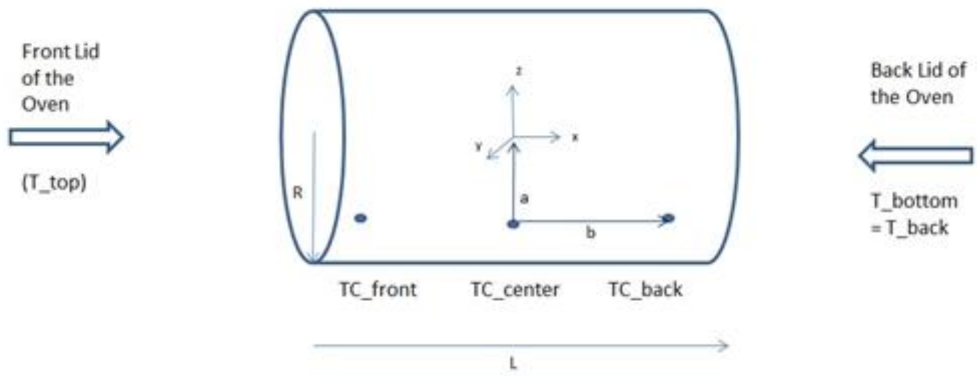

Figure A. 6 - View Factor Definitions between Oven and TCs

APPENDIX B. CODING

1. Substrate View Factor Coding

1.1. Top.m

```
function dF = viewtop(t, r)
global x y L

A = L/2;

num = r.*(r.*sin(t)).*( -A - y);
den = r.^2 + x.^2 - 2.*x.*r.*cos(t) + ( -A - y).^2;

dF = -num./(den.^2)/pi();
```

1.2. Sides.m

```
function dF = filamentsides(t, z)
global x y R

num = R.*(R.*sin(t)).*(x.*cos(t) - R);
den = R.^2 + x.^2 - 2.*x.*R.*cos(t) + (z-y).^2;

dF = -num./(den.^2)/pi();
```

1.3. Bottom.m

```
function dF = viewbottom(t, r)
global x y L

A = L/2;

num = -r.*(r.*sin(t)).*( +A - y);
den = r.^2 + x.^2 - 2.*x.*r.*cos(t) + ( +A - y).^2;

dF = -num./(den.^2)/pi();
```

2. Thermocouples View Factor Coding

2.1. View Factors between Thermocouples and Front Surface of the Oven (TC_front)

Each sub heading named as "top" and "bottom" represents the 2 areas of the front lid. Division depends on the placement of the thermocouple alignment on the axis of z=-b line and the codes named as "inner" represent the inner part of the double quadratic equation set.

2.1.1. TC_front_top.m

```
function dF = TC_Front_Top(t, r)
global x b L

num = -(r.*sin(t) + b).*(L/2 + x).*r;
den = r.^2 + 2.*r.*b.*sin(t) + b.^2 + (L/2 + x).^2;


dF = -num./(den.^2)/pi();
end
```

2.1.2. TC_front_top_inner.m

```
function dF = TC_Front_Top_Inner(t)
global x b L
for i = 1:length(t)
    tt = t(i);
    dF(i) = quad(@(r) ((r.*sin(tt)+b).*(L/2+x).*r./(((L/2+x).^2 +
b.^2 + r.^2 + (2.*r.*b.*sin(tt))).^2)/pi()), 0, b/sin(-tt));
end
end
```

2.1.3. TC_front_bottom_inner.m

```
function dF = TC_Front_Bottom_Inner(t)
global x b L R
for i = 1:length(t)
    tt = t(i);
    dF(i)  =  quad(@(r)  -((r.*sin(tt)+b).*(L/2+x).*r./(((L/2+x).^2
+ b.^2 + r.^2 + (2.*r.*b.*sin(tt))).^2)/pi()), b/sin(-tt), R);
end
end
```

2.2. View Factors between Thermocouples and Back Surface of the Oven (TC_back)

2.2.1. TC_back_top.m

```
function dF = TC_Front_Top(t, r)
global x b L
L = -L;
num = -(r.*sin(t) + b).*(L/2 + x).*r;
den = r.^2 + 2.*r.*b.*sin(t) + b.^2 + (L/2 + x).^2;
L = -L;


dF = num./(den.^2)/pi();
end
```

2.2.2. TC_back_bottom_inner.m

```
function dF = TC_Front_Bottom_Inner(t)
global x b L R
L = -L;
for i = 1:length(t)
    tt = t(i);
    dF(i)  = quad(@(r)  ((r.*sin(tt)+b).*(L/2+x).*r./(((L/2+x).^2 +
b.^2 + r.^2 + (2.*r.*b.*sin(tt))).^2)/pi()), b/sin(-tt), R);
end
L = -L;
end
```

2.3. View Factors between Thermocouples and Sides of the Oven (TC_sides)

2.3.1. TC_sides_top.m

```
function dF = TC_Sides_Top(t, z)
global x b R

num = R.*(R*sin(t) + b).*(R + b*sin(t));
den = R.^2 + 2.*R.*b.*sin(t) + b.^2 + (z-x).^2;

dF = num./(den.^2)/pi();
end
```

2.3.2. TC_sides_bottom.m

```
function dF = TC_Sides_Bottom(t, z)
global x b R

num = R.*(R*sin(t) + b).*(R + b*sin(t));
den = R.^2 + 2.*R.*b.*sin(t) + b.^2 + (z-x).^2;

dF = -num./(den.^2)/pi();
end
```

2.4. Coding for sum of the View Factors between Thermocouples and Oven

```
clear all
global x y R L b


% Geometric Constants
L = 33;            % Cylinder Length in cm
R = 16.400;            % Cylinder radius in cm
```

```
A = 10;              % Substrate Length in cm (square substrate)
filament_n = 12;     % Number of Filaments
filament_0 = 15;      % Location of the first filement - degrees
from the flat plane

a = 2               ;  % Location of front and back thermocouples
from the center of the oven
b = 8             ; % Distance of the thermocouples to the central
axis of the oven


% Simulation Parameters
delx = 1;          % Substrate Mesh Size x-dimension
dely = 1;          % Substrate Mesh Size y-dimension
delt = 0.1;          % Time step size
t_final=8000;          % Final time for the simulation
T_0 = 25;            % Initial Temperature
% load Tf.txt;            % Loading the profile of the filament
temperatures
% t = Tf(:,1);
% Tf = Tf(:,2:13);

% Mesh Definition
x_grid = [-A/2+delx/2:delx:A/2-delx/2];
y_grid = [-A/2+dely/2:dely:A/2-dely/2];
time_grid = [0:delt:t_final];
filaments = [0:30:360]/180*pi();

% % Initial Conditions
%  T(:,:,1)  =  ones(length(x_grid),  length(y_grid))  *  (T_0  +
273.15);
% Ts = [];                   % Assigning the temperatures of the
filaments
% for i = 1:12
%     Ts = [Ts [interp1(t,Tf(:,i),time_grid)]'];
% end
% Ts = Ts';
% Tt=interp1(t,Tf(:,1),time_grid);               % Temperature of
the top surface
% Tb=interp1(t,Tf(:,1),time_grid);               % Temperature of
the bottom surface
% Ta = 350;                                      % Temperature of
the air blown into the oven


% Physical Constants
stf_bol = 5.6704e-08;       % Stefan Boltmann Constant in W/m2/K4
emissivity = 1;             % Emissivity of the substrate surface
absorptivity = 1;                % Absorbtivity of the substrate
surface
k = 0.3;                          % Thermal Conductivity of the
substrate
h = 0;                               % Convective heat transfer
coefficient of the substrate surface
rho = 3.89;                 % Density of the substrate
Cp = 880;                   % Heat capacity of the substrate
```

```
C1 = delt * k / rho / delx / dely / Cp;

% View Factor Calculations for the thermocouples
initial = cputime;
% Thermocouples and the front surface
t1 = 2*pi() - asin(b/R);
t2 = pi() + asin(b/R);

x = -a;
    Ff_ft   =   dblquad(@TC_Front_Top,   0,   t2,   0,   R)   +
dblquad(@TC_Front_Top,     t1,     2*pi(),     0,     R)     +
quad(@TC_Front_Top_Inner, t2, t1);
    Ff_fb = quad(@TC_Front_Bottom_Inner, t2, t1);
x = 0;
    Fc_ft   =   dblquad(@TC_Front_Top,   0,   t2,   0,   R)   +
dblquad(@TC_Front_Top,     t1,     2*pi(),     0,     R)     +
quad(@TC_Front_Top_Inner, t2, t1);
    Fc_fb = quad(@TC_Front_Bottom_Inner, t2, t1);
x = a;
    Fb_ft   =   dblquad(@TC_Front_Top,   0,   t2,   0,   R)   +
dblquad(@TC_Front_Top,     t1,     2*pi(),     0,     R)     +
quad(@TC_Front_Top_Inner, t2, t1);
    Fb_fb = quad(@TC_Front_Bottom_Inner, t2, t1);

% Thermocouples and the back surface
x = -a;
    Ff_bt   =   dblquad(@TC_Back_Top,   0,   t2,   0,   R)   +
dblquad(@TC_Back_Top,     t1,     2*pi(),     0,     R)     +
quad(@TC_Back_Top_Inner, t2, t1);
    Ff_bb = quad(@TC_Back_Bottom_Inner, t2, t1);
x = 0;
    Fc_bt   =   dblquad(@TC_Back_Top,   0,   t2,   0,   R)   +
dblquad(@TC_Back_Top,     t1,     2*pi(),     0,     R)     +
quad(@TC_Back_Top_Inner, t2, t1);
    Fc_bb = quad(@TC_Back_Bottom_Inner, t2, t1);
x = a;
    Fb_bt   =   dblquad(@TC_Back_Top,   0,   t2,   0,   R)   +
dblquad(@TC_Back_Top,     t1,     2*pi(),     0,     R)     +
quad(@TC_Back_Top_Inner, t2, t1);
    Fb_bb = quad(@TC_Back_Bottom_Inner, t2, t1);

% Thermocouples and the Side Surfaces
x = -a;
    Ff_st   =   dblquad(@TC_Sides_Top,   0,   t2,   -L/2,   L/2)   +
dblquad(@TC_Sides_Top, t1, 2*pi(), -L/2, L/2);
    Ff_sb = dblquad(@TC_Sides_Bottom, t2, t1, -L/2, L/2);
x = 0;
    Fc_st   =   dblquad(@TC_Sides_Top,   0,   t2,   -L/2,   L/2)   +
dblquad(@TC_Sides_Top, t1, 2*pi(), -L/2, L/2);
    Fc_sb = dblquad(@TC_Sides_Bottom, t2, t1, -L/2, L/2);
x = a;
    Fb_st   =   dblquad(@TC_Sides_Top,   0,   t2,   -L/2,   L/2)   +
dblquad(@TC_Sides_Top, t1, 2*pi(), -L/2, L/2);
    Fb_sb = dblquad(@TC_Sides_Bottom, t2, t1, -L/2, L/2);

a
b
```

```
Fx_xx = [Ff_ft Ff_fb Ff_bt Ff_bb Ff_st Ff_sb; Fc_ft Fc_fb Fc_bt
Fc_bb Fc_st Fc_sb; Fb_ft Fb_fb Fb_bt Fb_bb Fb_st Fb_sb]
sum(Fx_xx')
```

APPENDIX C. SYSTEM DRAWINGS

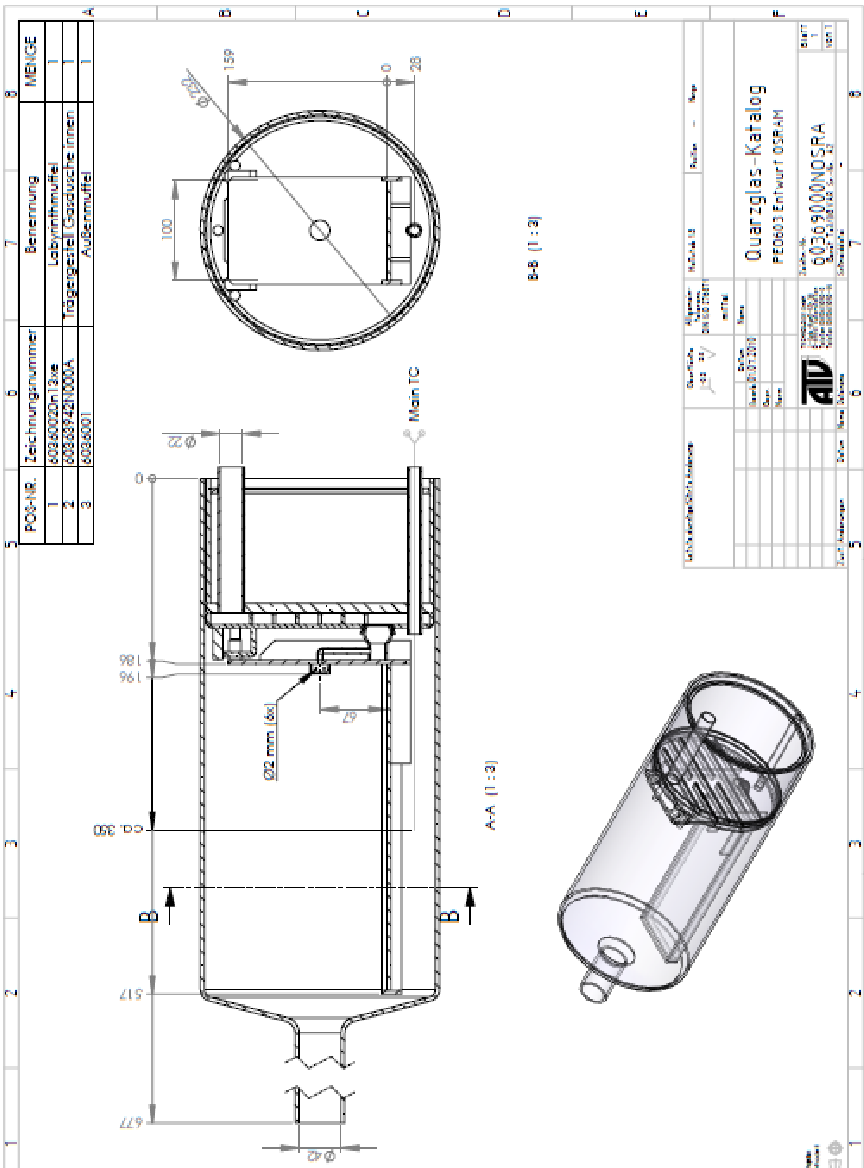

Figure C. 1 - Co-firing Oven Drawings

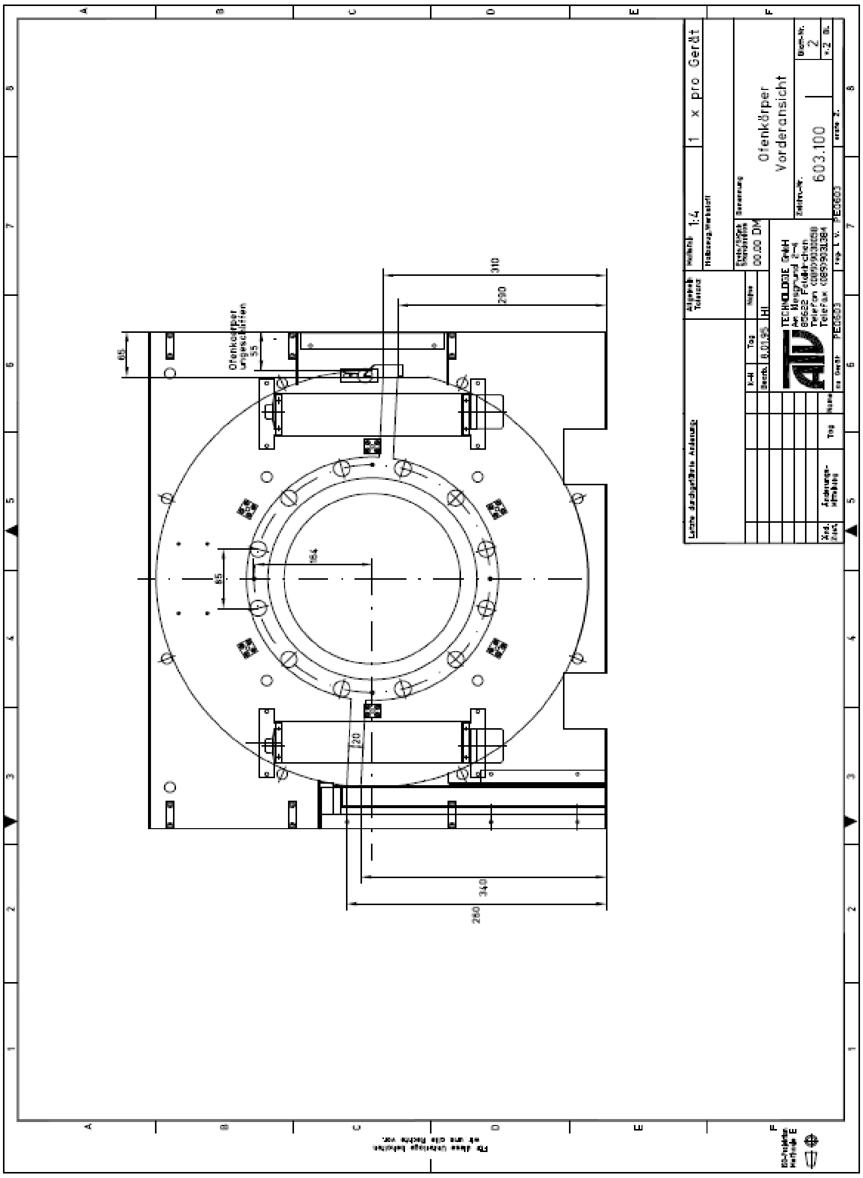

Figure C. 2 - Filament Positioning

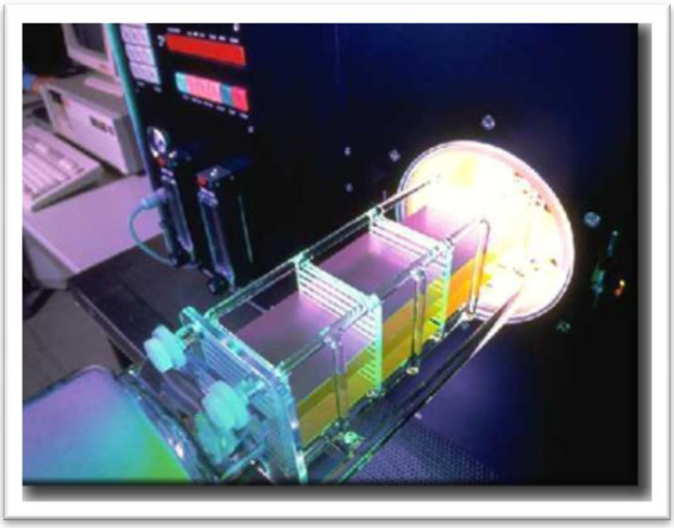

Figure C. 3 - Co-firing Oven (inside)

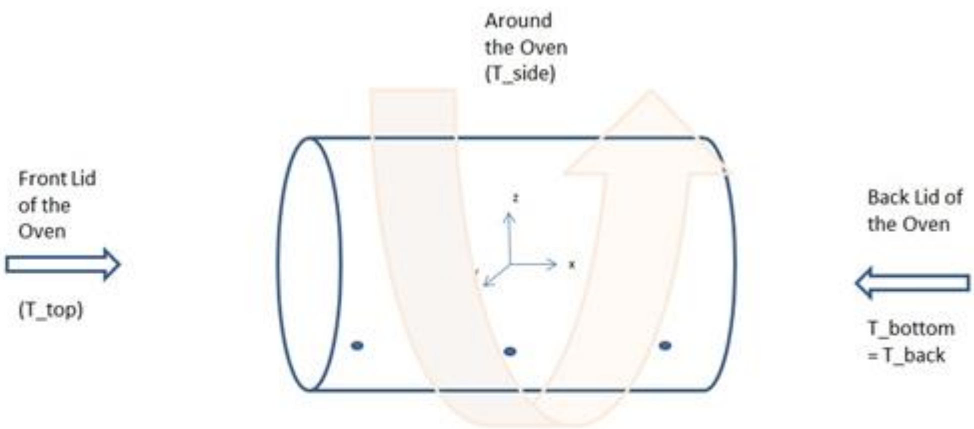

Figure C. 4 – Assignment of the Oven Temperatures

View Factors between (Fx_xx);

Oven \ TC	TC front		TC center		TC back	
	upper	Lower	upper	Lower	upper	Lower
Oven front	Ff_ft	Ff_fb	Fc_ft	Fc_fb	Fb_ft	Fb_fb
Oven sides	Ff_st	Ff_sb	Fc_st	Fc_sb	Fb_st	Fb_sb
Oven back	Ff_bt	Ff_bb	Fc_bt	Fc_bb	Fb_bt	Fb_bb

Fx_xx;
* First x: TC
* Second x: oven
* Third x: upper or lower surface of TCs

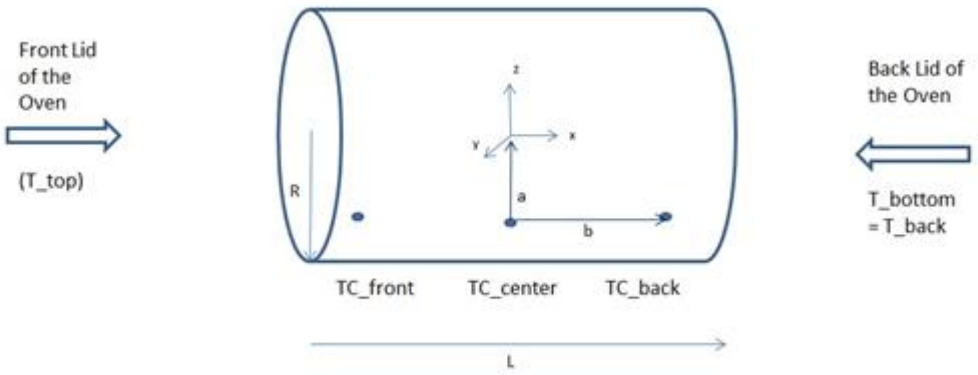

Figure C. 5 – Assignment of the View Factors

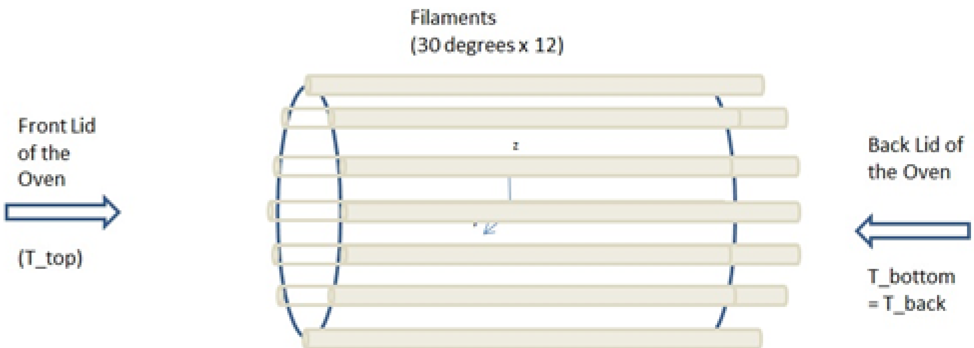

Figure C. 6 – Representation of the Heating Filaments

APPENDIX D. EXPERIMENTAL RESULTS

Note 1 – all time axes are in terms of seconds

Note 2 – filament power is % of maximum power

Note 3 – temperature axes are in terms of ºC

Run 01

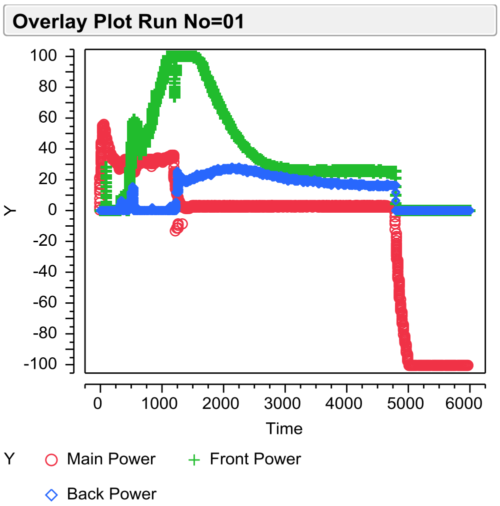

(a) Filament Power Trends

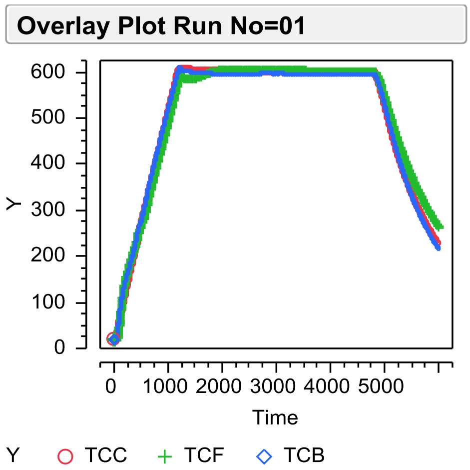

(b) Oven Thermocouple Temperatures Trends

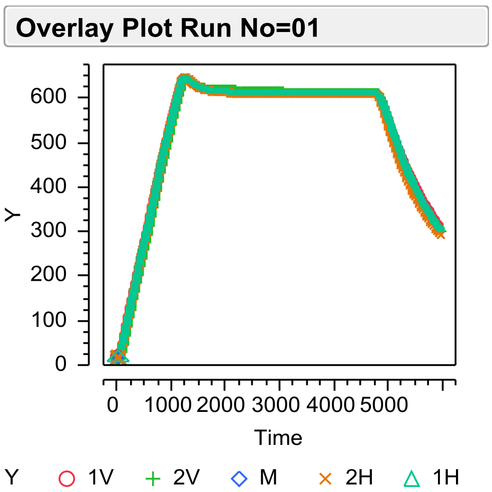

(c) Substrate Thermocouple Temperature Trends

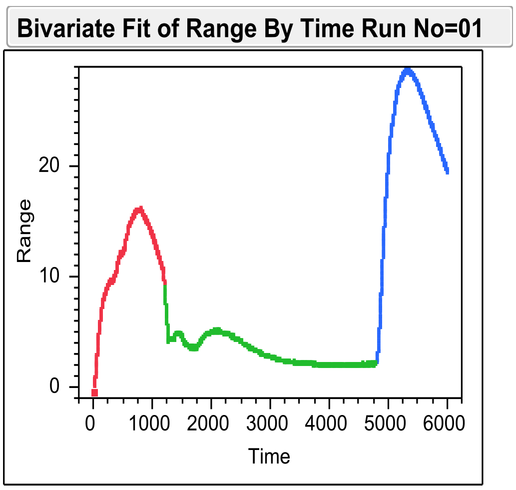

(d) Substrate Temperature Range Trends

Figure D. 1 - Trends for Run 01

Run 02

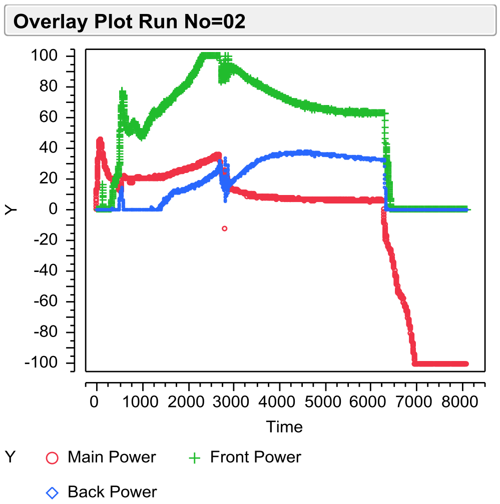

(a) Filament Power Trends

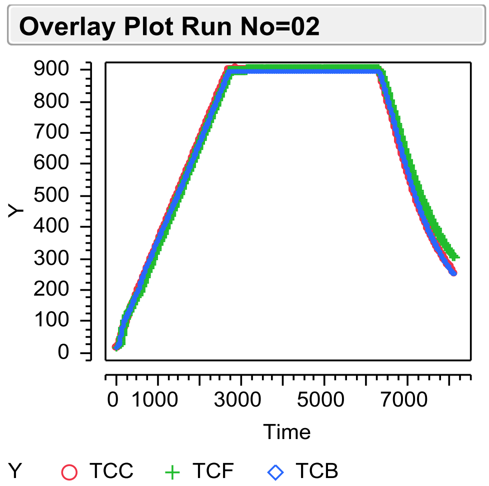

(b) Oven Thermocouple Temperatures Trends

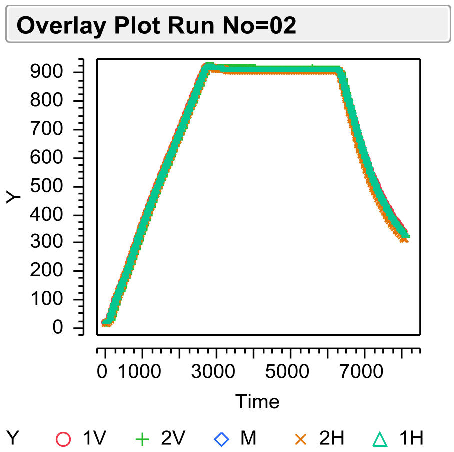

(c) Substrate Thermocouple Temperature Trends

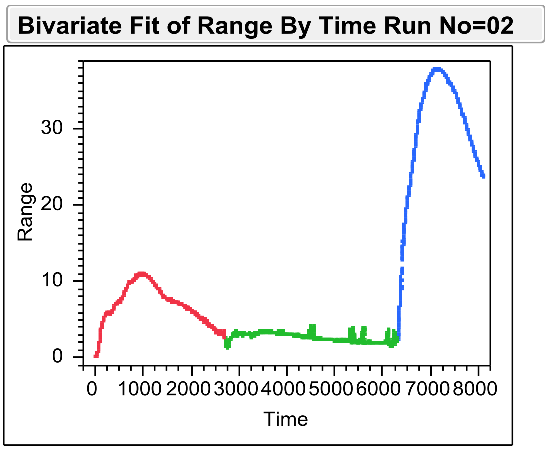

(d) Substrate Temperature Range Trends

Figure D. 2 - Trends for Run 02

Run 03

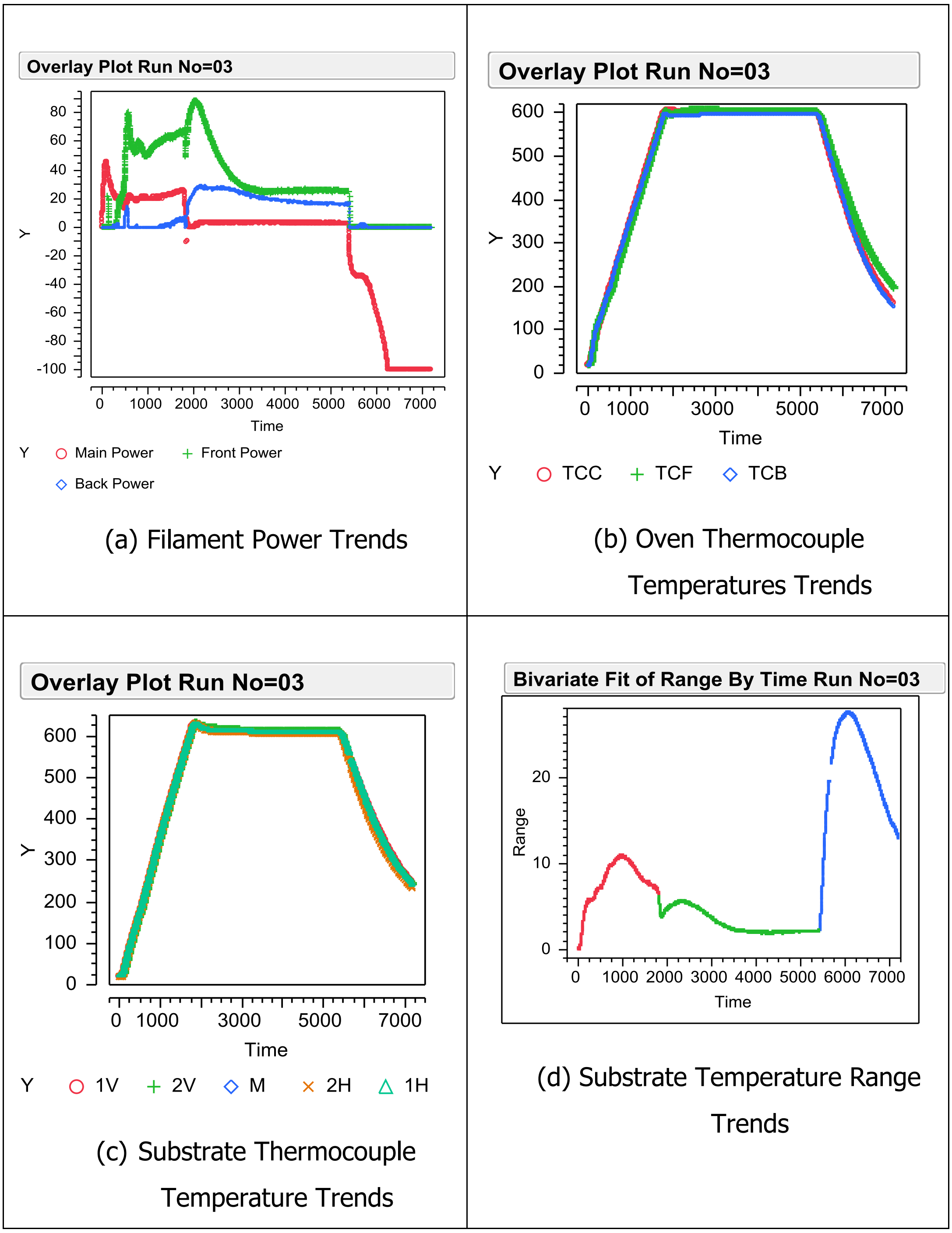

(a) Filament Power Trends

(b) Oven Thermocouple Temperatures Trends

(c) Substrate Thermocouple Temperature Trends

(d) Substrate Temperature Range Trends

Figure D. 3 – Trends for Run 03

Run 04

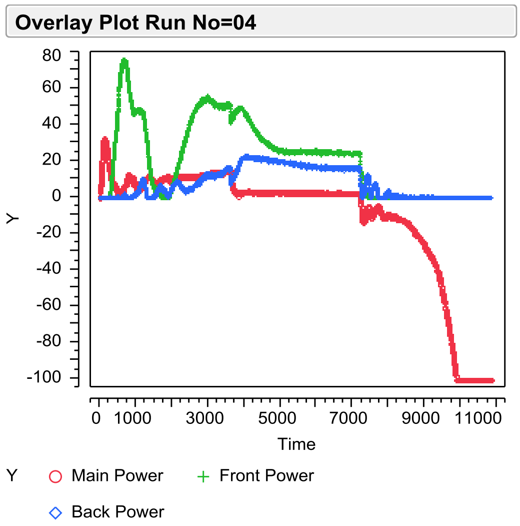

(a) Filament Power Trends

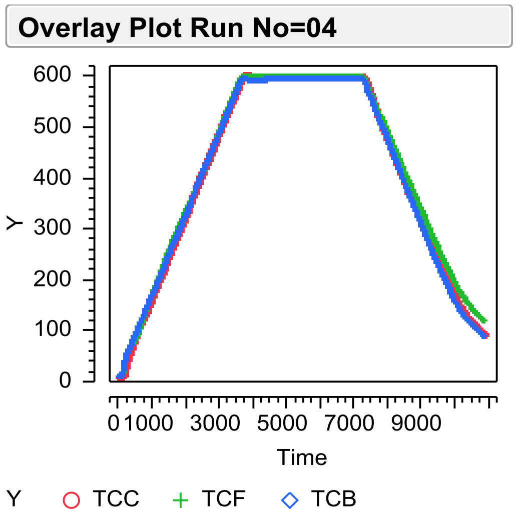

(b) Oven Thermocouple Temperatures Trends

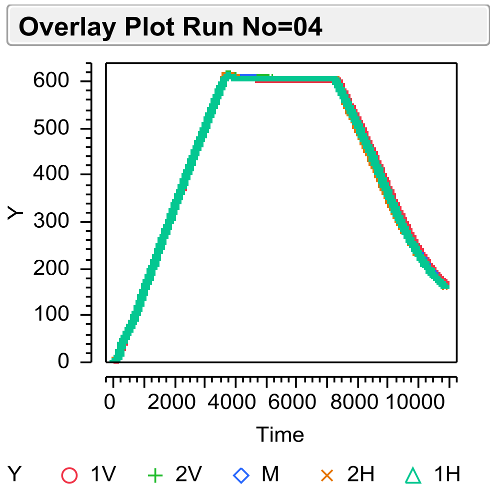

(c) Substrate Thermocouple Temperature Trends

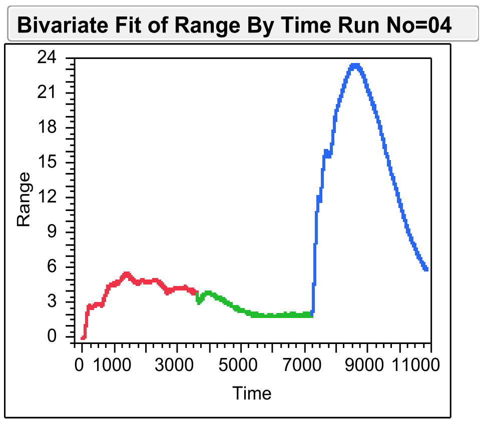

(d) Substrate Temperature Range Trends

Figure D. 4 – Trends for Run 04

Run 05

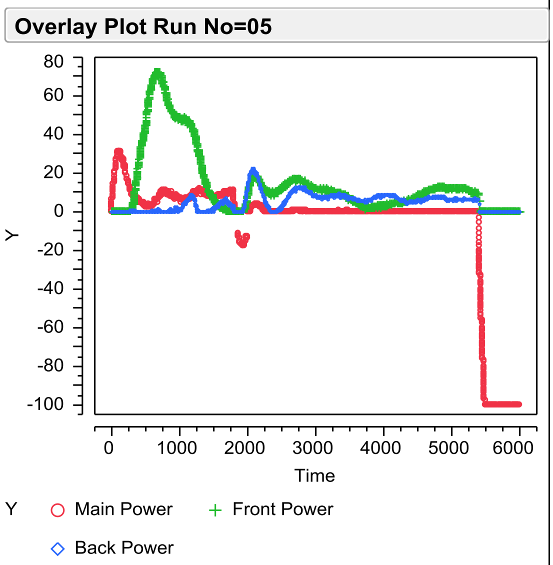

(a) Filament Power Trends

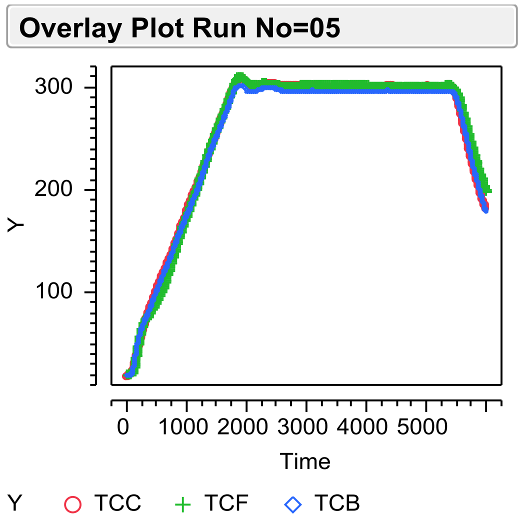

(b) Oven Thermocouple Temperatures Trends

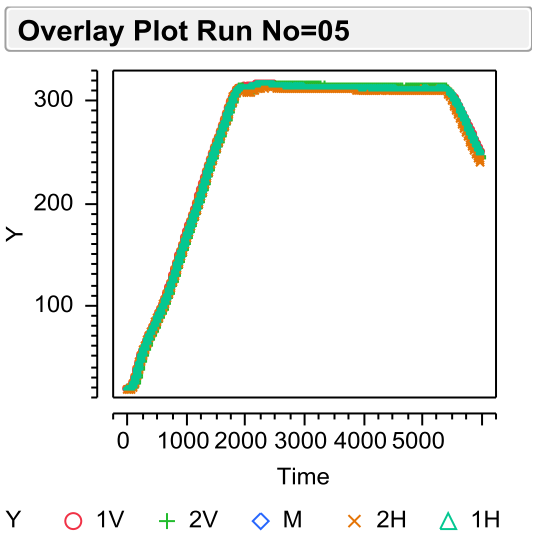

(c) Substrate Thermocouple Temperature Trends

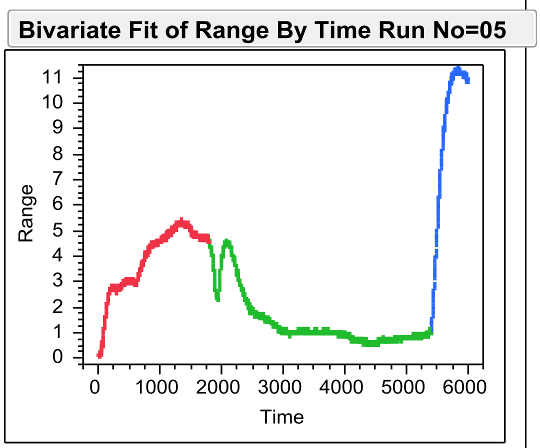

(d) Substrate Temperature Range Trends

Figure D. 5 – Trends for Run 05

Run 06

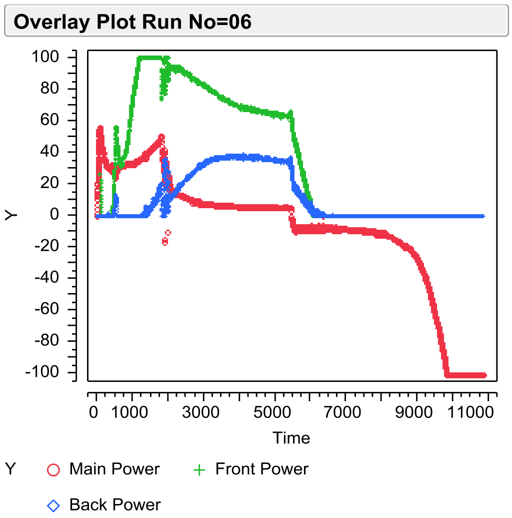

(a) Filament Power Trends

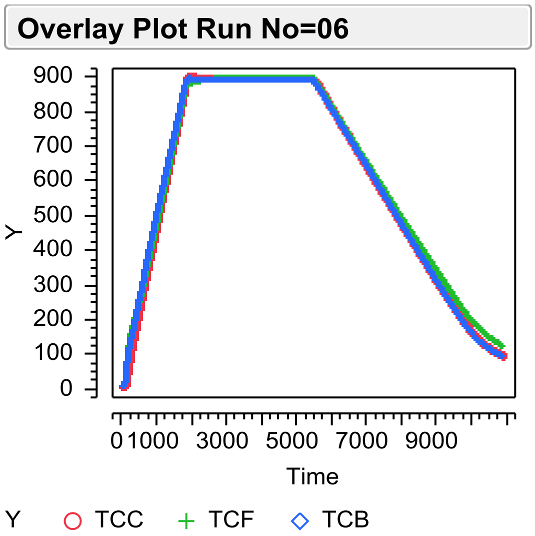

(b) Oven Thermocouple Temperatures Trends

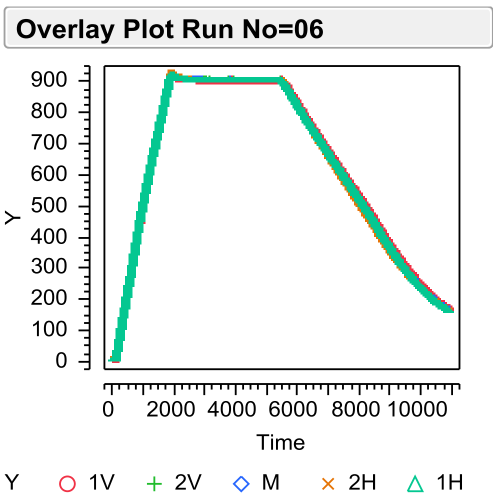

(c) Substrate Thermocouple Temperature Trends

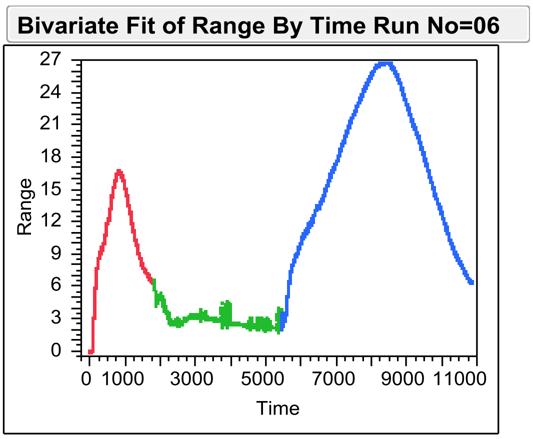

(d) Substrate Temperature Range Trends

Figure D. 6 – Trends for Run 06

Run 07

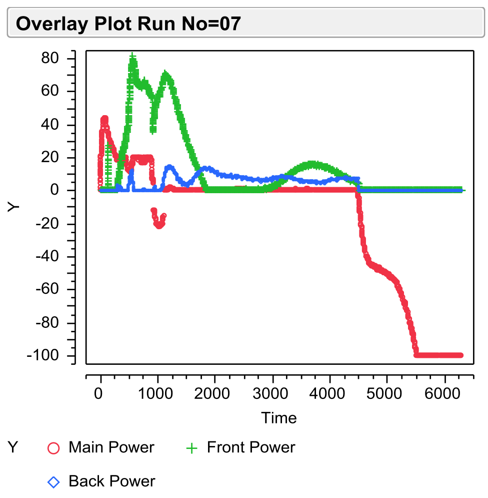

(a) Filament Power Trends

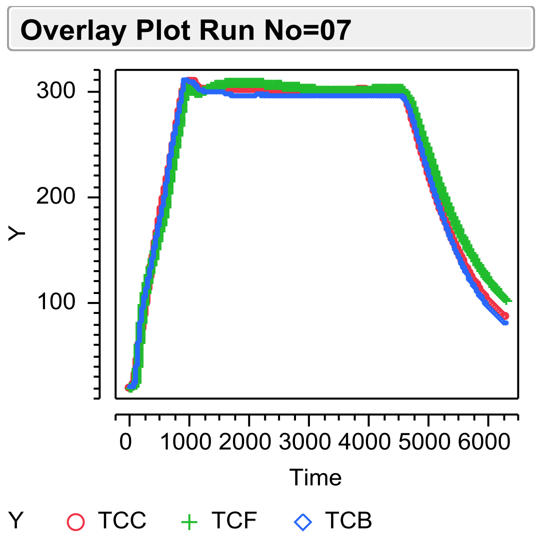

(b) Oven Thermocouple Temperatures Trends

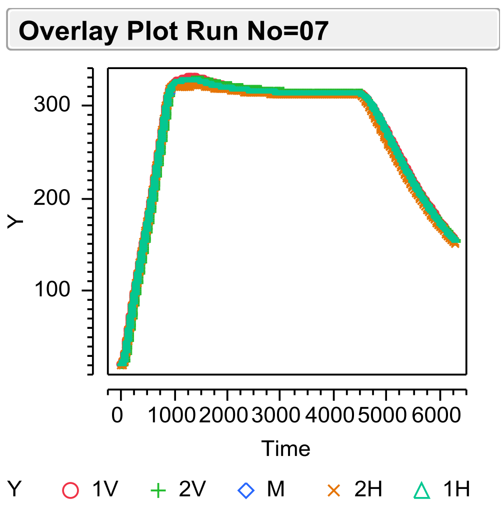

(c) Substrate Thermocouple Temperature Trends

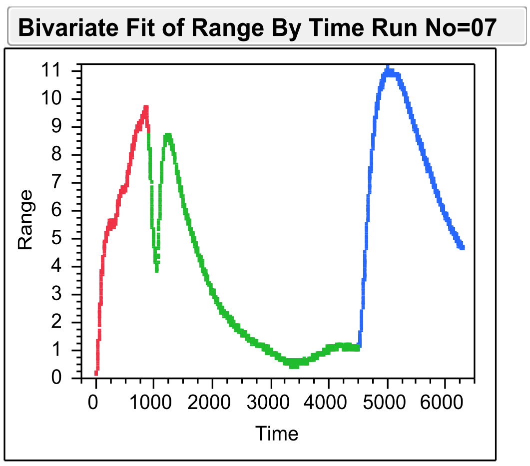

(d) Substrate Temperature Range Trends

Figure D. 7 - Trends for Run 07

Run 08

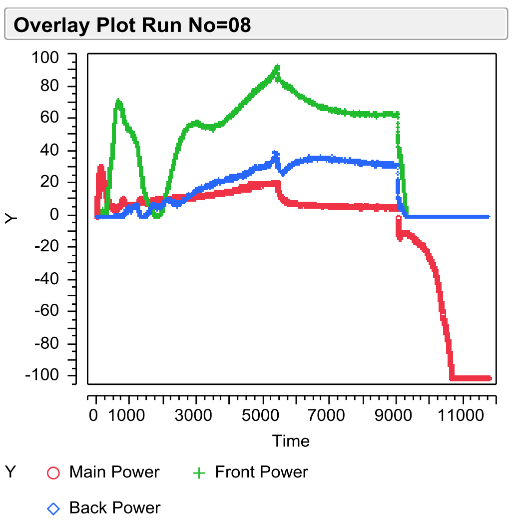

(a) Filament Power Trends

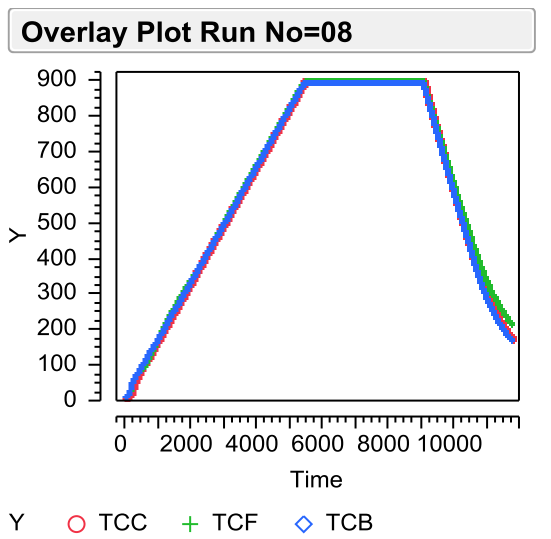

(b) Oven Thermocouple Temperatures Trends

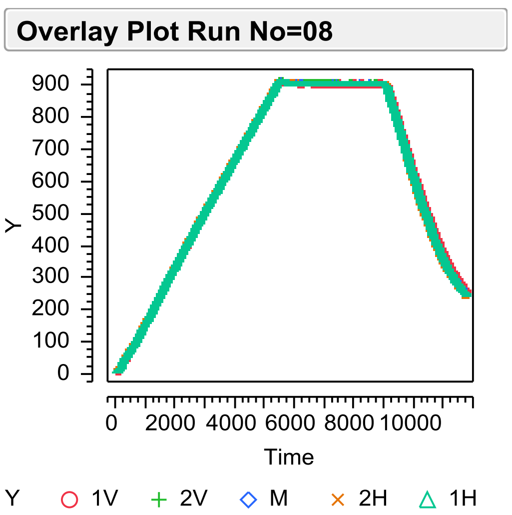

(c) Substrate Thermocouple Temperature Trends

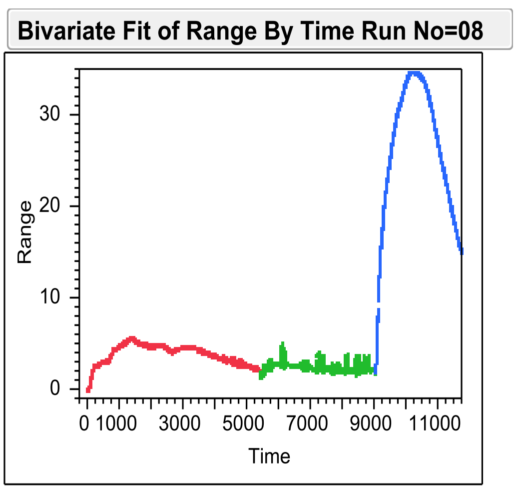

(d) Substrate Temperature Range Trends

Figure D. 8 – Trends for Run 08

Run 09

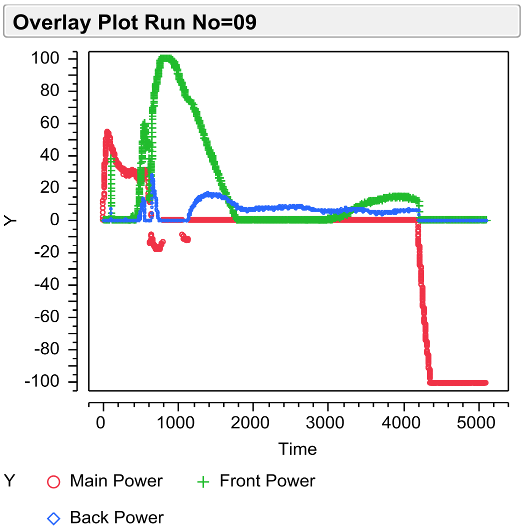

(a) Filament Power Trends

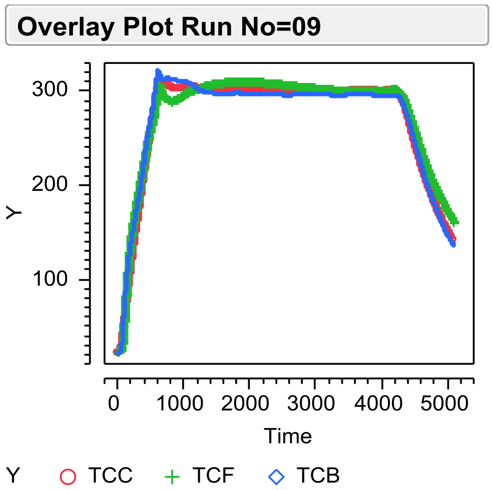

(b) Oven Thermocouple Temperatures Trends

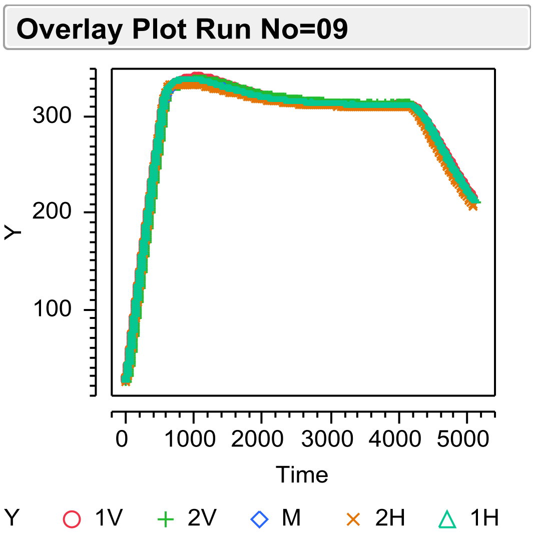

(c) Substrate Thermocouple Temperature Trends

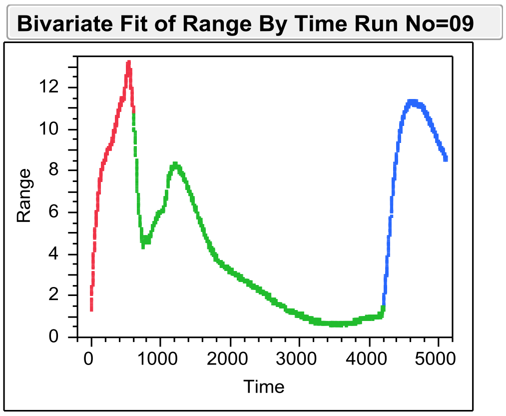

(d) Substrate Temperature Range Trends

Figure D. 9 – Trends for Run 09

Run 10

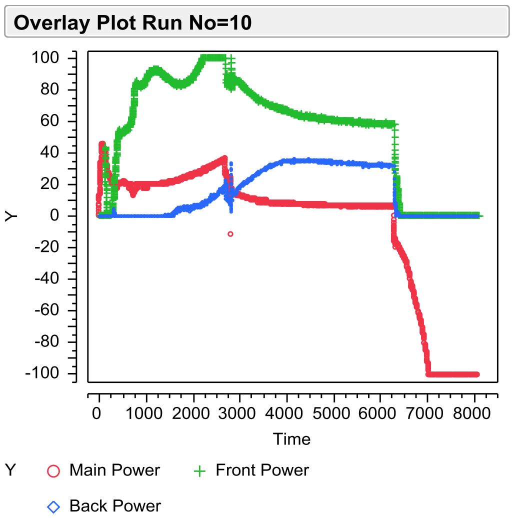

(a) Filament Power Trends

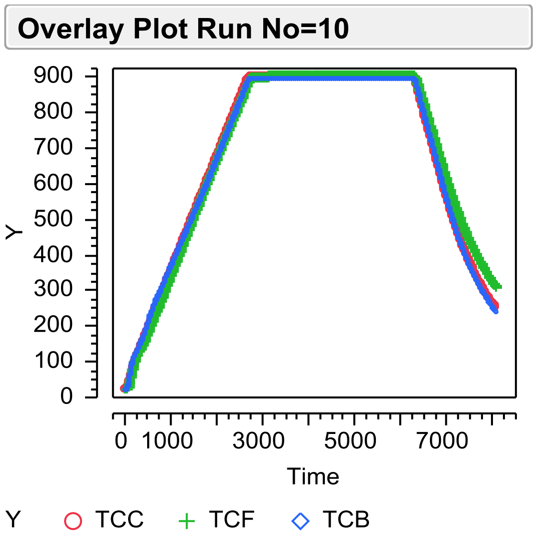

(b) Oven Thermocouple Temperatures Trends

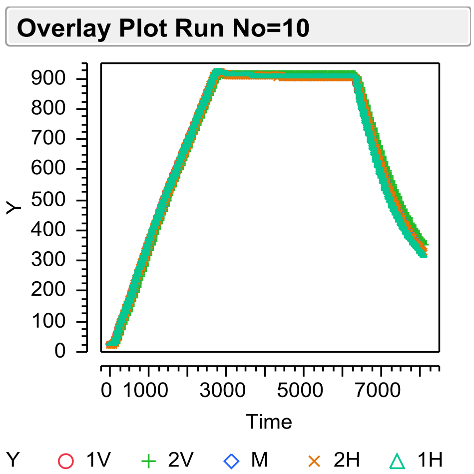

(c) Substrate Thermocouple Temperature Trends

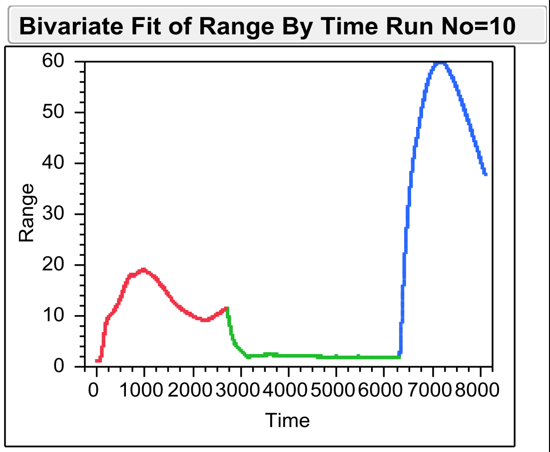

(d) Substrate Temperature Range Trends

Figure D. 10 – Trends for Run 10

Run 11

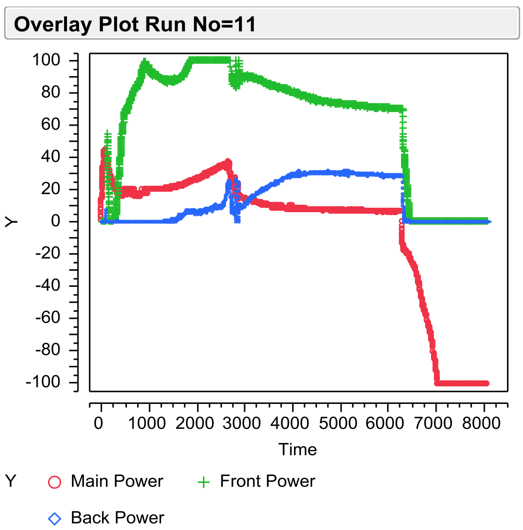

(a) Filament Power Trends

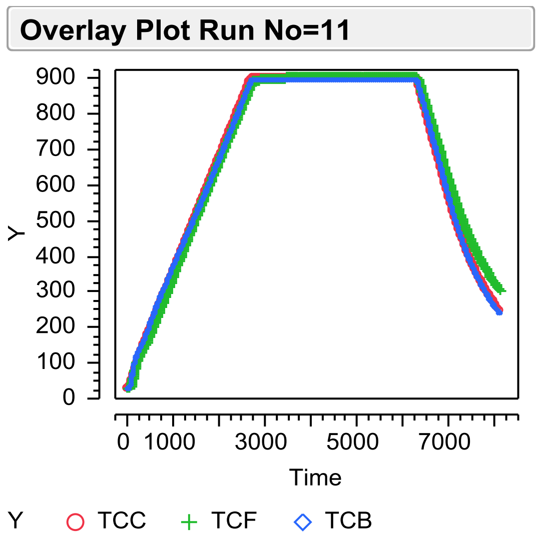

(b) Oven Thermocouple Temperatures Trends

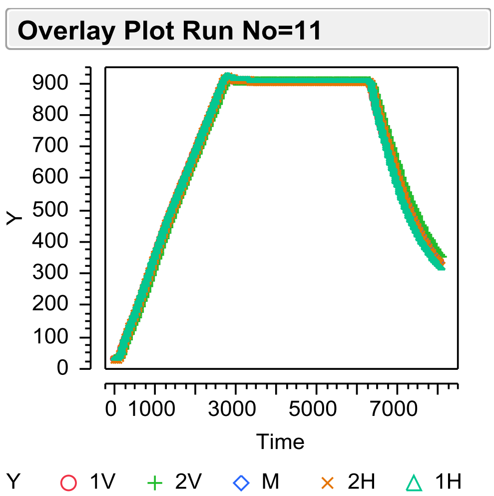

(c) Substrate Thermocouple Temperature Trends

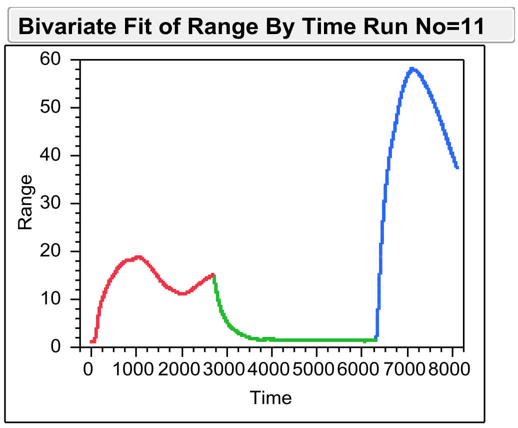

(d) Substrate Temperature Range Trends

Figure D. 11 – Trends for Run 11

Run 12

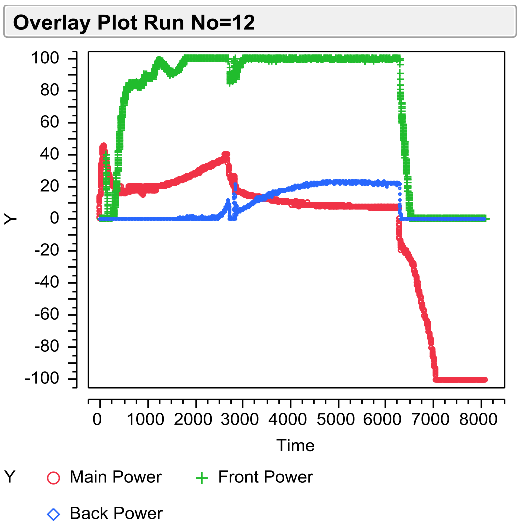

(a) Filament Power Trends

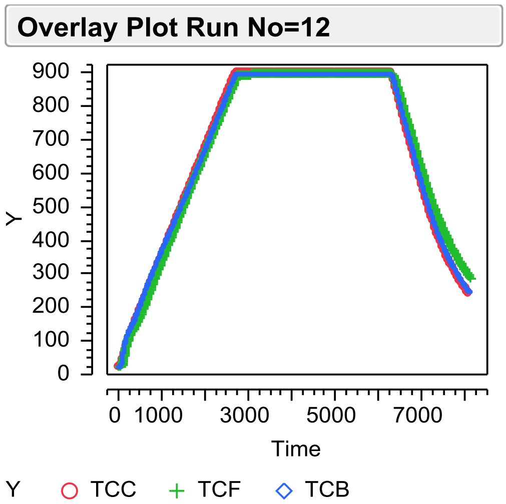

(b) Oven Thermocouple Temperatures Trends

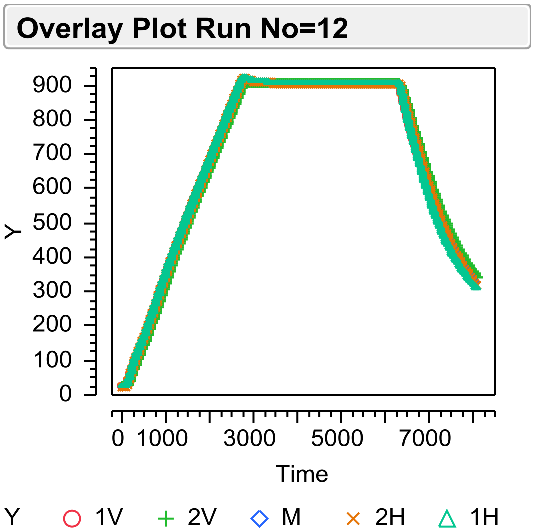

(c) Substrate Thermocouple Temperature Trends

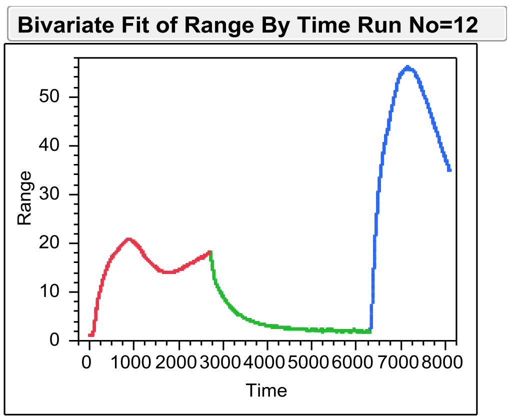

(d) Substrate Temperature Range Trends

Figure D. 12 - Trends for Run 12

Run 13

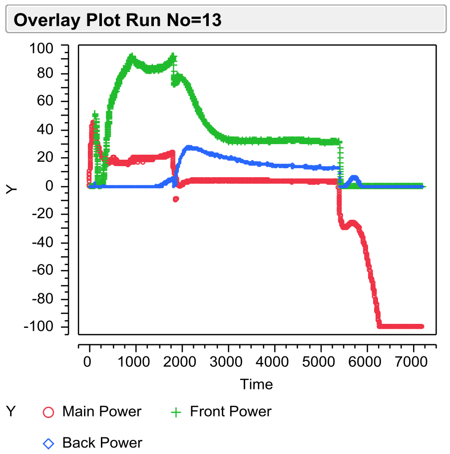

(a) Filament Power Trends

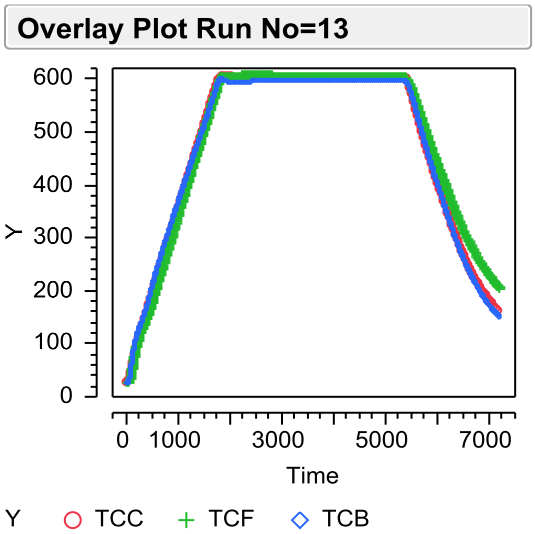

(b) Oven Thermocouple Temperatures Trends

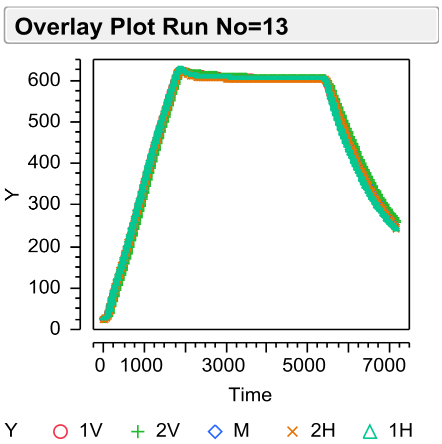

(c) Substrate Thermocouple Temperature Trends

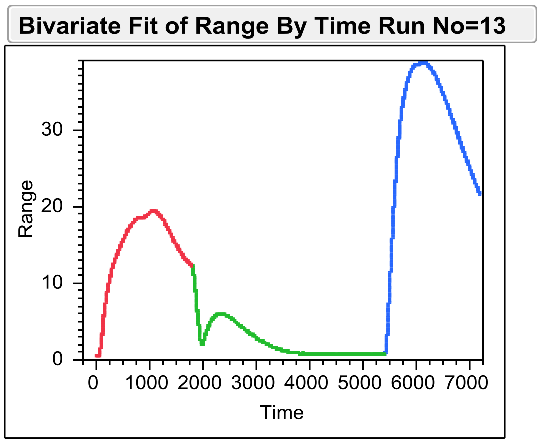

(d) Substrate Temperature Range Trends

Figure D. 13 - Trends for Run 13

APPENDIX E

ANSYS MODEL PREDICTIONS

(Note – this is an ANSYS standard output for one of the many simulations executed)

ANSYS

Project

First Saved	Wednesday, August 29, 2012
Last Saved	Sunday, September 02, 2012
Product Version	13.0 Release

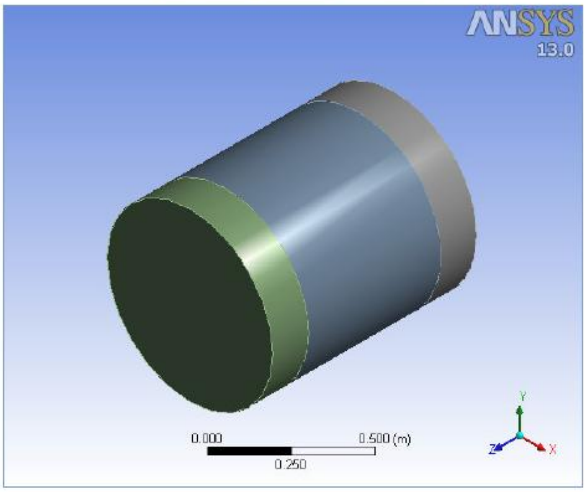

Contents

Units

TABLE 1

Unit System	Metric (m, kg, N, s, V, A) Degrees rad/s Celsius
Angle	Degrees
Rotational Velocity	rad/s
Temperature	Celsius

Model (A4)

Geometry

TABLE 2
Model (A4) > Geometry

Object Name	Geometry
State	Fully Defined
Definition	
Source	C:\Documents and Settings\User\Desktop\LTCC Oven Simulations\Dynamic Oven Simulation\Dynamic Oven Simulation_dp39_files\dp0\SYS\DM\SYS.agdb
Type	DesignModeler
Length Unit	Millimeters
Element Control	Manual
Display Style	Part Color
Bounding Box	
Length X	0.698 m
Length Y	0.698 m
Length Z	0.857 m
Properties	
Volume	0.27833 m³
Mass	144.13 kg
Scale Factor Value	1.
Statistics	
Bodies	39
Active Bodies	39
Nodes	26059
Elements	4773
Mesh Metric	None
Preferences	
Parameter Processing	Yes
Personal Parameter Key	DS
CAD Attribute Transfer	No
Named Selection Processing	No
Material Properties Transfer	No
CAD Associativity	Yes
Import Coordinate Systems	Yes
Reader Save Part File	No
Import Using Instances	Yes
Do Smart Update	No
Attach File Via Temp File	Yes
Temporary Directory	C:\Documents and Settings\User\Local Settings\Temp
Analysis Type	3-D
Enclosure and Symmetry Processing	Yes

TABLE 3
Model (A4) > Geometry > Parts

Object Name	*Substrate*
State	Meshed
Graphics Properties	
Visible	Yes
Transparency	1
Definition	
Suppressed	No
Stiffness Behavior	Flexible
Brick Integration Scheme	Full
Coordinate System	Default Coordinate System
Reference Temperature	By Environment
Material	
Assignment	Alumina
Nonlinear Effects	Yes
Thermal Strain Effects	Yes
Bounding Box	
Length X	0.2 m
Length Y	1.e-002 m
Length Z	0.2 m
Properties	
Volume	4.e-004 m³
Mass	1.58 kg
Centroid X	-6.17e-017 m
Centroid Y	5.e-003 m
Centroid Z	0. m
Moment of Inertia Ip1	5.2798e-003 kg·m²
Moment of Inertia Ip2	1.0533e-002 kg·m²
Moment of Inertia Ip3	5.2798e-003 kg·m²
Statistics	
Nodes	416
Elements	49
Mesh Metric	None

TABLE 4
Model (A4) > Geometry > Body Groups

Object Name	*Front_Filaments*	*Main_Filaments*	*Back_Filaments*
State	Meshed		
Graphics Properties			
Visible	Yes		
Definition			
Suppressed	No		
Assignment	Kanthal		
Coordinate System	Default Coordinate System		
Bounding Box			
Length X	0.29156 m	0.33682 m	0.29156 m
Length Y	0.29156 m	0.33682 m	0.29156 m
Length Z	4.e-003 m	0.507 m	4.e-003 m
Properties			
Volume	6.434e-005 m³	1.9113e-003 m³	6.434e-005 m³
Mass	0.3603 kg	10.704 kg	0.3603 kg
Centroid X	-6.3326e-009 m	5.0182e-017 m	-6.3326e-009 m
Centroid Y	-2.2513e-016 m	1.954e-017 m	1.6126e-016 m
Centroid Z	0.2515 m	-3.2099e-017 m	-0.2515 m
Moment of Inertia Ip1	2.089e-003 kg·m²	0.37232 kg·m²	2.089e-003 kg·m²
Moment of Inertia Ip2	2.089e-003 kg·m²	0.37232 kg·m²	2.089e-003 kg·m²
Moment of Inertia Ip3	4.177e-003 kg·m²	0.28841 kg·m²	4.177e-003 kg·m²
Statistics			
Nodes	1606	1680	1606
Elements	143	132	143
Mesh Metric	None		

TABLE 5

Model (A4) > Geometry > Front_Filaments > Parts

Object Name	*Solid*	*Solid*	*Solid*	*Solid*	*Solid*
State	Meshed				
Graphics Properties					
Visible	Yes				
Transparency	1				
Definition					
Suppressed	No				
Stiffness Behavior	Flexible				
Brick Integration Scheme	Full				
Coordinate System	Default Coordinate System				
Reference Temperature	By Environment				
Material					
Assignment	Kanthal				
Nonlinear Effects	Yes				
Thermal Strain Effects	Yes				
Bounding Box					
Length X	0.29156 m	7.2889e-002 m	0.10933 m	0.14578 m	0.18222 m
Length Y	0.29156 m	7.2889e-002 m	0.10933 m	0.14578 m	0.18222 m
Length Z	4.e-003 m				
Properties					
Volume	1.4454e-005 m³	3.4627e-006 m³	5.2946e-006 m³	7.1265e-006 m³	8.9584e-006 m³
Mass	8.0943e-002 kg	1.9391e-002 kg	2.965e-002 kg	3.9909e-002 kg	5.0167e-002 kg
Centroid X	-8.7305e-009 m	-7.4005e-017 m	-2.256e-017 m	-8.5234e-009 m	-6.4007e-009 m
Centroid Y	-4.2181e-016 m	5.1764e-017 m	-1.2981e-016 m	-2.2336e-016 m	4.9002e-016 m
Centroid Z	0.2515 m				
Moment of Inertia Ip1	8.3468e-004 kg·m²	1.1451e-005 kg·m²	4.0804e-005 kg·m²	9.9807e-005 kg·m²	1.9843e-004 kg·m²
Moment of Inertia Ip2	8.3468e-004 kg·m²	1.1451e-005 kg·m²	4.0804e-005 kg·m²	9.9807e-005 kg·m²	1.9843e-004 kg·m²
Moment of Inertia Ip3	1.6691e-003 kg·m²	2.2851e-005 kg·m²	8.1529e-005 kg·m²	1.9951e-004 kg·m²	3.9673e-004 kg·m²
Statistics					
Nodes	336	103	144	189	192
Elements	28	9	12	17	16
Mesh Metric	None				

TABLE 6

Model (A4) > Geometry > Front_Filaments > Parts

Object Name	*Solid*	*Solid*	*Solid*
State	Meshed		
Graphics Properties			
Visible	Yes		
Transparency	1		
Definition			
Suppressed	No		
Stiffness Behavior	Flexible		
Brick Integration Scheme	Full		
Coordinate System	Default Coordinate System		
Reference Temperature	By Environment		
Material			
Assignment	Kanthal		
Nonlinear Effects	Yes		
Thermal Strain Effects	Yes		
Bounding Box			
Length X	0.21867 m	0.25511 m	3.6444e-002 m
Length Y	0.21867 m	0.25511 m	3.6444e-002 m
Length Z	4.e-003 m		
Properties			
Volume	1.079e-005 m³	1.2622e-005 m³	1.6308e-006 m³
Mass	6.0426e-002 kg	7.0684e-002 kg	9.1327e-003 kg
Centroid X	1.7708e-008 m	-2.8064e-008 m	-2.464e-018 m
Centroid Y	-9.2317e-016 m	-6.2698e-017 m	4.5938e-017 m
Centroid Z	0.2515 m		
Moment of Inertia Ip1	3.4695e-004 kg·m²	5.5562e-004 kg·m²	1.2197e-006 kg·m²
Moment of Inertia Ip2	3.4695e-004 kg·m²	5.5562e-004 kg·m²	1.2197e-006 kg·m²
Moment of Inertia Ip3	6.9374e-004 kg·m²	1.1111e-003 kg·m²	2.4152e-006 kg·m²
Statistics			
Nodes	240	288	114
Elements	20	24	17
Mesh Metric	None		

TABLE 7
Model (A4) > Geometry > Main_Filaments > Parts

Object Name	*Solid*	*Solid*	*Solid*	*Solid*	*Solid*
State	Meshed				
Graphics Properties					
Visible	Yes				
Transparency	1				
Definition					
Suppressed	No				
Stiffness Behavior	Flexible				
Brick Integration Scheme	Full				
Coordinate System	Default Coordinate System				
Reference Temperature	By Environment				
Material					
Assignment	Kanthal				
Nonlinear Effects	Yes				
Thermal Strain Effects	Yes				
Bounding Box					
Length X	2.e-002 m				
Length Y	2.e-002 m				
Length Z	0.507 m				
Properties					
Volume	1.5928e-004 m³				
Mass	0.89196 kg				
Centroid X	-0.11597 m		-0.15841 m		-4.2446e-002 m
Centroid Y	0.11597 m	-0.11597 m	-4.2446e-002 m	4.2446e-002 m	0.15841 m
Centroid Z	-4.4444e-017 m	-2.4438e-016 m	-8.3403e-016 m	8.3942e-016 m	-7.4882e-016 m
Moment of Inertia Ip1	1.9032e-002 kg·m²				
Moment of Inertia Ip2	1.9032e-002 kg·m²				
Moment of Inertia Ip3	4.4147e-005 kg·m²				
Statistics					
Nodes	140				
Elements	11				
Mesh Metric	None				

TABLE 8
Model (A4) > Geometry > Main_Filaments > Parts

Object Name	*Solid*	*Solid*	*Solid*	*Solid*	*Solid*
State	Meshed				
Graphics Properties					
Visible	Yes				
Transparency	1				
Definition					
Suppressed	No				
Stiffness Behavior	Flexible				
Brick Integration Scheme	Full				
Coordinate System	Default Coordinate System				
Reference Temperature	By Environment				
Material					
Assignment	Kanthal				
Nonlinear Effects	Yes				
Thermal Strain Effects	Yes				
Bounding Box					
Length X	2.e-002 m				
Length Y	2.e-002 m				
Length Z	0.507 m				
Properties					
Volume	1.5928e-004 m³				
Mass	0.89196 kg				
Centroid X	4.2446e-002 m	0.11597 m	0.15841 m		0.11597 m
Centroid Y	0.15841 m	0.11597 m	4.2446e-002 m	-4.2446e-002 m	-0.11597 m
Centroid Z	7.5225e-016 m	2.2847e-016 m	-8.2583e-016 m	8.9194e-016 m	-3.1001e-016 m
Moment of Inertia Ip1	1.9032e-002 kg·m²				
Moment of Inertia Ip2	1.9032e-002 kg·m²				
Moment of Inertia Ip3	4.4147e-005 kg·m²				
Statistics					
Nodes	140				
Elements	11				
Mesh Metric	None				

TABLE 9
Model (A4) > Geometry > Main_Filaments > Parts

Object Name	*Solid*	*Solid*
State	Meshed	
Graphics Properties		
Visible	Yes	
Transparency	1	
Definition		
Suppressed	No	
Stiffness Behavior	Flexible	
Brick Integration Scheme	Full	
Coordinate System	Default Coordinate System	
Reference Temperature	By Environment	
Material		
Assignment	Kanthal	
Nonlinear Effects	Yes	
Thermal Strain Effects	Yes	
Bounding Box		
Length X	2.e-002 m	
Length Y	2.e-002 m	
Length Z	0.507 m	
Properties		
Volume	1.5928e-004 m^3	
Mass	0.89196 kg	
Centroid X	4.2446e-002 m	-4.2446e-002 m
Centroid Y	-0.15841 m	
Centroid Z	-9.2843e-016 m	8.3868e-016 m
Moment of Inertia Ip1	1.9032e-002 kg·m^2	
Moment of Inertia Ip2	1.9032e-002 kg·m^2	
Moment of Inertia Ip3	4.4147e-005 kg·m^2	
Statistics		
Nodes	140	
Elements	11	
Mesh Metric	None	

TABLE 10
Model (A4) > Geometry > Back_Filaments > Parts

Object Name	*Solid*	*Solid*	*Solid*	*Solid*	*Solid*
State	Meshed				
Graphics Properties					
Visible	Yes				
Transparency	1				
Definition					
Suppressed	No				
Stiffness Behavior	Flexible				
Brick Integration Scheme	Full				
Coordinate System	Default Coordinate System				
Reference Temperature	By Environment				
Material					
Assignment	Kanthal				
Nonlinear Effects	Yes				
Thermal Strain Effects	Yes				
Bounding Box					
Length X	0.29156 m	7.2889e-002 m	0.10933 m	0.14578 m	0.18222 m
Length Y	0.29156 m	7.2889e-002 m	0.10933 m	0.14578 m	0.18222 m
Length Z	4.e-003 m				
Properties					
Volume	1.4454e-005 m^3	3.4627e-006 m^3	5.2946e-006 m^3	7.1265e-006 m^3	8.9584e-006 m^3
Mass	8.0943e-002 kg	1.9391e-002 kg	2.965e-002 kg	3.9909e-002 kg	5.0167e-002 kg
Centroid X	-8.7305e-009 m	1.9887e-017 m	-4.6271e-017 m	-8.5234e-009 m	-6.4007e-009 m
Centroid Y	2.1577e-016 m	7.0056e-017 m	1.5659e-016 m	6.2714e-017 m	-5.3486e-017 m
Centroid Z	-0.2515 m				
Moment of Inertia Ip1	8.3468e-004 kg·m^2	1.1451e-005 kg·m^2	4.0804e-005 kg·m^2	9.9807e-005 kg·m^2	1.9843e-004 kg·m^2
Moment of Inertia Ip2	8.3468e-004 kg·m^2	1.1451e-005 kg·m^2	4.0804e-005 kg·m^2	9.9807e-005 kg·m^2	1.9843e-004 kg·m^2
Moment of Inertia Ip3	1.6691e-003 kg·m^2	2.2851e-005 kg·m^2	8.1529e-005 kg·m^2	1.9951e-004 kg·m^2	3.9673e-004 kg·m^2
Statistics					
Nodes	336	103	144	189	192
Elements	28	9	12	17	16
Mesh Metric	None				

TABLE 11
Model (A4) > Geometry > Back_Filaments > Parts

Object Name	*Solid*	*Solid*	*Solid*
State	Meshed		
Graphics Properties			
Visible	Yes		
Transparency	1		
Definition			
Suppressed	No		
Stiffness Behavior	Flexible		
Brick Integration Scheme	Full		
Coordinate System	Default Coordinate System		
Reference Temperature	By Environment		
Material			
Assignment	Kanthal		
Nonlinear Effects	Yes		
Thermal Strain Effects	Yes		
Bounding Box			
Length X	0.21867 m	0.25511 m	3.6444e-002 m
Length Y	0.21867 m	0.25511 m	3.6444e-002 m
Length Z	4.e-003 m		
Properties			
Volume	1.079e-005 m^3	1.2622e-005 m^3	1.6308e-006 m^3
Mass	6.0426e-002 kg	7.0684e-002 kg	9.1327e-003 kg
Centroid X	1.7708e-008 m	-2.8064e-008 m	-9.272e-018 m
Centroid Y	8.111e-016 m	-1.9867e-016 m	-1.6851e-017 m
Centroid Z	-0.2515 m		
Moment of Inertia Ip1	3.4695e-004 kg·m^2	5.5562e-004 kg·m^2	1.2197e-006 kg·m^2
Moment of Inertia Ip2	3.4695e-004 kg·m^2	5.5562e-004 kg·m^2	1.2197e-006 kg·m^2
Moment of Inertia Ip3	6.9374e-004 kg·m^2	1.1111e-003 kg·m^2	2.4152e-006 kg·m^2
Statistics			
Nodes	240	288	114
Elements	20	24	17
Mesh Metric	None		

TABLE 12
Model (A4) > Geometry > Parts

Object Name	*TCC*	*TCB*	*TCF*
State	Meshed		
Graphics Properties			
Visible	Yes		
Transparency	1		
Definition			
Suppressed	No		
Stiffness Behavior	Flexible		
Brick Integration Scheme	Full		
Coordinate System	Default Coordinate System		
Reference Temperature	By Environment		
Material			
Assignment	K-type TC		
Nonlinear Effects	Yes		
Thermal Strain Effects	Yes		
Bounding Box			
Length X	2.e-003 m		
Length Y	2.e-003 m		
Length Z	2.e-003 m		
Properties			
Volume	8.e-009 m³		
Mass	6.984e-005 kg		
Centroid X	-1.5728e-019 m	6.3635e-016 m	-4.1999e-016 m
Centroid Y	-9.e-002 m		
Centroid Z	-6.0137e-020 m	-0.225 m	0.225 m
Moment of Inertia Ip1	4.656e-011 kg·m²		
Moment of Inertia Ip2	4.656e-011 kg·m²		
Moment of Inertia Ip3	4.656e-011 kg·m²		
Statistics			
Nodes	756		
Elements	125		
Mesh Metric	None		

TABLE 13
Model (A4) > Geometry > Body Groups

Object Name	*Quartz_Tube*	*Insulation*
State	Meshed	
Graphics Properties		
Visible	Yes	
Definition		
Suppressed	No	
Assignment	Quartz	Insulation
Coordinate System	Default Coordinate System	
Bounding Box		
Length X	0.398 m	0.698 m
Length Y	0.398 m	0.698 m
Length Z	0.557 m	0.857 m
Properties		
Volume	1.7255e-002 m³	0.25863 m³
Mass	38.014 kg	93.108 kg
Centroid X	-1.4211e-016 m	-1.3054e-018 m
Centroid Y	6.2248e-018 m	-8.1446e-018 m
Centroid Z	4.1535e-016 m	5.6843e-017 m
Moment of Inertia Ip1	1.9772 kg·m²	9.8873 kg·m²
Moment of Inertia Ip2	1.9792 kg·m²	9.8873 kg·m²
Moment of Inertia Ip3	1.176 kg·m²	6.628 kg·m²
Statistics		
Nodes	11013	7470
Elements	2467	1464
Mesh Metric	None	

TABLE 14
Model (A4) > Geometry > Quartz_Tube > Parts

Object Name	*Left_Quartz*	*Back_Quartz*	*Right_Quartz*	*Front_Quartz*
State	Meshed			
Graphics Properties				
Visible	Yes			
Transparency	1			
Definition				
Suppressed	No			
Stiffness Behavior	Flexible			
Brick Integration Scheme	Full			
Coordinate System	Default Coordinate System			
Reference Temperature	By Environment			
Material				
Assignment	Quartz			
Nonlinear Effects	Yes			
Thermal Strain Effects	Yes			
Bounding Box				
Length X	0.199 m	0.398 m	0.199 m	0.398 m
Length Y	0.398 m			
Length Z	0.517 m	2.e-002 m	0.517 m	2.e-002 m
Properties				
Volume	6.1395e-003 m³	2.4882e-003 m³	6.1395e-003 m³	2.4882e-003 m³
Mass	13.525 kg	5.4815 kg	13.525 kg	5.4815 kg
Centroid X	-0.12013 m	-2.6836e-017 m	0.12013 m	-2.5833e-017 m
Centroid Y	-1.8913e-017 m	6.4205e-017 m	7.42e-018 m	7.3203e-018 m
Centroid Z	-3.6113e-018 m	-0.2685 m	2.907e-017 m	0.2685 m
Moment of Inertia Ip1	0.53953 kg·m²	5.3902e-002 kg·m²	0.53953 kg·m²	5.3902e-002 kg·m²
Moment of Inertia Ip2	0.34534 kg·m²	5.3902e-002 kg·m²	0.34534 kg·m²	5.3902e-002 kg·m²
Moment of Inertia Ip3	0.2854 kg·m²	0.10744 kg·m²	0.2854 kg·m²	0.10744 kg·m²
Statistics				
Nodes	4565	1501	4247	1466
Elements	616	649	572	630
Mesh Metric	None			

TABLE 15
Model (A4) > Geometry > Insulation > Parts

Object Name	*Back_Insulation*	*Side_Insulation*	*Front_Insulation*
State	Meshed		
Graphics Properties			
Visible	Yes		
Transparency	1		
Definition			
Suppressed	No		
Stiffness Behavior	Flexible		
Brick Integration Scheme	Full		
Coordinate System	Default Coordinate System		
Reference Temperature	By Environment		
Material			
Assignment	Insulation		
Nonlinear Effects	Yes		
Thermal Strain Effects	Yes		
Bounding Box			
Length X	0.698 m		
Length Y	0.698 m		
Length Z	0.15 m	0.557 m	0.15 m
Properties			
Volume	5.7397e-002 m³	0.14384 m³	5.7397e-002 m³
Mass	20.663 kg	51.782 kg	20.663 kg
Centroid X	-1.1014e-017 m	5.0674e-018 m	-7.5672e-018 m
Centroid Y	-3.0388e-018 m	-1.0499e-017 m	-7.3497e-018 m
Centroid Z	-0.3535 m	1.2287e-017 m	0.3535 m
Moment of Inertia Ip1	0.66138 kg·m²	3.4003 kg·m²	0.66138 kg·m²
Moment of Inertia Ip2	0.66138 kg·m²	3.4003 kg·m²	0.66138 kg·m²
Moment of Inertia Ip3	1.2457 kg·m²	4.1366 kg·m²	1.2457 kg·m²
Statistics			
Nodes	2065	3932	2065
Elements	372	720	372
Mesh Metric	None		

TABLE 16
Model (A4) > Coordinate Systems > Coordinate System

Object Name	*Global Coordinate System*	*Front_Filament_Plane*	*H1_plane*	*H2_plane*	*M_plane*
State	Fully Defined				
Definition					
Type	Cartesian				
Coordinate System ID	0.	Program Controlled			
Origin					
Origin X	0. m		8.e-002 m	-8.e-002 m	0. m
Origin Y	0. m		5.e-003 m		
Origin Z	0. m	0.2515 m	-8.e-002 m		0. m
Define By		Global Coordinates			
Location		Defined			
Directional Vectors					
X Axis Data	[1. 0. 0.]	[0. 0. -1.]	[1. 0. 0.]		
Y Axis Data	[0. 1. 0.]				
Z Axis Data	[0. 0. 1.]	[1. 0. 0.]	[0. 0. 1.]		
Principal Axis					
Axis		X			
Define By		Fixed Vector			
Orientation About Principal Axis					
Axis		Y			
Define By		Fixed Vector			
Transformations					
Base Configuration		Absolute			
Transformed Configuration		[0. 0. 0.2515]	[8.e-002 5.e-003 -8.e-002]	[-8.e-002 5.e-003 -8.e-002]	[0. 5.e-003 0.]

TABLE 17
Model (A4) > Coordinate Systems > Coordinate System

Object Name	*TC_back_plane*	*TC_center_plane*	*TC_front_plane*	*V1_plane*	*V2_plane*
State	Fully Defined				
Definition					
Type	Cartesian				
Coordinate System ID	Program Controlled				
Origin					
Define By	Global Coordinates				
Origin X	0. m			8.e-002 m	-8.e-002 m
Origin Y	-9.e-002 m			5.e-003 m	
Origin Z	-0.225 m	0. m	0.225 m	8.e-002 m	
Location	Defined				
Principal Axis					
Axis	X				
Define By	Fixed Vector				
Orientation About Principal Axis					
Axis	Y				
Define By	Fixed Vector				
Directional Vectors					
X Axis Data	[1. 0. 0.]				
Y Axis Data	[0. 1. 0.]				
Z Axis Data	[0. 0. 1.]				
Transformations					
Base Configuration	Absolute				
Transformed Configuration	[0. -9.e-002 -0.225]	[0. -9.e-002 0.]	[0. -9.e-002 0.225]	[8.e-002 5.e-003 8.e-002]	[-8.e-002 5.e-003 8.e-002]

TABLE 18
Model (A4) > Connections

Object Name	*Connections*
State	Fully Defined
Auto Detection	
Generate Automatic Connection On Refresh	Yes
Transparency	
Enabled	Yes

TABLE 19
Model (A4) > Connections > Contacts

Object Name	*Contacts*	*Contacts 2*
State	Fully Defined	
Definition		
Connection Type	Contact	
Scope		
Scoping Method	Geometry Selection	
Geometry	All Bodies	
Auto Detection		
Tolerance Type	Slider	
Tolerance Slider	0.	
Tolerance Value	3.2681e-003 m	
Face/Face	Yes	No
Face/Edge	No	
Edge/Edge	No	
Priority	Include All	
Group By	Bodies	
Search Across	Bodies	

TABLE 20
Model (A4) > Connections > Contacts > Contact Regions

Object Name	*Contact Region 3*	*Contact Region 4*	*Contact Region 7*	*Contact Region 10*	*Contact Region 6*
State	Fully Defined				
Scope					
Scoping Method	Geometry Selection				
Contact	1 Face				
Target	1 Face				
Contact Bodies	Left_Quartz	Back_Quartz	Right_Quartz	Front_Quartz	Back_Quartz
Target Bodies	Side_Insulation	Back_Insulation	Side_Insulation	Front_Insulation	Side_Insulation
Definition					
Type	Bonded				
Scope Mode	Automatic				
Behavior	Symmetric				
Suppressed	No				
Advanced					
Formulation	Pure Penalty				
Thermal Conductance	Program Controlled				
Pinball Region	Program Controlled				

TABLE 21
Model (A4) > Connections > Contacts > Contact Regions

Object Name	*Contact Region 8*
State	Fully Defined
Scope	
Scoping Method	Geometry Selection
Contact	1 Face
Target	1 Face
Contact Bodies	Front_Quartz
Target Bodies	Side_Insulation
Definition	
Type	Bonded
Scope Mode	Automatic
Behavior	Symmetric
Suppressed	No
Advanced	
Formulation	Pure Penalty
Thermal Conductance	Program Controlled
Pinball Region	Program Controlled

TABLE 22
Model (A4) > Connections > Contacts 2 > Contact Regions

Object Name	*Bonded - Front_Insulation To Side_Insulation*	*Bonded - Back_Insulation To Side_Insulation*
State	Fully Defined	
Scope		
Scoping Method	Geometry Selection	
Contact	1 Body	
Target	1 Body	
Contact Bodies	Front_Insulation	Back_Insulation
Target Bodies	Side_Insulation	
Definition		
Type	Bonded	
Scope Mode	Manual	
Behavior	Symmetric	
Suppressed	No	
Advanced		
Formulation	Pure Penalty	
Thermal Conductance	Program Controlled	
Pinball Region	Program Controlled	

TABLE 23
Model (A4) > Mesh

Object Name	*Mesh*
State	Solved
Defaults	
Physics Preference	Mechanical
Relevance	0
Sizing	
Use Advanced Size Function	Off
Relevance Center	Coarse
Element Size	Default
Initial Size Seed	Active Assembly
Smoothing	Medium
Transition	Fast
Span Angle Center	Coarse
Minimum Edge Length	2.e-003 m
Inflation	
Use Automatic Inflation	None
Inflation Option	Smooth Transition
Transition Ratio	0.272
Maximum Layers	5
Growth Rate	1.2
Inflation Algorithm	Pre
View Advanced Options	No
Advanced	
Shape Checking	Standard Mechanical
Element Midside Nodes	Program Controlled
Straight Sided Elements	No
Number of Retries	Default (4)
Extra Retries For Assembly	Yes
Rigid Body Behavior	Dimensionally Reduced
Mesh Morphing	Disabled
Defeaturing	
Pinch Tolerance	Please Define
Generate Pinch on Refresh	No
Automatic Mesh Based Defeaturing	On
Defeaturing Tolerance	Default
Statistics	
Nodes	26059
Elements	4773
Mesh Metric	None

TABLE 24

Model (A4) > Mesh > Mesh Controls

Object Name	*Insulation*	*Automatic Method*	*Main Filament Mesh*	*Front Filament Mesh*	*Back Filament Mesh*
State	Fully Defined				
Scope					
Scoping Method	Named Selection				
Named Selection	Insulation	Quartz Tube	Main Filaments	Front Filaments	Back Filaments
Definition					
Suppressed	No				
Method	MultiZone	Automatic	MultiZone		
Mapped Mesh Type	Hexa		Hexa	Hexa/Prism	
Free Mesh Type	Not Allowed		Not Allowed		
Element Midside Nodes	Use Global Setting				
Src/Trg Selection	Automatic		Automatic		
Source	Program Controlled		Program Controlled		
Advanced					
Mesh Based Defeaturing	Off		Off		
Minimum Edge Length	1.2504 m		6.2832e-002 m	8.9361e-002 m	
Write ICEM CFD Files	No		No		

TABLE 25

Model (A4) > Mesh > Mesh Controls

Object Name	*Substrate Mesh*
State	Fully Defined
Scope	
Scoping Method	Geometry Selection
Geometry	1 Body
Definition	
Suppressed	No
Type	Element Size
Element Size	3.e-002 m
Behavior	Soft

TABLE 26

Model (A4) > Named Selections > Named Selections

Object Name	*Insulation*	*Quartz Tube*	*Main Filaments*	*Back Filaments*	*Front Filaments*
State	Fully Defined				
Scope					
Scoping Method	Geometry Selection				
Geometry	3 Bodies	4 Bodies	12 Bodies	8 Bodies	
Definition					
Send to Solver	Yes				
Visible	Yes				
Program Controlled Inflation	Exclude				
Statistics					
Type	Manual				
Total Selection	3 Bodies	4 Bodies	12 Bodies	8 Bodies	
Suppressed	0				
Hidden	0				

TABLE 27

Model (A4) > Named Selections > Named Selections

Object Name	*Main Left Filaments*	*Main Right Filaments*	*Radiating Surfaces*
State	Fully Defined		
Scope			
Scoping Method	Geometry Selection		
Geometry	6 Bodies		128 Faces
Definition			
Send to Solver	Yes		
Visible	Yes		
Program Controlled Inflation	Exclude		
Statistics			
Type	Manual		
Total Selection	6 Bodies		128 Faces
Suppressed	0		
Hidden	0		

Transient Thermal (A5)

TABLE 28

Model (A4) > Analysis

Object Name	*Transient Thermal (A5)*
State	Solved
Definition	
Physics Type	Thermal
Analysis Type	Transient
Solver Target	Mechanical APDL
Options	
Generate Input Only	No

TABLE 29

Model (A4) > Transient Thermal (A5) > Initial Condition

Object Name	*Initial Temperature*
State	Fully Defined
Definition	
Initial Temperature	Uniform Temperature
Initial Temperature Value	22. °C

TABLE 30
Model (A4) > Transient Thermal (A5) > Analysis Settings

Object Name	*Analysis Settings*
State	Fully Defined
Step Controls	
Number Of Steps	1.
Current Step Number	1.
Step End Time	7000. s
Auto Time Stepping	On
Define By	Time
Initial Time Step	10. s
Minimum Time Step	10. s
Maximum Time Step	100. s
Time Integration	On
Solver Controls	
Solver Type	Program Controlled
Radiosity Controls	
Flux Convergence	1.e-004
Maximum Iteration	1000.
Solver Tolerance	0.1
Over Relaxation	0.1
Hemicube Resolution	10.
Nonlinear Controls	
Heat Convergence	Program Controlled
Temperature Convergence	Program Controlled
Line Search	Program Controlled
Nonlinear Formulation	Program Controlled
Output Controls	
Calculate Thermal Flux	Yes
Calculate Results At	All Time Points
Analysis Data Management	
Solver Files Directory	C:\Documents and Settings\User\Desktop\LTCC Oven Simulations\Dynamic Oven Simulation\Dynamic Oven Simulation_dp39_files\dp0\SYS\MECH\
Future Analysis	None
Scratch Solver Files Directory	
Save MAPDL db	No
Delete Unneeded Files	No
Nonlinear Solution	Yes
Solver Units	Active System
Solver Unit System	mks

TABLE 31
Model (A4) > Transient Thermal (A5) > Loads

Object Name	*Radiation*	*Main Filament Power*	*Front Filament Power*	*Back Filament Power*	*Blower on the Left*
State	Fully Defined				
Scope					
Scoping Method	Named Selection				Geometry Selection
Named Selection	Radiating Surfaces	Main Filaments	Front Filaments	Back Filaments	
Geometry					1 Face
Definition					
Type	Radiation	Internal Heat Generation			Convection
Correlation	Surface to Surface				
Emissivity	1. (step applied)				
Ambient Temperature	22. °C (step applied)				22. °C (step applied)
Enclosure	1.				
Suppressed	No				
Magnitude		Run 01 Main	Run 01 Front		
Film Coefficient					Stagnant Air - Horizontal Cyl

FIGURE 1
Model (A4) > Transient Thermal (A5) > Radiation

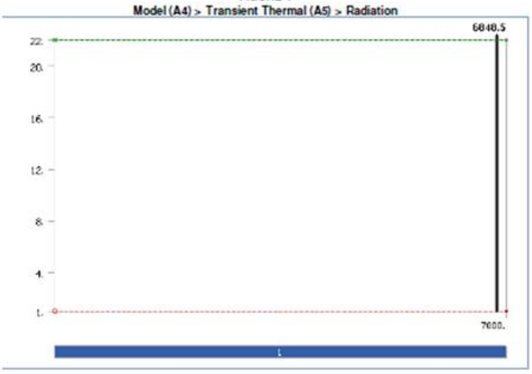

FIGURE 2
Model (A4) > Transient Thermal (A5) > Main Filament Power

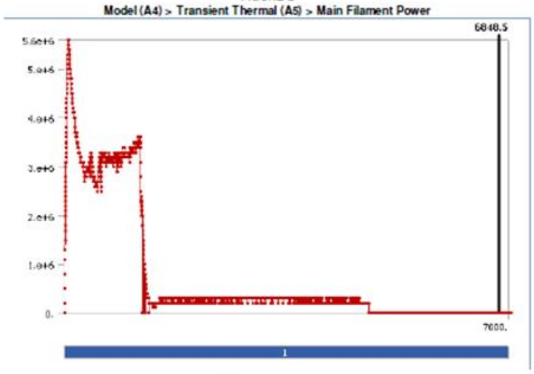

FIGURE 3

Model (A4) > Transient Thermal (A5) > Front Filament Power

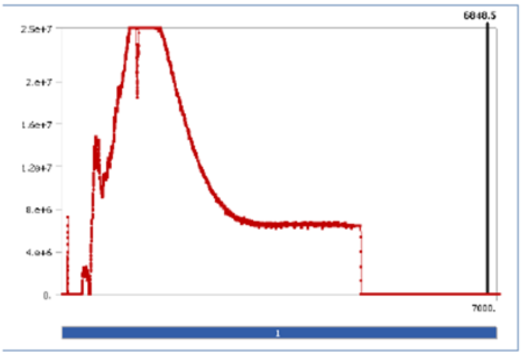

FIGURE 4

Model (A4) > Transient Thermal (A5) > Back Filament Power

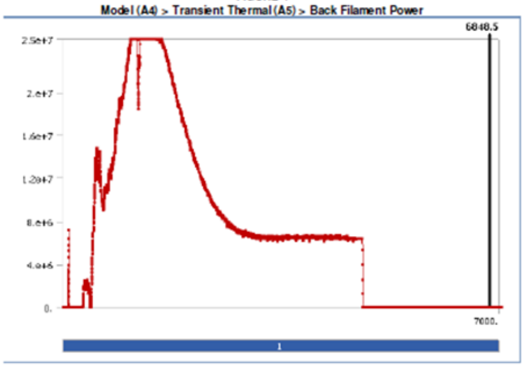

FIGURE 5

Model (A4) > Transient Thermal (A5) > Blower on the Left

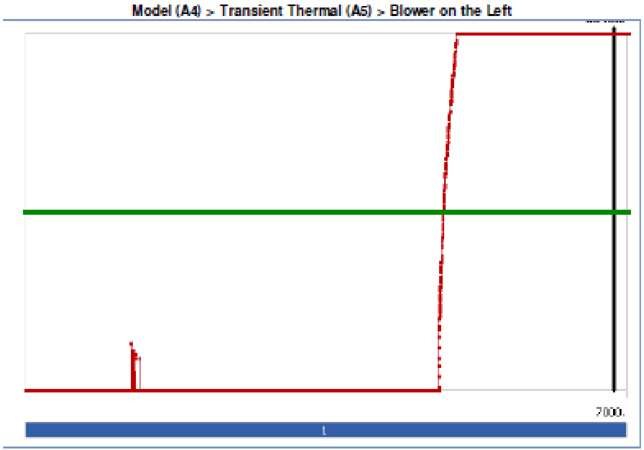

TABLE 33

Model (A4) > Transient Thermal (A5) > Loads

Object Name	*Insulation Convection Sides*	*Insulation Convection Front and Back*
State	Fully Defined	
Scope		
Scoping Method	Geometry Selection	
Geometry	3 Faces	2 Faces
Definition		
Type	Convection	
Film Coefficient	Stagnant Air - Horizontal Cyl	Stagnant Air - Vertical Planes
Coefficient Type	Average Film Temperature	
Ambient Temperature	22. °C (step applied)	
Edit Tabular Data	Film Coefficient	
Suppressed	No	

FIGURE 6

Model (A4) > Transient Thermal (A5) > Insulation Convection Sides

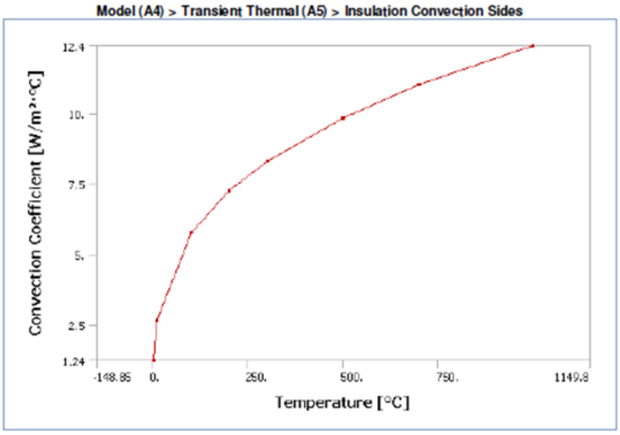

TABLE 34

Model (A4) > Transient Thermal (A5) > Insulation Convection Sides

Temperature [°C]	Convection Coefficient [W/m²·°C]
1.	1.24
10.	2.67
100.	5.76
200.	7.25
300.	8.3
500.	9.84
700.	11.01
1000.	12.4

FIGURE 7
Model (A4) > Transient Thermal (A5) > Insulation Convection Front and Back

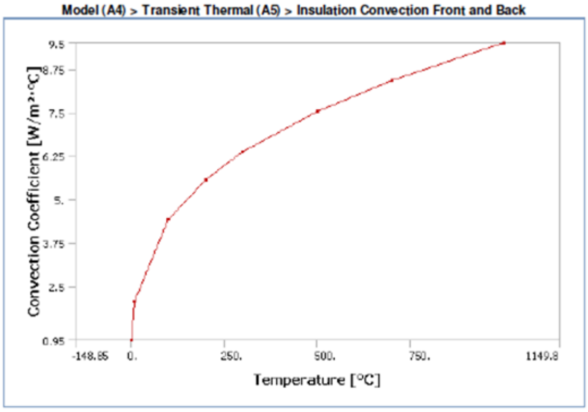

TABLE 35
Model (A4) > Transient Thermal (A5) > Insulation Convection Front and Back

Temperature [°C]	Convection Coefficient [W/m²·°C]
1.	0.95
10.	2.05
100.	4.41
200.	5.56
300.	6.36
500.	7.54
700.	8.43
1000.	9.5

TABLE 36
Model (A4) > Transient Thermal (A5) > Solution

Object Name	*Solution (A6)*
State	Solved
Adaptive Mesh Refinement	
Max Refinement Loops	1.
Refinement Depth	2.
Information	
Status	Done

TABLE 37
Model (A4) > Transient Thermal (A5) > Solution (A6) > Solution Information

Object Name	*Solution Information*
State	Solved
Solution Information	
Solution Output	Solver Output
Update Interval	2.5 s
Display Points	All

TABLE 38
Model (A4) > Transient Thermal (A5) > Solution (A6) > Solution Information > Result Charts

Object Name	*Temperature - Global Maximum*	*Temperature - Global Minimum*
State	Solved	
Scope		
Scoping Method	Global Maximum	Global Minimum
Definition		
Type	Temperature	
Results		
Minimum	30.466 °C	11.347 °C
Maximum	797.64 °C	22.129 °C

FIGURE 8
Model (A4) > Transient Thermal (A5) > Solution (A6) > Solution Information > Temperature - Global Maximum

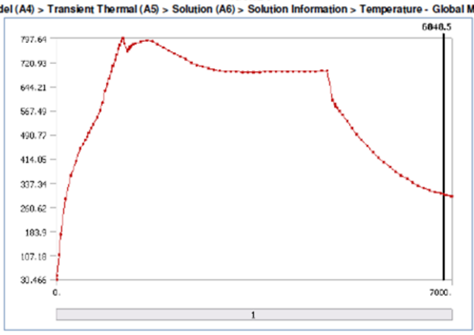

FIGURE 9
Model (A4) > Transient Thermal (A5) > Solution (A6) > Solution Information > Temperature - Global Minimum

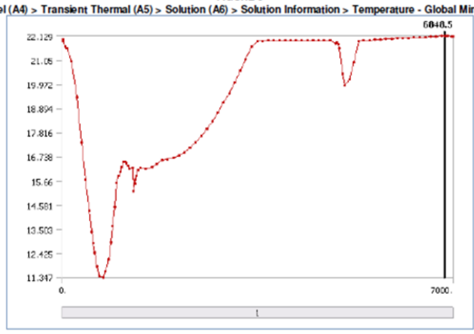

TABLE 39
Model (A4) > Transient Thermal (A5) > Solution (A6) > Results

Object Name	*Insulation Outer*	*Quartz Tube Left*	*Quartz Tube Right*	*Main Filaments*	*Substrate*
State	Solved				
Scope					
Scoping Method	Geometry Selection			Named Selection	Geometry Selection
Geometry	5 Faces	1 Face			1 Body
Named Selection				Main Filaments	
Definition					
Type	Temperature				
By	Time				
Display Time	Last				
Calculate Time History	Yes				
Identifier					
Results					
Minimum	22.168 °C	22.108 °C	39.437 °C	153.42 °C	194.9 °C
Maximum	41.533 °C	77.531 °C	255.21 °C	244.21 °C	228.82 °C
Minimum Occurs On	Front_Insulation			Solid	
Maximum Occurs On	Front_Insulation			Solid	
Minimum Value Over Time					
Minimum	16.849 °C	22.035 °C		30.438 °C	22.005 °C
Maximum	22.168 °C	612.62 °C	611.33 °C	701.17 °C	652.8 °C
Maximum Value Over Time					
Minimum	22.004 °C	22.26 °C	22.215 °C	30.466 °C	22.014 °C
Maximum	41.533 °C	681.44 °C	673.03 °C	728.98 °C	657.35 °C
Information					
Time	7000. s				
Load Step	1				
Substep	100				
Iteration Number	2689				

FIGURE 11
Model (A4) > Transient Thermal (A5) > Solution (A6) > Quartz Tube Left

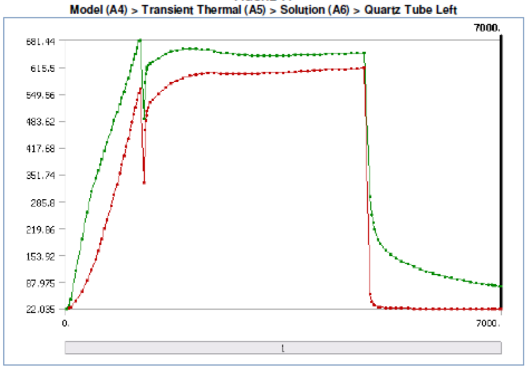

FIGURE 10
Model (A4) > Transient Thermal (A5) > Solution (A6) > Insulation Outer

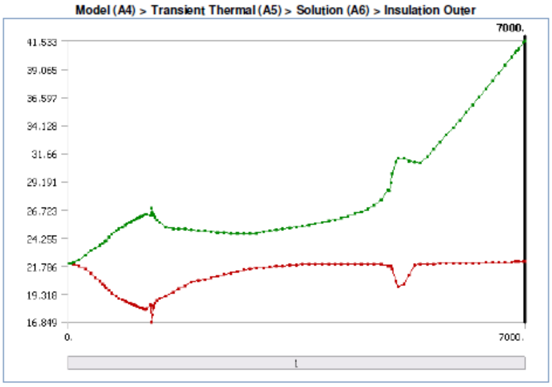

TABLE 40
Model (A4) > Transient Thermal (A5) > Solution (A6) > Insulation Outer

Time [s]	Minimum [°C]	Maximum [°C]
10.	21.998	22.004
20.	21.995	22.01
50.	21.985	22.041
80.	21.964	22.086
170.	21.796	22.362
260.	21.497	22.748
350.	21.112	23.107
419.4	20.774	23.349
481.82	20.433	23.562
525.41	20.151	23.776
551.67	19.991	23.901
577.93	19.868	24.019
621.61	19.615	24.274
665.29	19.381	24.519
729.17	19.115	24.827
780.81	18.95	25.038
825.9	18.828	25.2
870.99	18.698	25.357
904.77	18.615	25.463
938.56	18.529	25.571
975.73	18.425	25.693
1008.1	18.349	25.792
1040.2	18.271	25.892
1069.	18.209	25.978
1097.1	18.146	26.065
1125.3	18.097	26.144
1153.4	18.043	26.227
1181.6	17.991	26.311
1209.7	18.024	26.333
1261.9	18.319	26.179
1279.3	16.849	26.84
1289.3	17.515	26.484
1299.3	18.153	26.279
1309.3	18.299	26.189
1326.	18.492	26.04
1364.1	18.722	25.786
1402.2	18.874	25.579
1502.2	19.169	25.206
1602.2	19.471	25.02
1695.9	19.763	25.029
1789.7	20.053	24.992
1889.7	20.324	24.939
1989.7	20.463	24.883
2089.7	20.603	24.827
2189.7	20.743	24.777
2289.7	20.885	24.739
2389.7	21.027	24.702
2489.7	21.166	24.666
2589.7	21.297	24.645
2689.7	21.419	24.639
2789.7	21.501	24.644
2889.7	21.573	24.655
2989.7	21.637	24.757
3089.7	21.694	24.851
3189.7	21.745	24.94
3289.7	21.791	25.024
3389.7	21.835	25.107
3489.7	21.87	25.19
3589.7	21.894	25.277
3689.7	21.913	25.373
3789.7	21.911	25.48
3889.7	21.91	25.593
3989.7		25.719
4089.7	21.911	25.854
4189.7	21.914	26.006
4289.7	21.918	26.171
4389.7	21.923	26.351
4489.7	21.926	26.547
4589.7		26.762
4689.7	21.927	27.114
4789.7	21.928	27.57
4889.7	21.766	28.416
4923.	21.802	28.376
4945.3	21.751	29.056
4967.6	21.558	29.879
5016.6	20.413	30.884
5065.5	19.912	31.24
5148.7	20.173	31.187
5232.	20.949	31.008
5315.3	21.882	30.871
5398.5	21.926	30.794
5498.5	21.937	31.374
5598.5	21.953	31.982
5698.5	21.969	32.61
5798.5	21.987	33.252
5898.5	22.006	33.909
5998.5	22.013	34.576
6098.5	22.02	35.252
6198.5	22.031	35.936
6298.5	22.043	36.624
6398.5	22.057	37.318
6498.5	22.073	38.014
6598.5	22.09	38.714
6698.5	22.108	39.415
6798.5	22.127	40.118
6848.5	22.136	40.469
6873.5	22.141	40.645
6898.5	22.146	40.821
6973.5	22.162	41.347
7000.	22.168	41.533

TABLE 41
Model (A4) > Transient Thermal (A5) > Solution (A6) > Quartz Tube Left

Time [s]	Minimum [°C]	Maximum [°C]
10.	22.035	22.26
20.	22.127	22.898
50.	23.377	30.624
80.	25.938	45.636
170.	41.429	116.38
260.	63.548	192.81
350.	91.073	258.7
419.4	117.18	309.63
481.82	142.7	342.16
525.41	164.89	362.04
551.67	180.26	376.39
577.93	194.7	388.01
621.61	218.22	410.97
665.29	240.28	431.2
729.17	273.84	460.03
780.81	302.4	483.69
825.9	328.24	504.87
870.99	355.76	525.25
904.77	376.18	539.55
938.56	396.69	555.23
975.73	420.	572.98
1008.1	440.32	588.46
1040.2	461.16	605.02
1069.	479.86	619.41
1097.1	498.61	634.24
1125.3	516.7	648.34
1153.4	534.68	663.2
1181.6	552.65	678.42
1209.7	562.22	681.44
1261.9	331.97	488.71
1279.3	461.59	576.83
1289.3	483.87	598.72
1299.3	497.95	609.1
1309.3	507.33	614.66
1326.	516.7	619.31
1364.1	527.75	624.43
1402.2	535.14	628.16
1502.2	549.51	637.39
1602.2	564.02	647.82
1695.9	575.15	654.48
1789.7	582.28	656.93
1889.7	589.12	659.41
1989.7	594.27	660.53
2089.7	596.77	659.3
2189.7	598.89	658.13
2289.7	600.77	657.2
2389.7	600.28	653.93
2489.7	599.05	650.32
2589.7	599.31	649.18
2689.7	599.24	647.5
2789.7	598.99	645.93
2889.7	598.82	644.57
2989.7	599.29	644.29
3089.7	599.68	643.79
3189.7	600.27	643.74
3289.7	600.61	643.22
3389.7	601.09	643.23
3489.7	601.76	643.34
3589.7	602.87	644.1
3689.7	604.03	644.86
3789.7	605.3	645.77
3889.7	605.6	645.43
3989.7	606.75	646.34
4089.7	607.21	646.24
4189.7	608.51	647.35
4289.7	609.14	647.57
4389.7	609.59	
4489.7	609.95	647.63
4589.7	611.46	648.94
4689.7	612.11	649.18
4789.7	612.62	649.38
4889.7	59.069	298.62
4923.	37.961	253.34
4945.3	33.434	233.68
4967.6	30.368	217.47
5016.6	26.744	191.81
5065.5	25.861	180.03
5148.7	24.893	166.67
5232.	24.241	156.1
5315.3	23.762	147.26
5398.5	23.415	139.67
5498.5	23.112	131.85
5598.5	22.889	125.04
5698.5	22.722	119.06
5798.5	22.595	113.75
5898.5	22.496	109.01
5998.5	22.419	104.74
6098.5	22.358	100.88
6198.5	22.308	97.362
6298.5	22.265	94.153
6398.5	22.23	91.214
6498.5	22.2	88.504
6598.5	22.176	85.996
6698.5	22.155	83.673
6798.5	22.137	81.513
6848.5	22.129	80.471
6873.5	22.125	79.961
6898.5	22.121	79.458
6973.5	22.111	78.028
7000.	22.108	77.531

FIGURE 13
Model (A4) > Transient Thermal (A5) > Solution (A6) > Main Filaments

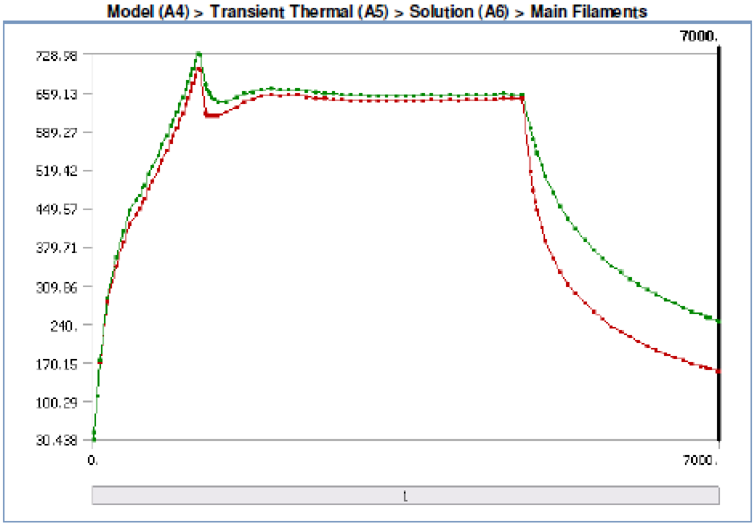

FIGURE 14
Model (A4) > Transient Thermal (A5) > Solution (A6) > Substrate

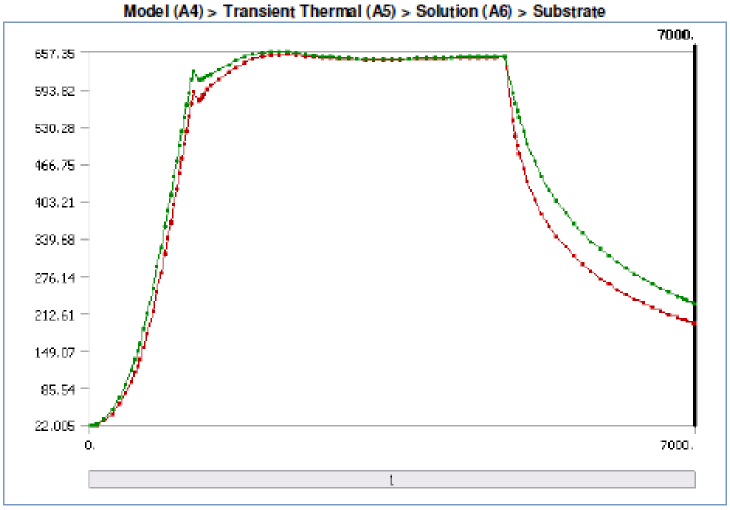

FIGURE 12
Model (A4) > Transient Thermal (A5) > Solution (A6) > Quartz Tube Right

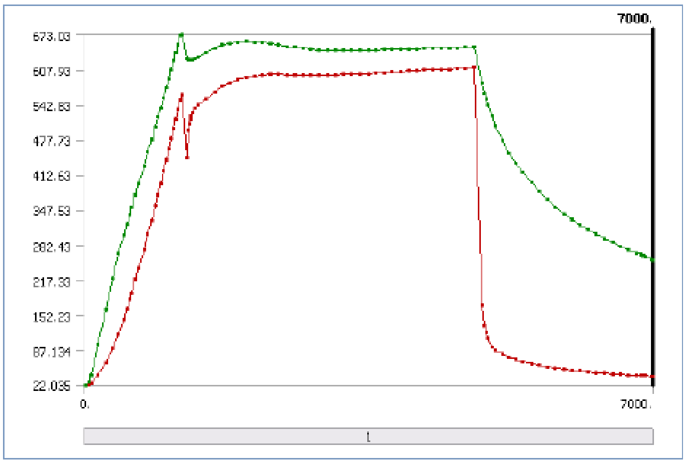

TABLE 42

Model (A4) > Transient Thermal (A5) > Solution (A6) > Quartz Tube Right

Time [s]	Minimum [°C]	Maximum [°C]
10.	22.035	22.215
20.	22.125	22.733
50.	23.36	28.794
80.	25.938	40.489
170.	41.429	96.842
260.	63.548	161.4
350.	91.073	220.51
419.4	117.18	267.54
481.82	142.7	299.81
525.41	164.89	321.77
551.67	180.26	338.49
577.93	194.7	352.28
621.61	218.22	376.34
665.29	240.28	397.34
729.17	273.84	428.6
780.81	302.4	454.8
825.9	328.24	478.16
870.99	355.76	502.2
904.77	376.18	519.29
938.56	396.69	536.83
975.73	420.	556.85
1008.1	440.32	574.09
1040.2	461.16	592.09
1069.	479.86	607.87
1097.1	498.61	623.99
1125.3	516.7	639.07
1153.4	534.68	654.44
1181.6	552.65	669.96
1209.7	562.22	673.03
1261.9	444.19	628.75
1279.3	494.64	626.61
1289.3	507.83	626.47
1299.3	516.46	626.23
1309.3	522.36	625.93
1326.	528.49	627.07
1364.1	536.46	628.5
1402.2	542.45	630.78
1502.2	554.03	638.74
1602.2	566.8	648.76
1695.9	576.82	655.06
1789.7	583.24	657.17
1889.7	589.32	659.41
1989.7	593.88	660.53
2089.7	596.08	659.3
2189.7	597.8	658.13
2289.7	599.36	657.2
2389.7	598.75	653.93
2489.7	597.46	650.32
2589.7	597.76	649.18
2689.7	597.74	647.5
2789.7	597.53	645.93
2889.7	597.4	644.57
2989.7	597.89	644.29
3089.7	598.3	643.79
3189.7	598.9	643.74
3289.7	599.27	643.22
3389.7	599.75	643.23
3489.7	600.43	643.34
3589.7	601.54	644.1
3689.7	602.71	644.86
3789.7	603.97	645.77
3889.7	604.28	645.43
3989.7	605.43	646.34
4089.7	605.89	646.24
4189.7	607.2	647.35
4289.7	607.83	647.57
4389.7	608.28	
4489.7	608.64	647.63
4589.7	610.16	648.94
4689.7	610.82	649.18
4789.7	611.33	649.38
4889.7	171.62	582.77
4923.	134.01	564.72
4945.3	120.68	553.38
4967.6	109.79	542.69
5016.6	93.614	521.87
5065.5	87.568	503.51
5148.7	80.249	476.79
5232.	74.561	454.03
5315.3	69.958	434.18
5398.5	66.138	416.61
5498.5	62.337	398.06
5598.5	59.132	381.49
5698.5	56.405	366.59
5798.5	54.045	353.05
5898.5	51.989	340.68
5998.5	50.175	329.3
6098.5	48.564	319.63
6198.5	47.124	310.67
6298.5	45.829	302.28
6398.5	44.663	294.42
6498.5	43.6	287.
6598.5	42.626	279.98
6698.5	41.736	273.35
6798.5	40.919	267.07
6848.5	40.524	264.
6873.5	40.333	262.49
6898.5	40.148	261.
6973.5	39.629	256.71
7000.	39.437	255.21

TABLE 43
Model (A4) > Transient Thermal (A5) > Solution (A6) > Main Filaments

Time [s]	Minimum [°C]	Maximum [°C]
10.	30.438	30.466
20.	43.457	43.545
50.	108.75	109.49
80.	171.32	173.28
170.	279.94	287.61
260.	346.01	360.16
350.	387.77	407.55
419.4	422.02	446.16
481.82	437.01	463.21
525.41	447.53	473.8
551.67	459.11	485.4
577.93	465.46	491.53
621.61	484.02	510.53
665.29	497.57	524.61
729.17	518.28	545.89
780.81	536.24	564.48
825.9	552.98	581.69
870.99	568.89	597.64
904.77	580.14	608.71
938.56	593.77	622.31
975.73	608.93	637.37
1008.1	622.21	650.54
1040.2	636.67	664.92
1069.	648.86	676.94
1097.1	662.03	689.96
1125.3	674.21	701.96
1153.4	687.59	715.33
1181.6	701.17	728.98
1209.7	699.73	726.77
1261.9	621.56	671.85
1279.3	617.3	664.06
1289.3	616.66	660.6
1299.3	616.2	657.29
1309.3	616.22	654.63
1326.	616.29	650.81
1364.1	616.78	644.81
1402.2	617.48	641.67
1502.2	622.33	642.41
1602.2	632.31	649.98
1695.9	640.97	656.65
1789.7	645.51	659.07
1889.7	651.94	663.29
1989.7	654.52	665.71
2089.7	653.54	664.5
2189.7	653.82	664.7
2289.7	654.08	664.88
2389.7	650.88	661.53
2489.7	647.71	658.24
2589.7	647.59	658.1
2689.7	646.76	657.22
2789.7	645.22	655.52
2889.7	644.41	654.63
2989.7	644.04	654.13
3089.7	643.71	653.67
3189.7	643.61	653.45
3289.7	643.38	653.1
3389.7	643.24	652.94
3489.7	643.37	652.91
3589.7	643.93	653.3
3689.7	644.64	653.87
3789.7	645.48	654.6
3889.7	644.11	652.91
3989.7	645.67	654.48
4089.7	644.74	653.29
4189.7	646.59	655.2
4289.7	645.91	654.3
4389.7	645.69	653.93
4489.7	645.56	653.74
4589.7	647.97	656.25
4689.7	647.55	655.67
4789.7	647.47	655.47
4889.7	515.11	593.96
4923.	481.79	574.44
4945.3	462.48	561.94
4967.6	445.42	550.06
5016.6	415.49	526.85
5065.5	390.93	506.17
5148.7	358.93	476.77
5232.	333.35	451.79
5315.3	312.26	430.24
5398.5	294.44	411.39
5498.5	276.48	391.77
5598.5	261.09	374.48
5698.5	247.69	359.1
5798.5	235.86	345.27
5898.5	225.32	332.74
5998.5	215.83	321.29
6098.5	207.23	310.78
6198.5	199.35	301.29
6298.5	192.05	292.53
6398.5	185.32	284.37
6498.5	179.09	276.71
6598.5	173.29	269.49
6698.5	167.89	262.7
6798.5	162.83	256.28
6848.5	160.38	253.16
6873.5	159.18	251.62
6898.5	157.99	250.1
6973.5	154.6	245.73
7000.	153.42	244.21

TABLE 44
Model (A4) > Transient Thermal (A5) > Solution (A6) > Substrate

Time [s]	Minimum [°C]	Maximum [°C]
10.	22.005	22.014
20.	22.019	22.049
50.	22.29	22.556
80.	22.942	23.678
170.	29.264	32.568
260.	40.952	47.839
350.	58.53	69.707
419.4	76.712	92.047
481.82	96.304	115.57
525.41	112.05	134.77
551.67	122.57	147.77
577.93	133.84	161.33
621.61	154.98	186.17
665.29	178.05	212.45
729.17	216.09	254.73
780.81	249.72	291.47
825.9	281.25	325.3
870.99	314.81	360.83
904.77	340.8	387.77
938.56	367.57	415.03
975.73	397.87	445.43
1008.1	424.64	471.83
1040.2	451.61	498.17
1069.	475.94	521.62
1097.1	499.8	544.53
1125.3	523.44	566.79
1153.4	546.82	588.57
1181.6	569.91	609.91
1209.7	589.78	625.6
1261.9	573.52	609.58
1279.3	575.4	609.15
1289.3	577.79	609.9
1299.3	580.48	610.92
1309.3	583.11	612.01
1326.	586.69	613.69
1364.1	593.44	616.72
1402.2	599.2	619.36
1502.2	611.02	626.53
1602.2	622.28	635.59
1695.9	631.66	643.51
1789.7	638.5	648.7
1889.7	644.39	653.09
1989.7	648.77	656.13
2089.7	650.86	657.14
2189.7	652.05	657.35
2289.7	652.8	657.29
2389.7	651.78	655.6
2489.7	649.82	653.07
2589.7	648.73	651.56
2689.7	647.7	650.11
2789.7	646.5	648.66
2889.7	645.44	647.36
2989.7	644.79	646.64
3089.7	644.28	646.05
3189.7	644.02	645.75

Time [s]	Minimum [°C]	Maximum [°C]
1789.7	638.5	648.7
1889.7	644.39	653.09
1989.7	648.77	656.13
2089.7	650.86	657.14
2189.7	652.05	657.35
2289.7	652.8	657.29
2389.7	651.78	655.6
2489.7	649.82	653.07
2589.7	648.73	651.56
2689.7	647.7	650.11
2789.7	646.5	648.66
2889.7	645.44	647.36
2989.7	644.79	646.64
3089.7	644.28	646.05
3189.7	644.02	645.75
3289.7	643.71	645.34
3389.7	643.54	645.14
3489.7	643.49	645.08
3589.7	643.73	645.42
3689.7	644.19	645.93
3789.7	644.82	646.62
3889.7	644.87	646.65
3989.7	645.36	647.18
4089.7	645.48	647.3
4189.7	646.15	647.99
4289.7	646.47	648.32
4389.7	646.59	648.45
4489.7	646.61	648.48
4589.7	647.47	649.31
4689.7	647.94	649.76
4789.7	648.18	650.02
4889.7	541.39	588.74
4923.	514.4	569.42
4945.3	498.56	556.98
4967.6	484.33	545.1
5016.6	458.44	521.63
5065.5	436.47	500.66
5148.7	406.7	470.7
5232.	382.18	445.04
5315.3	361.49	422.84
5398.5	343.7	403.39
5498.5	325.49	383.04
5598.5	309.67	365.1
5698.5	295.75	349.11
5798.5	283.37	334.73
5898.5	272.25	321.7
5998.5	262.17	309.82
6098.5	252.98	298.9
6198.5	244.55	288.84
6298.5	236.77	279.52
6398.5	229.57	270.85
6498.5	222.86	262.76
6598.5	216.6	255.18
6698.5	210.73	248.06
6798.5	205.21	241.37

TABLE 45

Model (A4) > Transient Thermal (A5) > Solution (A6) > Results

Object Name	*Main Filaments_2500s*	*Main Filaments_3500s*	*Main Filaments_4500s*
State	Solved		
Scope			
Scoping Method	Named Selection		
Named Selection	Main Filaments		
Definition			
Type	Temperature		
By	Time		
Display Time	2500. s	3500. s	4500. s
Calculate Time History	Yes		
Identifier			
Results			
Minimum	647.7 °C	643.43 °C	645.81 °C
Maximum	658.22 °C	652.95 °C	654. °C
Minimum Occurs On	Solid		
Maximum Occurs On	Solid		
Minimum Value Over Time			
Minimum	30.438 °C		
Maximum	701.17 °C		
Maximum Value Over Time			
Minimum	30.466 °C		
Maximum	728.98 °C		
Information			
Time	2500. s	3500. s	4500. s
Load Step	1		
Substep	48	58	68
Iteration Number	387	437	486

FIGURE 15

Model (A4) > Transient Thermal (A5) > Solution (A6) > Main Filaments_2500s

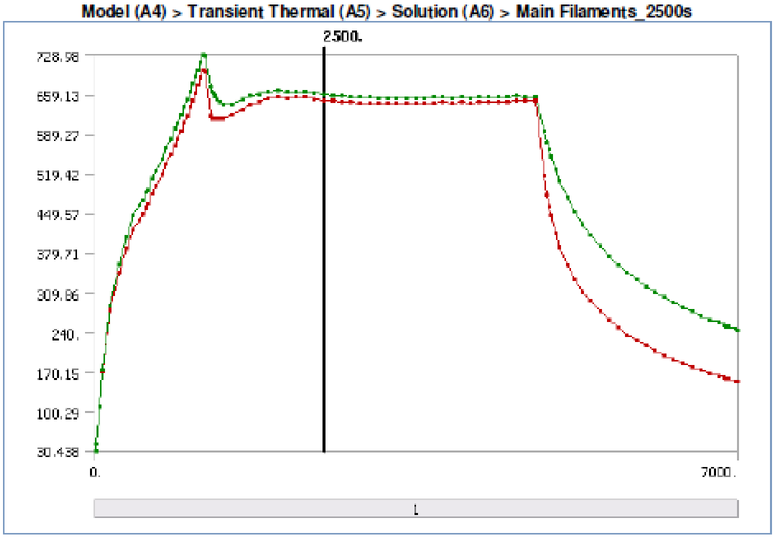

FIGURE 16

Model (A4) > Transient Thermal (A5) > Solution (A6) > Main Filaments_3500s

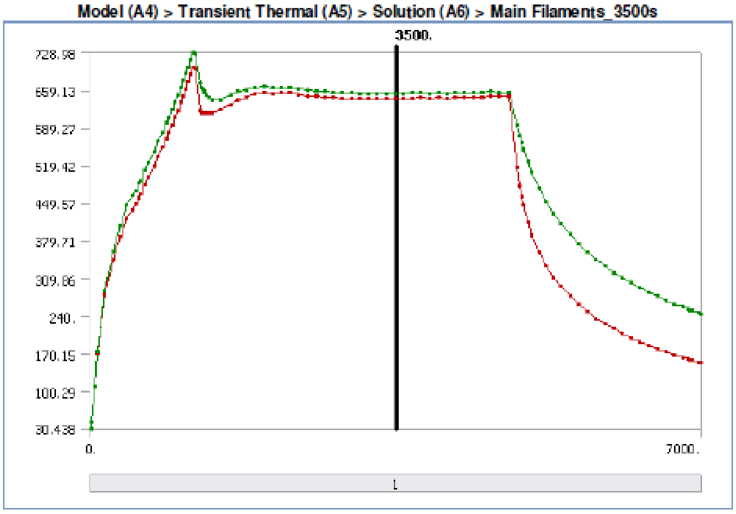

TABLE 46
Model (A4) > Transient Thermal (A5) > Solution (A6) > Main Filaments_2500s

Time [s]	Minimum [°C]	Maximum [°C]
10.	30.438	30.466
20.	43.457	43.545
50.	108.75	109.49
80.	171.32	173.28
170.	279.94	287.61
260.	346.01	360.16
350.	387.77	407.55
419.4	422.02	446.16
481.82	437.01	463.21
525.41	447.53	473.8
551.67	459.11	485.4
577.93	465.46	491.53
621.61	484.02	510.53
665.29	497.57	524.61
729.17	518.28	545.89
780.81	536.24	564.48
825.9	552.98	581.69
870.99	568.89	597.64
904.77	580.14	608.71
938.56	593.77	622.31
975.73	608.93	637.37
1008.1	622.21	650.54
1040.2	636.67	664.92
1069.	648.86	676.94
1097.1	662.03	689.96
1125.3	674.21	701.96
1153.4	687.59	715.33
1181.6	701.17	728.98
1209.7	699.73	726.77
1261.9	621.56	671.85
1279.3	617.3	664.06
1289.3	616.66	660.6
1299.3	616.2	657.29
1309.3	616.22	654.63
1326.	616.29	650.81
1364.1	616.78	644.81
1402.2	617.48	641.67
1502.2	622.33	642.41
1602.2	632.31	649.98
1695.9	640.97	656.65
1789.7	645.51	659.07
1889.7	651.94	663.29
1989.7	654.52	665.71
2089.7	653.54	664.5
2189.7	653.82	664.7
2289.7	654.08	664.88
2389.7	650.88	661.53
2489.7	647.71	658.24
2589.7	647.59	658.1
2689.7	646.76	657.22
2789.7	645.22	655.52
2889.7	644.41	654.63
2989.7	644.04	654.13
3089.7	643.71	653.67
3189.7	643.61	653.45
3289.7	643.38	653.1
3389.7	643.24	652.94
3489.7	643.37	652.91
3589.7	643.93	653.3
3689.7	644.64	653.87
3789.7	645.48	654.6
3889.7	644.11	652.91
3989.7	645.67	654.48
4089.7	644.74	653.29
4189.7	646.59	655.2
4289.7	645.91	654.3
4389.7	645.69	653.93
4489.7	645.56	653.74
4589.7	647.97	656.25
4689.7	647.55	655.67
4789.7	647.47	655.47
4889.7	515.11	593.96
4923.	481.79	574.44
4945.3	462.48	561.94
4967.6	445.42	550.06
5016.6	415.49	526.85
5065.5	390.93	506.17
5148.7	358.93	476.77
5232.	333.35	451.79
5315.3	312.26	430.24
5398.5	294.44	411.39
5498.5	276.48	391.77
5598.5	261.09	374.48
5698.5	247.69	359.1
5798.5	235.86	345.27
5898.5	225.32	332.74

TABLE 47
Model (A4) > Transient Thermal (A5) > Solution (A6) > Main Filaments_3500s

Time [s]	Minimum [°C]	Maximum [°C]
10.	30.438	30.466
20.	43.457	43.545
50.	108.75	109.49
80.	171.32	173.28
170.	279.94	287.61
260.	346.01	360.16
350.	387.77	407.55
419.4	422.02	446.16
481.82	437.01	463.21
525.41	447.53	473.8
551.67	459.11	485.4
577.93	465.46	491.53
621.61	484.02	510.53
665.29	497.57	524.61
729.17	518.28	545.89
780.81	536.24	564.48
825.9	552.98	581.69
870.99	568.89	597.64
904.77	580.14	608.71
938.56	593.77	622.31
975.73	608.93	637.37
1008.1	622.21	650.54
1040.2	636.67	664.92
1069.	648.86	676.94
1097.1	662.03	689.96
1125.3	674.21	701.96
1153.4	687.59	715.33
1181.6	701.17	728.98
1209.7	699.73	726.77
1261.9	621.56	671.85
1279.3	617.3	664.06
1289.3	616.66	660.6
1299.3	616.2	657.29
1309.3	616.22	654.63
1326.	616.29	650.81
1364.1	616.78	644.81
1402.2	617.48	641.67
1502.2	622.33	642.41
1602.2	632.31	649.98
1695.9	640.97	656.65
1789.7	645.51	659.07
1889.7	651.94	663.29
1989.7	654.52	665.71
2089.7	653.54	664.5
2189.7	653.82	664.7
2289.7	654.08	664.88
2389.7	650.88	661.53
2489.7	647.71	658.24
2589.7	647.59	658.1
2689.7	646.76	657.22
2789.7	645.22	655.52
2989.7	644.04	654.13
3089.7	643.71	653.67
3189.7	643.61	653.45
3289.7	643.38	653.1
3389.7	643.24	652.94
3489.7	643.37	652.91
3589.7	643.93	653.3
3689.7	644.64	653.87
3789.7	645.48	654.6
3889.7	644.11	652.91
3989.7	645.67	654.48
4089.7	644.74	653.29
4189.7	646.59	655.2
4289.7	645.91	654.3
4389.7	645.69	653.93
4489.7	645.56	653.74
4589.7	647.97	656.25
4689.7	647.55	655.67
4789.7	647.47	655.47
4889.7	515.11	593.96
4923.	481.79	574.44
4945.3	462.48	561.94
4967.6	445.42	550.06
5016.6	415.49	526.85
5065.5	390.93	506.17
5148.7	358.93	476.77
5232.	333.35	451.79
5315.3	312.26	430.24
5398.5	294.44	411.39
5498.5	276.48	391.77
5598.5	261.09	374.48
5698.5	247.69	359.1
5798.5	235.86	345.27
5898.5	225.32	332.74
5998.5	215.83	321.29
6098.5	207.23	310.78
6198.5	199.35	301.29
6298.5	192.05	292.53
6398.5	185.32	284.37
6498.5	179.09	276.71
6598.5	173.29	269.49
6698.5	167.89	262.7
6798.5	162.83	256.28
6848.5	160.38	253.16
6873.5	159.18	251.62
6898.5	157.99	250.1
6973.5	154.6	245.73
7000.	153.42	244.21

FIGURE 17

Model (A4) > Transient Thermal (A5) > Solution (A6) > Main Filaments_4500s

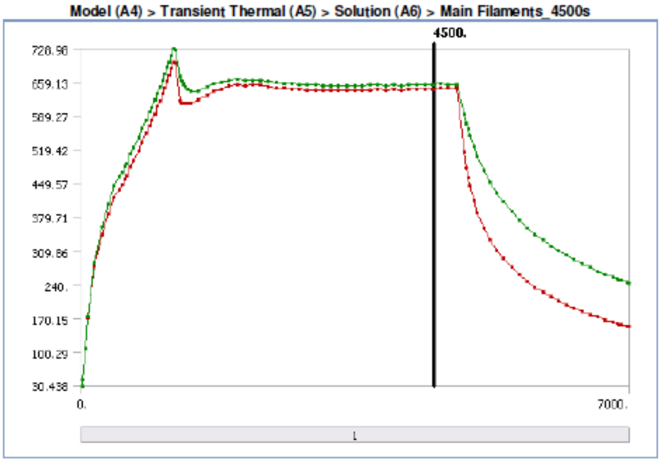

TABLE 49

Model (A4) > Transient Thermal (A5) > Solution (A6) > Probes

Object Name	*TCC*	*TCF*	*TCB*	*H1*	*H2*
State	Solved				
Definition					
Type	Temperature				
Location Method	Geometry Selection			Coordinate System	
Geometry	1 Body				
Location				H1_plane	H2_plane
X Coordinate				8.e-002 m	-8.e-002 m
Y Coordinate				5.e-003 m	
Z Coordinate				-8.e-002 m	
Options					
Display Time	End Time				
Spatial Resolution	Use Maximum				
Results					
Temperature	187.55 °C	191.88 °C	192.09 °C	227.74 °C	197.8 °C
Maximum Value Over Time					
Temperature	658.32 °C	687.22 °C	688.35 °C	655.28 °C	654.82 °C
Minimum Value Over Time					
Temperature	22. °C				
Information					
Time	7000. s				
Load Step	1				
Substep	100				
Iteration Number	2689				

TABLE 48

Model (A4) > Transient Thermal (A5) > Solution (A6) > Main Filaments 4500s

Time [s]	Minimum [°C]	Maximum [°C]
10.	30.438	30.466
20.	43.457	43.545
50.	108.75	109.49
80.	171.32	173.28
170.	279.94	287.61
260.	346.01	360.16
350.	387.77	407.55
419.4	422.02	446.16
481.82	437.01	463.21
525.41	447.53	473.8
551.67	459.11	485.4
577.93	465.46	491.53
621.61	484.02	510.53
665.29	497.57	524.61
729.17	518.28	545.89
780.81	536.24	564.48
825.9	552.98	581.69
870.99	568.89	597.64
904.77	580.14	608.71
938.56	593.77	622.31
975.73	608.93	637.37
1008.1	622.21	650.54
1040.2	636.67	664.92
1069.	648.86	676.94
1097.1	662.03	689.96
1125.3	674.21	701.96
1153.4	687.59	715.33
1181.6	701.17	728.98
1209.7	699.73	726.77
1261.9	621.56	671.85
1279.3	617.3	664.06
1289.3	616.66	660.6
1299.3	616.2	657.29
1309.3	616.22	654.63
1326.	616.29	650.81
1364.1	616.78	644.81
1402.2	617.48	641.67
1502.2	622.33	642.41
1602.2	632.31	649.98
1695.9	640.97	656.65
1789.7	645.51	659.07
1889.7	651.94	663.29
1989.7	654.52	665.71
2089.7	653.54	664.5
2189.7	653.82	664.7
2289.7	654.08	664.88
2389.7	650.88	661.53
2489.7	647.71	658.24
2589.7	647.59	658.1
2689.7	646.76	657.22
2789.7	645.22	655.52
2889.7	644.41	654.63
2989.7	644.04	654.13
3089.7	643.71	653.67
3189.7	643.61	653.45
3289.7	643.38	653.1
3389.7	643.24	652.94
3489.7	643.37	652.91
3589.7	643.93	653.3
3689.7	644.64	653.87
3789.7	645.48	654.6
3889.7	644.11	652.91
3989.7	645.67	654.48
4089.7	644.74	653.29
4189.7	646.59	655.2
4289.7	645.91	654.3
4389.7	645.69	653.93
4489.7	645.56	653.74
4589.7	647.97	656.25
4689.7	647.55	655.67
4789.7	647.47	655.47
4889.7	515.11	593.96
4923.	481.79	574.44
4945.3	462.48	561.94
4967.6	445.42	550.06
5016.6	415.49	526.85
5065.5	390.93	506.17
5148.7	358.93	476.77
5232.	333.35	451.79
5315.3	312.26	430.24
5398.5	294.44	411.39
5498.5	276.48	391.77
5598.5	261.09	374.48
5698.5	247.69	359.1
5798.5	235.86	345.27
5898.5	225.32	332.74
5998.5	215.83	321.29
6098.5	207.23	310.78
6198.5	199.35	301.29
6298.5	192.05	292.53
6398.5	185.32	284.37
6498.5	179.09	276.71
6598.5	173.29	269.49
6698.5	167.89	262.7
6798.5	162.83	256.28
6848.5	160.38	253.16
6873.5	159.18	251.62
6898.5	157.99	250.1

FIGURE 18
Model (A4) > Transient Thermal (A5) > Solution (A6) > TCC

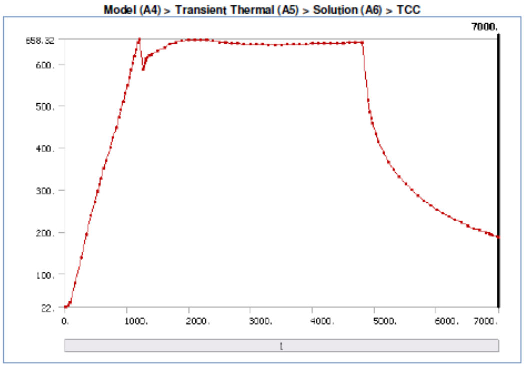

FIGURE 19
Model (A4) > Transient Thermal (A5) > Solution (A6) > TCF

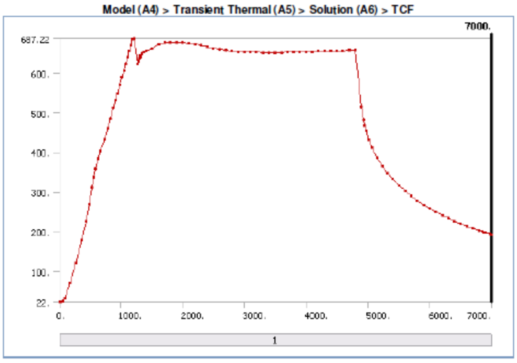

FIGURE 20
Model (A4) > Transient Thermal (A5) > Solution (A6) > TCB

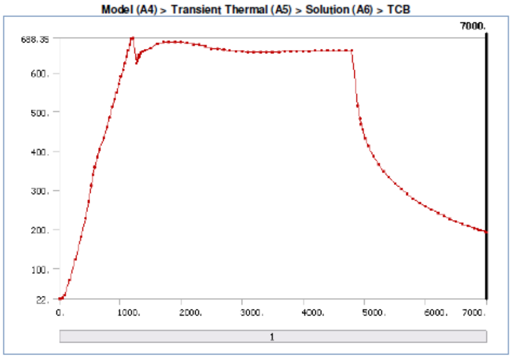

FIGURE 21
Model (A4) > Transient Thermal (A5) > Solution (A6) > H1

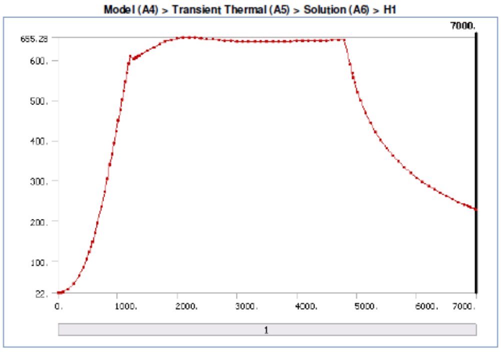

FIGURE 22
Model (A4) > Transient Thermal (A5) > Solution (A6) > H2

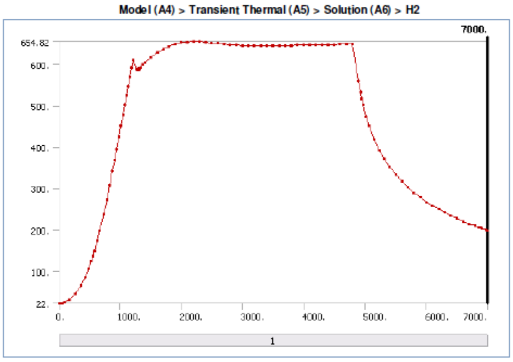

FIGURE 23
Model (A4) > Transient Thermal (A5) > Solution (A6) > M

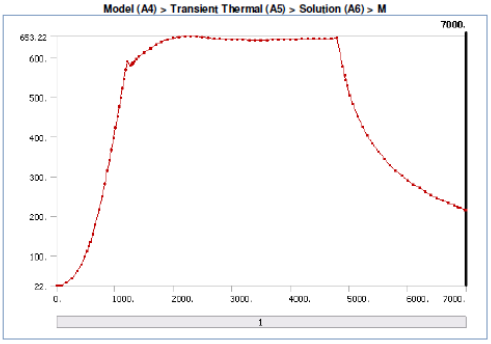

TABLE 50
Model (A4) > Transient Thermal (A5) > Solution (A6) > Probes

Object Name	*M*	*V1*	*V2*	*M_2500s*	*M_3500s*
State	Solved				
Definition					
Type	Temperature				
Location Method	Coordinate System				
Location	M_plane	V1_plane	V2_plane	M_plane	
X Coordinate	0. m	8.e-002 m	-8.e-002 m	0. m	
Y Coordinate	5.e-003 m				
Z Coordinate	0. m	8.e-002 m		0. m	
Options					
Display Time	End Time			2500. s	3500. s
Results					
Temperature	214.25 °C	227.75 °C	197.92 °C	650.33 °C	643.58 °C
Maximum Value Over Time					
Temperature	653.22 °C	654.75 °C	654.49 °C	653.22 °C	
Minimum Value Over Time					
Temperature	22. °C				
Information					
Time	7000. s			2500. s	3500. s
Load Step	1				
Substep	100			48	58
Iteration Number	2689			387	437

FIGURE 24
Model (A4) > Transient Thermal (A5) > Solution (A6) > V1

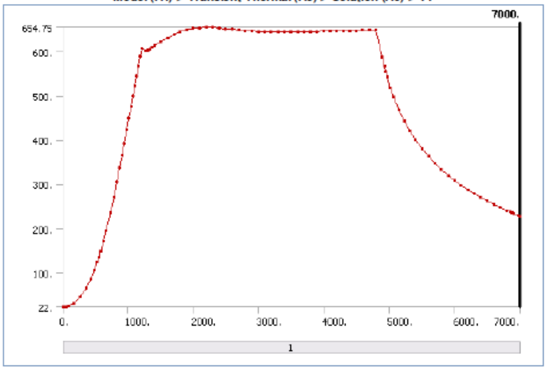

FIGURE 25
Model (A4) > Transient Thermal (A5) > Solution (A6) > V2

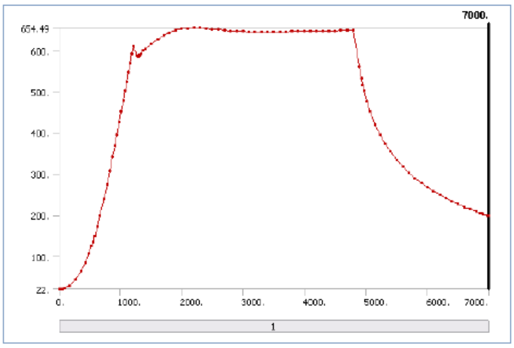

FIGURE 26
Model (A4) > Transient Thermal (A5) > Solution (A6) > M_2500s

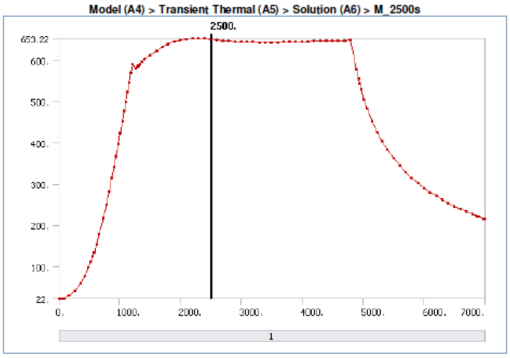

FIGURE 27
Model (A4) > Transient Thermal (A5) > Solution (A6) > M_3500s

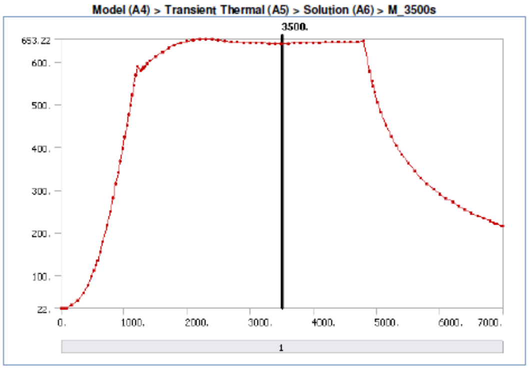

TABLE 51
Model (A4) > Transient Thermal (A5) > Solution (A6) > Probes

Object Name	*M_4500s*
State	Solved
Definition	
Type	Temperature
Location Method	Coordinate System
Location	M_plane
X Coordinate	0. m
Y Coordinate	5.e-003 m
Z Coordinate	0. m
Options	
Display Time	4500. s
Results	
Temperature	646.79 °C
Maximum Value Over Time	
Temperature	653.22 °C
Minimum Value Over Time	
Temperature	22. °C
Information	
Time	4500. s
Load Step	1
Substep	68
Iteration Number	486

FIGURE 28
Model (A4) > Transient Thermal (A5) > Solution (A6) > M_4500s

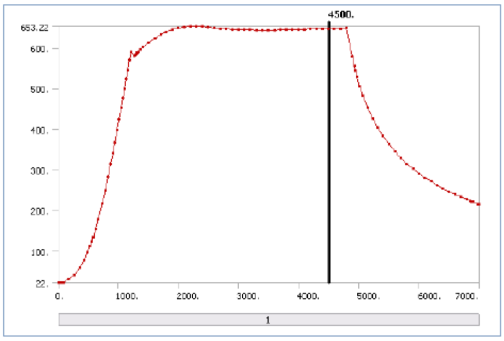

Material Data

Alumina

TABLE 52
Alumina > Constants

Density	3950 kg m^-3
Thermal Conductivity	22 W m^-1 C^-1
Specific Heat	930 J kg^-1 C^-1

Kanthal

TABLE 53
Kanthal > Constants

Density	5600 kg m^-3
Specific Heat	420 J kg^-1 C^-1
Thermal Conductivity	30 W m^-1 C^-1

K-type TC

TABLE 54
K-type TC > Constants

Density	8730 kg m^-3
Specific Heat	448 J kg^-1 C^-1
Thermal Conductivity	19.2 W m^-1 C^-1

Quartz

TABLE 55
Quartz > Constants

Density	2203 kg m^-3
Specific Heat	200 J kg^-1 C^-1
Thermal Conductivity	0.25 W m^-1 C^-1

Insulation

TABLE 56
Insulation > Constants

Density	360 kg m^-3
Thermal Conductivity	0.1 W m^-1 C^-1
Specific Heat	680 J kg^-1 C^-1